FLUENT INCORPORATED

10 Cavendish Court, Centerra Resource Park
Lebanon, New Hampshire 03766-1442 · USA
Telephone: (603) 643-2600
Fax: (603) 643-3967

Final Report

CFD Modeling of the Vermont Yankee Steam Dryer Phase - II

TM-675

Prepared for:

Entergy Nuclear Operations
Entergy Nuclear Vermont Yankee
320 Governor Hunt Rd.
Vernon, VT, 05354

By:

John Straus, Ph.D.
Senior Consulting Engineer

Reviewed by:

Karl Kühlert, Dr.-Ing.
Customer Service Team Leader, Power Generation

May 20, 2005

1. Executive Summary

In support of the Entergy VY Uprate program, Fluent performed CFD analyses of the VY reactor at 100% and 120% load conditions in two phases. Phase I work was a feasibility study on the application of LES modeling to the flow within the dryer. The Phase I study showed that an LES model could be successfully applied to the dryer model. As a result of the Phase I work, a broader understanding of the flow field within the dryer was established. Pressure signals were recorded at several locations within the dryer and processed through a signal analyzer.

This report documents the LES modeling results generated under Phase II of the CFD project. The model employed under this second phase included several modeling improvements to raise the overall accuracy of the Phase I model. The model geometry was modified to: 1) include the two 6" dams on the top of the dryer, 2) include the smooth inner radius at each steam outlet nozzle, 3) extend the outlet pipes beyond the strain gages, and include a common outlet header.

Improvements to the physical models consisted of 1) an ideal-gas representation of the steam for compressibility, and 2) improved boundary condition definition. Improvements to the boundary condition definition were made by extending the inlet to the domain to the base of the dryer. To preserve a workable model, a LES-appropriate mesh was included in only one of the plenum regions. A coarser mesh was used elsewhere.

A user-defined function (UDF) was developed to write out surface pressure data (Δp) across the walls of the dryer. This UDF could be applied manually to full (Fluent) data sets, or employed automatically during a simulation to produce high temporal resolution surface Δp data on the dryer.

The compressible flow, LES simulations of the Entergy VY dryer provide considerable insight into the flow field within the upper vessel. Two LES simulations were performed, one for the 100% load condition, and one for the 120% load condition. Global flow features for both cases were described with the aid of velocity and pressure contours, velocity vector plots, and pathline trajectories. The simulations confirmed the complex transient nature of the flow within the vessel. The steam jets entering the dome are observed to interact with each other in a transient manner. Vortical flow structures are observed in the plenums as the flow is forced to feed into the steam nozzles. These global flow features are observed in both the 100% load and 120% load cases.

During the data acquisition phase, surface Δp, mass-weighted averaged pressures, and mass flow rates were recorded at high sampling rates. This information complemented the graphical data by focusing on signal characteristics. Surface Δp data were recorded for both the 100% and 120% load conditions for a total of 2.25 seconds and 1.8 seconds, respectively. The data sets were supplied to Entergy to be used as inputs for additional structural analyses. Surface-averaged and point Δp histories were extracted from the surface Δp data file. This data, together with mass-weighted average pressures at the strain gages and at the inlet to the steam line hosting strain-gage-1 (sg1), was processed in an FFT spectrum analyzer.

The main conclusions regarding the forces on the face plate:

- The mean pressure loads on the face plate are 0.8 psi for 100% and 1.1 psi for 120%
- The mean pressure loads scale with square of velocity.

- Significant pressure fluctuations on the face plate originating from hydrodynamic effects have a frequency lower than 30 Hz. Complex flow structures and vortices in the plenum are responsible for these pressure fluctuations.

- Some pressure fluctuations on the face plate with frequencies higher than 30 Hz have been identified and are associated with acoustic modes. The mean frequencies of the pressure bands are around 40 Hz and 60 Hz.

- The time averaged load on the left gusset is 0.8 psi for the 100% case and 1.04 psi for the 120% case.

- Signals at the strain gage location are considerably stronger than at the face plate.

- The CFD model time step and modeling parameters were developed to accurately simulate hydrodynamic effects. Because the LES simulation included compressibility, acoustic effects are also captured. Accurate depiction of acoustic load amplitude would require a much smaller time step and result in an order of magnitude increase in the solution time.

2. Introduction

Entergy Nuclear Operations is seeking a license from the NRC for an extended power uprate (EPU) for Vermont Yankee (VY) to operate at 120% of current output levels. Of significance to this request are repeated structural failures of the steam dryer in a larger GE boiling water reactor (Exelon Quad Cities) following an extended power uprate. The observed failure at Quad Cities is currently believed to result from cyclic stressing of the panel walls of the steam dryer adjacent to the main steam piping nozzles. The NRC has requested Entergy to analytically demonstrate that the EPU conditions will not result in steam dryer structural failures. Entergy has undertaken an in-depth analysis of the stresses imposed on the VY steam dryer under current and uprate conditions. This analysis is based on a multidisciplinary approach. Included in this approach is a computational fluids dynamics (CFD) analysis of the flow in and about the steam dryer of the VY plant at 100% and 120% current licensed thermal power.

A project between Entergy and Fluent was arranged to develop a CFD model of the VY steam dryer. Phase I of this work consisted of a feasibility study that included both an unsteady Reynolds-Averaged Navier-Stokes (URANS) based simulation as well as a Large-Eddy simulation (LES) to isolate the effects of local vortex shedding. The URANS model simulated the entire upper vessel and dryer and a short section of the steam pipes. The LES simulation employed a highly refined mesh, consistent with LES requirements, on a truncated domain, to keep the simulation tractable. The Phase I work proved that LES modeling of the dryer could be performed and showed the presence of vortical structures at the vessel steam nozzle.

Phase II was established to improve the accuracy of the model by executing the recommendations that resulted from the Phase I work. These recommendations addressed the uncertainties associated with the simplifying assumptions used in the setup of the Phase I work. Specifically, the Phase II modeling included flow compressibility. Furthermore, the plenum and vessel head flow were coupled. The latter was accomplished by performing the LES simulation on a model encompassing the full upper vessel and dryer. To make this analysis tractable, the LES

simulation was performed on a hybrid mesh that retained an LES-appropriate mesh in only one of the plenum regions. The remainder of the domain was defined with a relatively coarse mesh. The concept of using the LES model on a relatively coarse mesh was tested as part of the Phase II work. This test consisted of a comparison of results generated from the use of the LES and URANS models on a coarse mesh to ensure that the LES model would not produce significantly different results from the URANS simulation. In the hybrid mesh, the LES model results on the coarse portion of the mesh would provide the boundary condition data for the fine mesh region.

The Phase II work also incorporated refinements to the geometry. Specifically, six-inch high dams along the top surface of the dryer, neglected in the Phase I geometry, were included. Furthermore, the main steam pipes were extended to a point beyond the location of the strain gages used for assessing local steam pressures in the pipes. The balance of the steam lines to the Turbine control valves were analytically represented to preserve pressure loss and flow coupling between the lines.

Lastly, a customized C-program (user defined function or UDF) was developed to write out pressure histories along all surfaces of the dryer. The sampling rate for this data is consistent with Phase I monitor data.

The scope of this report encompasses the modeling approach for the Phase II studies, and the results for the 100% and 120% load analyses. The Vermont Yankee technical representative for this phase of the project provided the geometry data, operating conditions, project direction and reviewer resources. GE provided a CFD model to initiate this modeling and Entergy provided the drawings listed in Table 1.

Table 1. Summary of drawings used to create the CFD model.

Description	VY Drawing	Revision
Main Steam Piping	5920 569	7
	570	5
	571	5
	ISI-RPV-105	
RPV		
	ISI-RPV-100	1
	ISI-RPV-101	1
	ISI-RPV-102	1
	ISI-RPV-103	3
	5920 18	8
	5920 24	10
	5920 103	3
	5920 105	6
	5920 3773 sh3	11
Steam Dryer	5920 493	2
	5920 494	1
	5920 876	0
	5920 877	1
	5920 878	1
	5920 879	1
	5920 880	1
	5920 881	1
	5920 882	1
	5920 883	1
	5920 884	1
Dryer Modification		
GE Drawings from VYDC-2003-012		
	234C6402 sh1-6	1
	234C6397Sh1	
	234C6631-6652 Sh1	0
	234C6649 Sh2	0
	234C6651 Sh2	0

3. Model Set-Up and Technical Approach

The LES analysis performed under Phase I lacked flow coupling between the plenum and vessel head. As part of the simplifying assumptions used in Phase I, a fixed boundary condition based on URANS results was used to define the inlet conditions for the clipped domain of the LES model. Under the Phase II work, the flows between the two regions are coupled by resolving the entire domain for the LES simulation. The original LES mesh is retained, and the remainder of the vessel geometry is meshed with a coarse mesh. The combination of the fine and coarse resolution is referred to as a hybrid mesh. Conceptually, the fixed boundary condition employed in Phase I is replaced with a dynamic condition defined by an LES solution on the coarse section of the hybrid mesh.

The success of obtaining an LES solution on the hybrid mesh hinged on the capacity for the LES model to sufficiently resolve the flow field on the coarse mesh. The concept of using the LES model on a coarse mesh was tested by comparing LES and URANS-based results on a coarse mesh. The test involved a visual comparison of the flow field between a URANS solution and an LES solution on the model meshed entirely with a coarse mesh. Specifically, the mesh resolution was consistent with the refined mesh used for the refined RANS calculations of Phase I. Comparisons were made at the plane that defined the inlet boundary condition to the clipped domain for the LES study of Phase I.

Following the test, LES solutions for the 100% power load and 120% loads were calculated. The modeling approach for all LES simulations followed that of the Phase I work. A compressible URANS solution was first established before the LES solution was calculated. Following the switch to the LES model, sufficient solution time was permitted to allow the transition transients to pass through the domain. After the solution became established, time-averaged data, and dryer surface pressure data were recorded.

3.1 Geometry and Mesh

The complete 3D model developed for Phase I simulations was the basis for the 3D model for the Phase II work (Figures 1, 2, and 3). Two six-inch dams were added to the top of the original dryer geometry. The smooth inner radius was added to each steam outlet nozzle. The outlet pipes were extended to include the two-stage ninety-degree turn and lengthened to include the strain gage locations. For the comparison study, the domain ended at the strain gages. For the LES studies, the steam lines were extended further from the strain gages and the pressure drop and flow coupling of the balance of the piping to the turbine control valves was analytically represented. This analytical representation included porous media and a common plenum (yellow pipe in Figure 3). The properties of the porous media are discussed in section 3.3.

Two different meshes were created. The first mesh was a uniformly sized coarse mesh used to compare the LES model solution with a URANS simulation. The resolution used was similar to that of the refined mesh used in the Phase I analysis (average cell size of 1.5 inches in the plenum). This coarse mesh contained roughly 1.9 million mixed elements.

To generate the second mesh, three different regions were distinguished, one plenum with steamlines with a LES appropriate mesh, one plenum with steamlines with a coarse mesh, and the dome and dryer. The LES appropriate mesh was confined to the same region represented in the clipped domain model used for the Phase I work and used a similar resolution (0.65 inches within

the plenum). For the opposite plenum, a coarse mesh with a resolution of approximately 1.5 inches was used. This resolution is consistent with the first test mesh and the refined RANS mesh of the Phase I work. A considerable number of cells were required to transition from the high resolution mesh to the low resolution mesh in the dome (Figures 4 and 5). The mesh size in the dome and the dryer was similar to the finest mesh in this area used in Phase I. The (hybrid) mesh contained roughly 4.6 million cells.

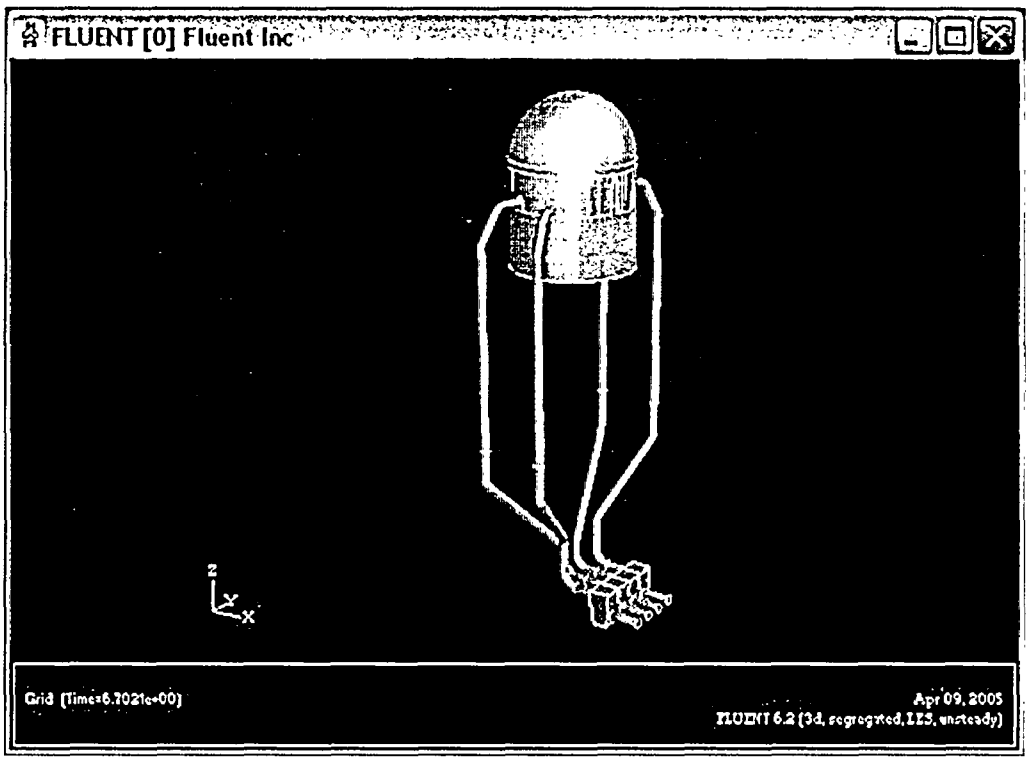

Figure 1. Full 3D Geometry of upper vessel, steam pipes, and common outlet plenum.

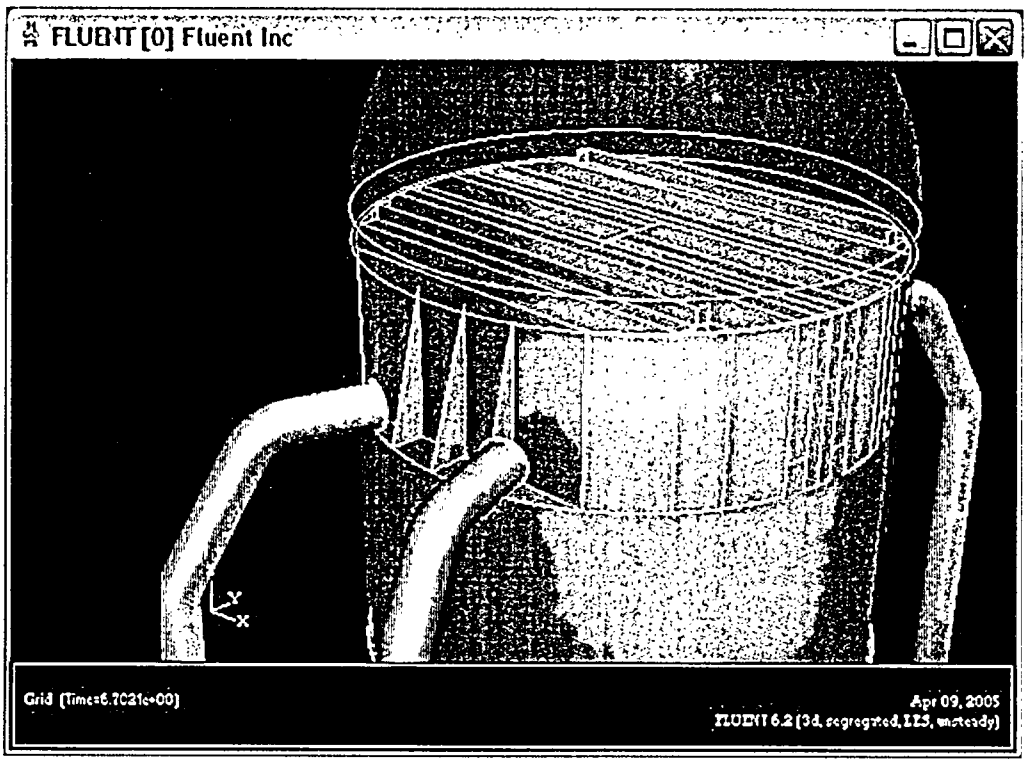

Figure 2. Close up view of 6" dams and outlet pipes.

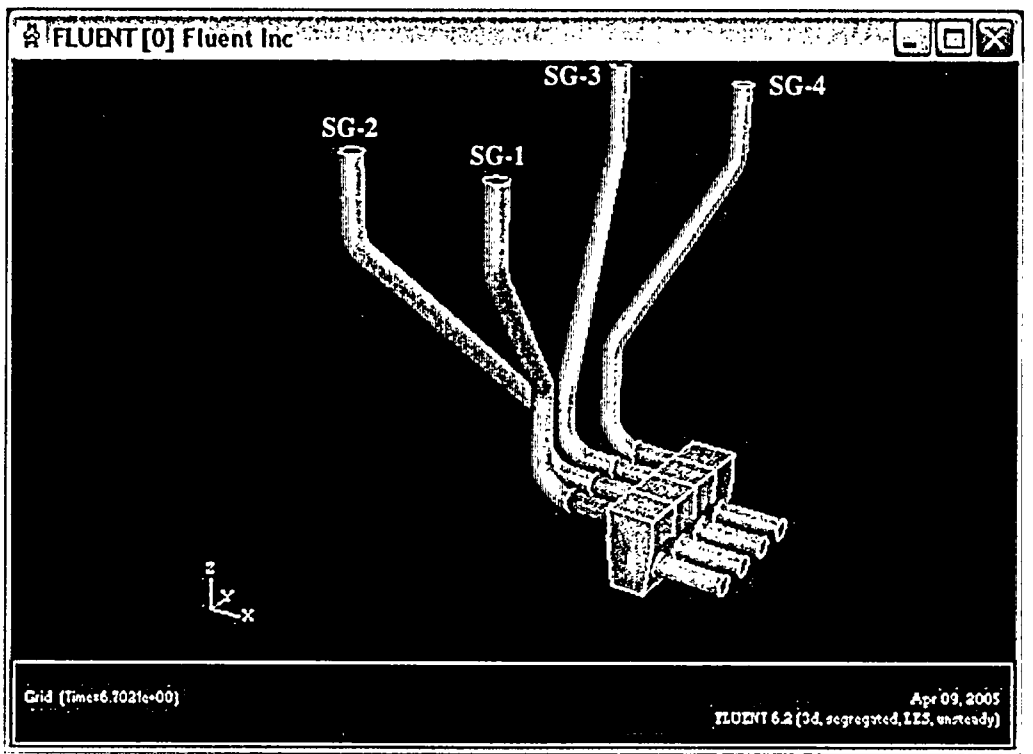

Figure 3. Strain gage location (top) and common outlet plenum

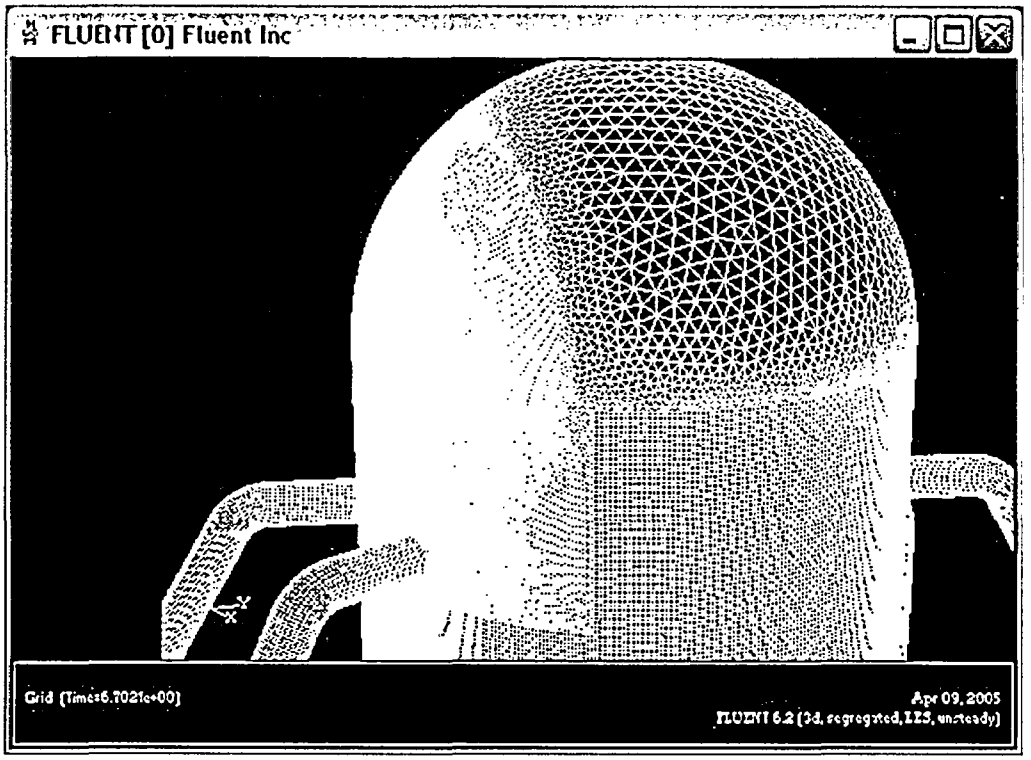

Figure 4. External view of LES mesh – coarse mesh transition

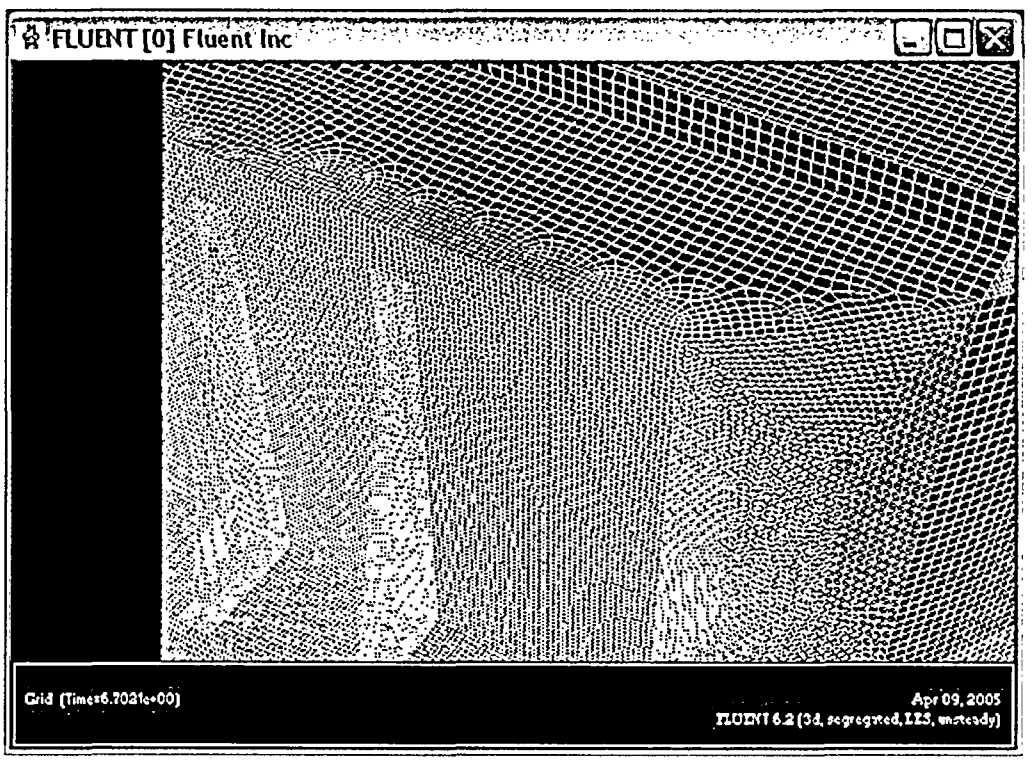

Figure 5. Internal view of LES mesh – coarse mesh transition

3.2 Operating Conditions and Physical Model Assumptions

Conditions in the dryer involve the flow of saturated steam (water vapor) at 7.067 MPa (1025 psia) and 560 K. Simulations were performed for both 100% and 120% load. At 100% power load, steam flows through the dryer at a rate of 813 kg/sec (6.46E6 lbm/hr). At 120% load, steam flows through the dryer at a rate of 996.1 kg/sec (7.906+E6 lbm/hr). Liquid droplets are assumed to be completely removed from the flow through the dryer vane assemblies.

To improve on the model simulation used in the Phase I studies, the flow in the dryer was modeled to be compressible. Density was modeled using the ideal gas law. To account for real gas effects, a compressibility factor was included in the ideal gas equation of state such that the correct density would be calculated for the known saturated temperature and pressure. The compressibility factor was accounted for through the modification of the molecular weight of water vapor (24.55 instead of 18.012 kg/kmol). The steam density under saturated conditions is 36.912 kg/m^3 and a constant molecular viscosity of 1.8991 x 10^{-5} kg/m-s was used (data obtained from NIST website and cross-checked with textbook thermodynamic tables). Computed average densities ranged from 38 kg/m^3 at 100% load to 38.6 kg/m^3 at 120% load, approximately 4% from the density under saturated conditions.

The energy equation was solved to track the changes in local temperature. It was assumed that the difference between the total and static temperature at the inlet of the dryer is small because of the low flow velocities at this location. The inlet total temperature was therefore set at 560K. All external walls were assumed to be adiabatic. Heat fluxes across internal walls were assumed to be negligible because the temperature of the fluid is quite uniform throughout the dryer region. Variations from the mean fluid temperatures could arise in the plenum in areas with high flow velocity because of compressibility effects.

The flow was modeled to be turbulent and unsteady. As with Phase I, the Realizable k-ε model was used for the URANS analysis. For the URANS analyses, the momentum and energy equations were discretized using a second-order upwind formulation. For the LES analyses, the momentum equations were discretized using a bounded, central differencing scheme to reduce numerical diffusion. The dynamic Smagorinsky-Lilly model was used to model subgrid scale stresses. [Refer to Fluent v6.2 User's Guide for further information.]

3.3 Boundary Conditions

Boundary conditions for the Phase II work were similar to that for the Phase I work. For compressible flow, a fixed uniform mass flux is specified at the inlet boundary, rather than a fixed velocity. For 100% load, steam is introduced into the computational domain at the inlets at a uniform rate of 76.59 kg/m^2-sec in a direction normal to the inlet boundaries (+z-axis). For 120% load, steam is introduced into the domain at 91.91 kg/m^2-sec. As in Phase I, the flow is assumed to be mildly turbulent with an intensity of 2%. This moderate level of turbulence is often times used in CFD as a boundary condition when turbulence quantities are unknown. The turbulence level at the inlet does not have any impact on the flow in the dryer because the turbulence field becomes fully developed as it traverses through the inlet path of the dryer.

Following entry into the steam dryer domain, the steam flow navigates through the dryer liquid separation components. As before, the dryer vane assemblies were represented using a porous media lumped parameter model. The porous media resistance was defined to be anisotropic and restricted the flow along the vessel axis and in the direction normal to the vertical faceplates.

Uniform flow resistance coefficients for the 100% and 120% cases were applied to the porous media and were based on a pressure drop of ~0.5 psi at 120% power (Vermont Yankee Extended Power Uprate Task T0304: Reactor Internal Pressure Differences and Fuel Lift Evaluation, GE-NE-0000-0009-5746-01 Revision 0, May 2003).

The flow encounters a second set of porous media just upstream of the common outlet plenum representing the balance of the steam system not explicitly included in the model. The porous media was designed to provide an overall pressure loss from the RPV to the turbine control valve of ~39.6 psi at 100% power (based on Plant Instrumentation 4/19/2005 11:00:00 RPV Pressure is (B048) 1007.109psig and Throttle steam pressure is (T006) 967.506psig at (B022) 6.559 M#/hr). The simulated pressure drop was 38 psi. Therefore the resistance provided by the porous media was appropriate to preserve the steam property change from the vessel to the strain gage location.

The outlet boundaries are defined as constant pressure boundaries. The outlet pressure was set to 6.957 MPa (1009 psia) and used for both the 100% load and 120% load cases.

As for Phase I, all wall boundaries were defined as no-slip boundaries. The standard wall-function was used to relate local fluid conditions with local wall shear stresses for both turbulence models. Local y+ values typically ranged from 30 to 25000 along the dryer walls. y+ is a dimensionless variable commonly used to represent the distance from a wall in a turbulent boundary layer; $y+ = y\, \upsilon^* / \nu_w$, $\upsilon^* = (\tau_w / \rho_w)^{1/2}$. Within the plenum (LES side), y+ values were on the order of 3000-15000.

3.4 Solution Procedure

Three distinct LES simulations, as described above, were performed: (1) test of the LES model on a coarse mesh with a comparison with URANS results, (2) LES simulation on the hybrid mesh at 100% load, and (3) LES simulation on the hybrid mesh as 120% load. The URANS and LES simulations used to test the LES model on the coarse mesh were run at 100% power load. The compressible flow LES solution was preceded and seeded by the compressible flow URANS solution. The same procedure was used for the LES simulation for 100% load on the hybrid mesh. However, since the 120% load case was run after the 100% load case, the 120% LES simulation was seeded by the 100% load LES simulation.

All transient solutions were obtained using the iterative time-advancing (ITA) segregated solver using standard solution controls in Fluent 6.2. The non-iterative time advancing scheme (NITA) used for the Phase I calculations were determined to be less efficient for these mildly compressible flow cases. When performing the test runs, a maximum time step size of 0.0025 seconds was used for the URANS phase of the calculation and a maximum time step size of 0.0003 seconds was used for the LES portion. For the LES hybrid runs at 100% power load, a maximum time step size of 0.0005 seconds was used. A maximum time step size of 0.0004 seconds was used for the 120% load case. This time step size is consistent with a local Courant number of ~1 for a conservatively assumed local velocity of 40 m/sec in the plenum region.

As with the Phase I calculations, each LES calculation on the hybrid mesh consisted of two phases, the startup calculation phase and the data-sampling phase. Pressures at points L2 and L6 on the vertical faceplate were typically monitored over time to gage the progress of the solution. The locations of these points are provided in Table 2 and Figure 6 (other points shown in Table 2 were used in the Phase I analyses). In general, for entry into the data-sampling phase, data registers used to record time-averaged velocities and pressures were created and initialized.

For the LES hybrid runs, full data sets were recorded roughly every 0.25 seconds (simulated) for the 100% power load case, and every 0.2 seconds for the 120% load case. The information contained in these data sets includes local velocities, pressures, turbulence, and fluid properties. 17 full data sets were saved for the 100% load case and 18 data sets for the 120% load case. For the Phase I work, data acquired at a higher sampling frequency (0.0002 seconds) was recorded only for pressure at six distinct points. For the Phase II work, a customized UDF was created to write out to disk the pressure data at similarly high frequencies (0.001 second intervals for the 100% power load and 0.0008 second intervals for 120% load) at all 140,517 cell locations along all dryer wall surfaces. The UDF can also be applied manually to any of the full data sets to extract the pressure distribution data for the corresponding time. The Fluent wall zone IDs for which the data was exported are provided in Appendix A1.

Rather than recording absolute pressures, the UDF was written to record local pressure differences. If the flow was numerically resolved on both sides of the wall, the pressure difference across a given point on the wall was calculated based on the local pressures at the cell centers on either side of the wall. If the flow was resolved on only one side of the wall, the pressure on the non-resolved side was assumed to be that at the inlet to the domain. Except along the cylindrical surface of the dryer, a positively valued pressure difference was defined to be aligned with the positive coordinate axes. Along the cylindrical surface, positive pressure differentials were defined as inwards, towards the geometrical axis of the vessel. Coordinate directions can be seen in Figure 2. The origin is located along the axis of the vessel and aligned vertically with the lower horizontal surface of the plenum.

The format of the file written by the UDF is shown in Figure 7. Columns were separated with spaces. A total of 140,517 columns were required to accommodate all cell faces of all dryer walls. If applied manually to one of the full data sets, only the first row of pressure data is reported.

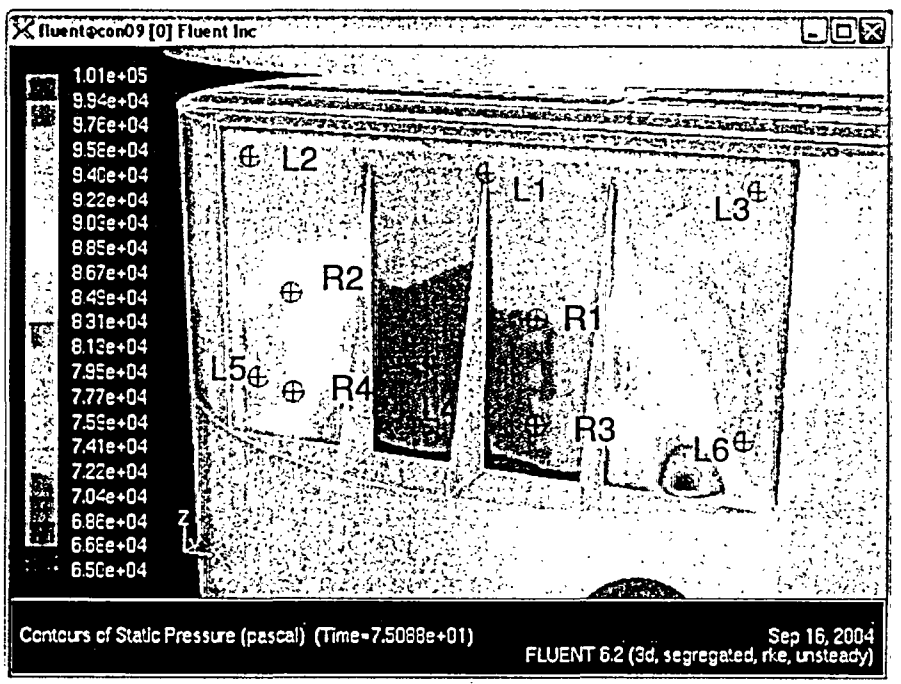

Figure 6. Location of monitoring points.

Table 2. Location of point monitors for LES simulation*

Point monitor ID	x-position (in)	y-position (in)	z-position (in)
L1	0	-84.25	56
L2	-48	-84.25	56
L3	48	-84.25	56
L4	0	-84.25	12
L5	-48	-84.25	12
L6	48	-84.25	12

*Origin elevation is aligned with horizontal face plate and located on vessel axis

Zone-ID-1	Zone-ID-1	Zone-ID-1	Zone-ID-j	Zone-ID-N	. .
x-coordinate-1	x-coordinate-2	x-coordinate-3	x-coordinate-i	x-coordinate-i	
y-coordinate-1	y-coordinate-2	y-coordinate-3	y-coordinate-i	y-coordinate-i	
z-coordinate-1	z-coordinate-2	z-coordinate-3	z-coordinate-i	z-coordinate-i	
Face Area-1	Face Area-2	Face Area-3	Face Area-i	Face Area-i	
P_{t1}	P_{t1}	P_{t1}	P_{t1}	P_{t1}	
P_{t2}	P_{t2}	P_{t2}	P_{t2}	P_{t2}	
.					
.					

Figure 7. Format of UDF output for pressure differences

4. Simulation Results

Solutions were obtained on the full vessel 3D model with a coarse mesh for the LES – URANS comparison, and on the hybrid mesh for the 100% power and 120% power to provide pressure data for stress analysis. The solutions for these cases are described in this section.

4.1 LES Coarse Mesh Applicability Test

To test the applicability of the LES model on a coarse mesh, a URANS solution and an LES solution were established on a coarse mesh and their results compared. The resolution of the coarse mesh was similar to that of the refined mesh studies of Phase I (cell size of ~1.5 inches in the plenum).

To gage the applicability of the LES model on the coarse mesh, instantaneous and mean pressures from both solutions on the vertical face plate were compared (Figures 8-11). Furthermore, results were compared along the interface at which the transition between the fine mesh and the coarse mesh takes place in the hybrid mesh. Along this plane, mean pressures and velocity magnitudes were compared (Figures 12-15).

Since different turbulence models were employed, identical solutions were not expected. For the hybrid mesh model to be successful, it was expected that the LES model on the coarse mesh sufficiently represent the conditions at the interface boundary. Figures 8 through 15 show just this case.

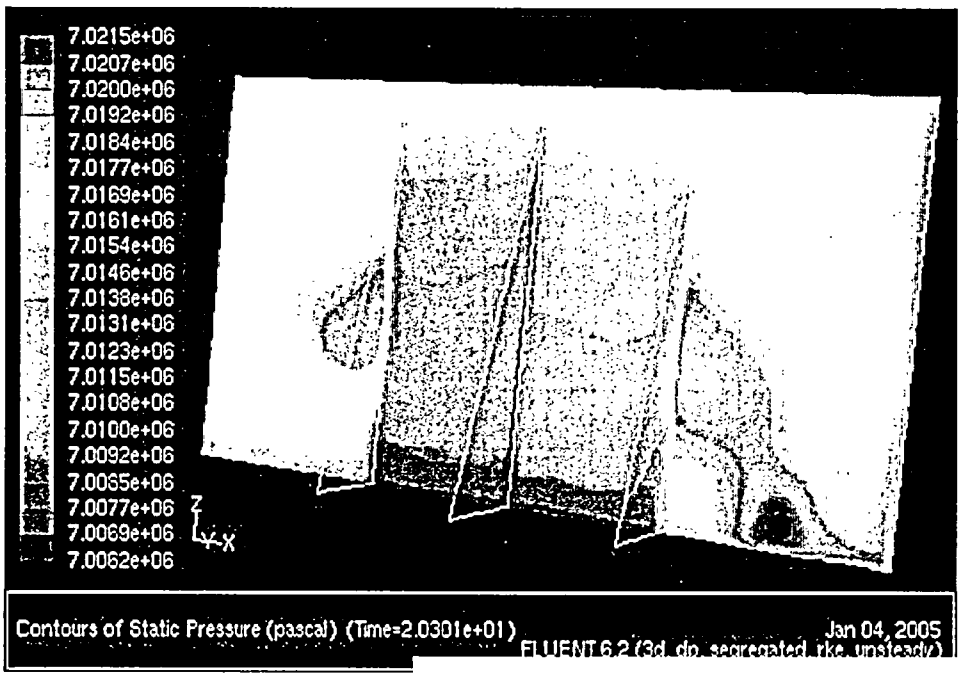

Figure 8. Instantaneous static pressure contours (LES side) derived from URANS model on coarse mesh.

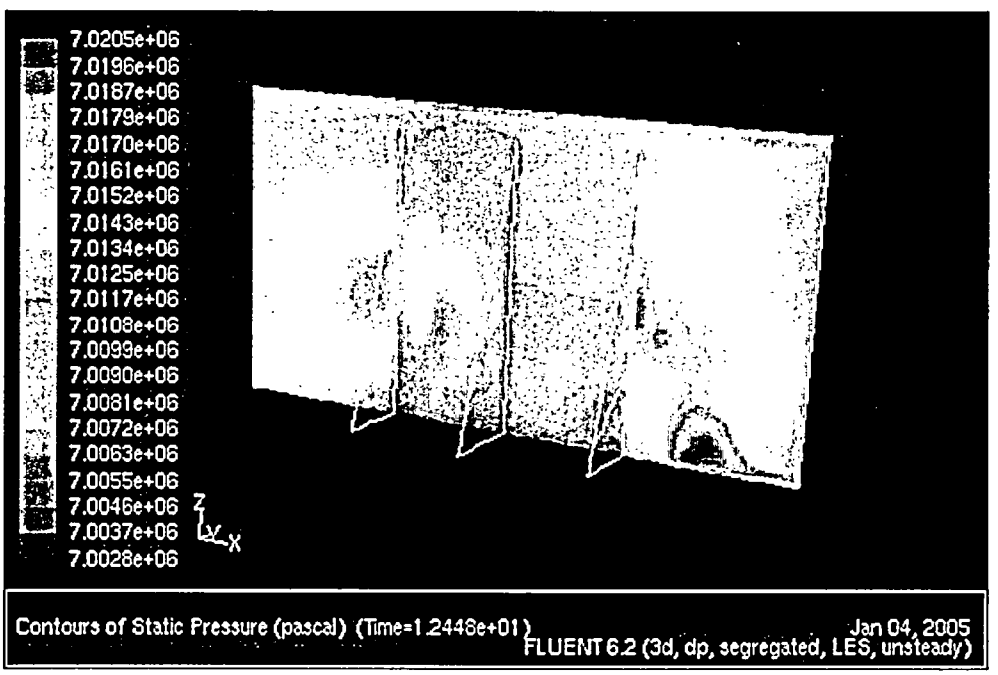

Figure 9. Instantaneous static pressure contours (LES side) derived from LES model on coarse mesh.

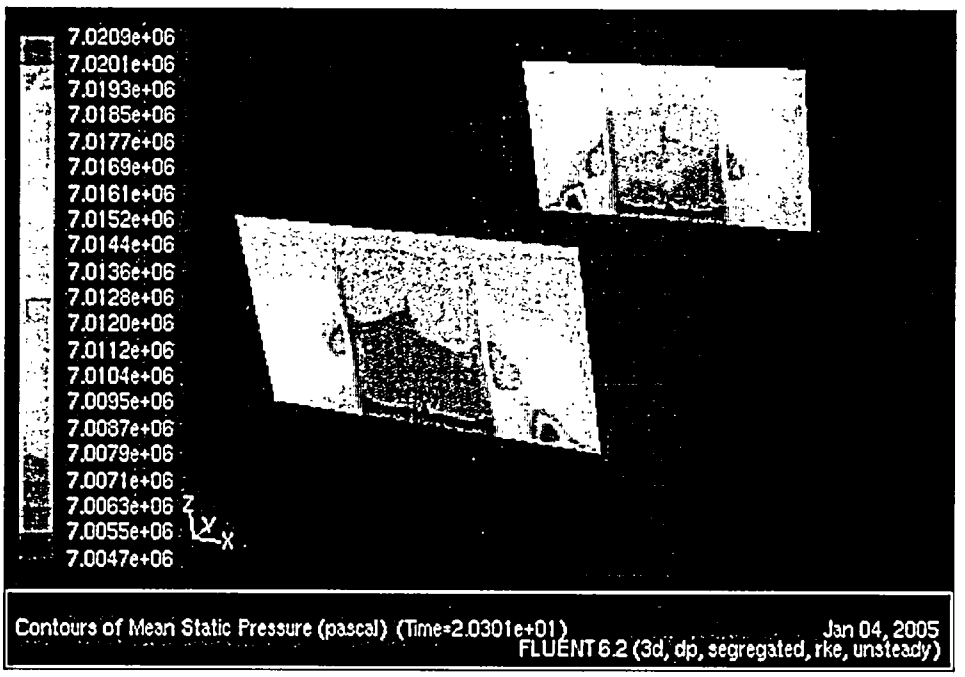

Figure 10. Mean static pressure contours derived from URANS model on coarse mesh.

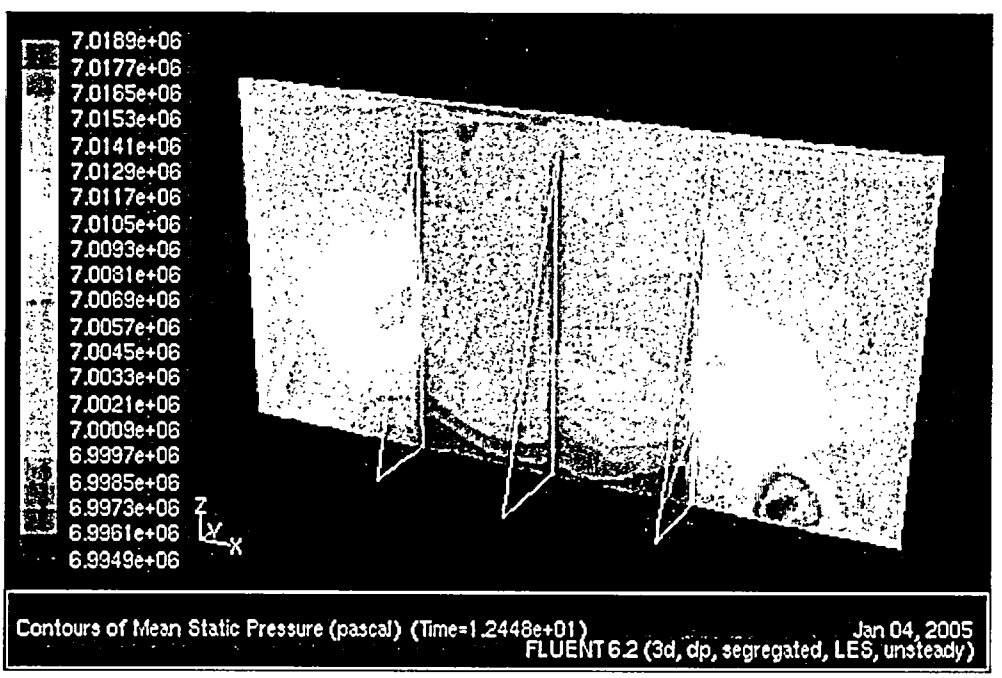

Figure 11. Mean static pressure contours (LES Side) derived from LES model on coarse mesh.

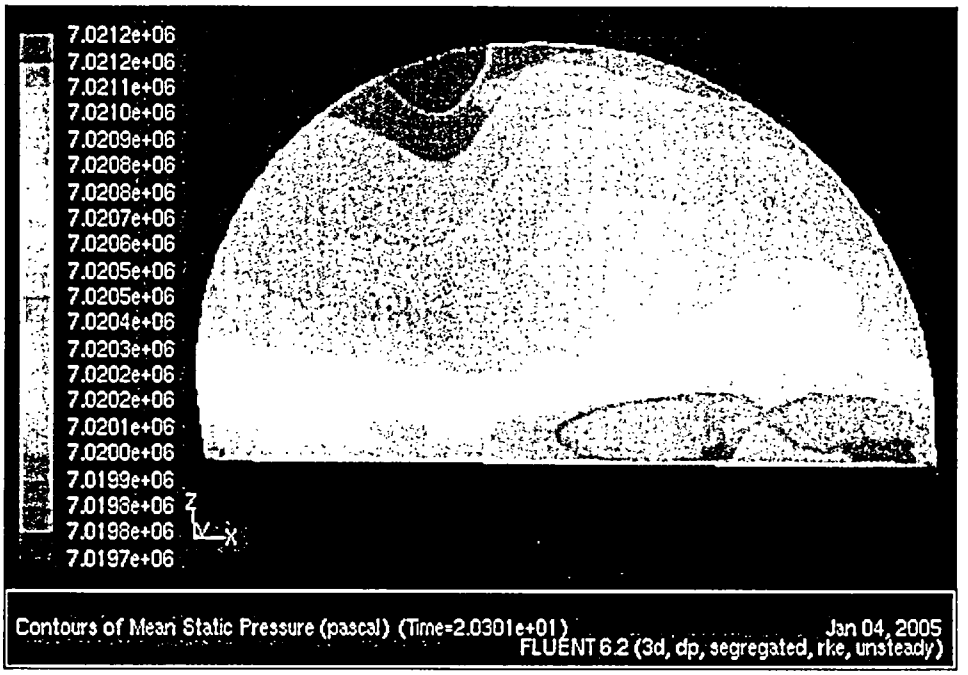

Figure 12. Mean static pressure contours along mesh interface derived from URANS model on coarse mesh.

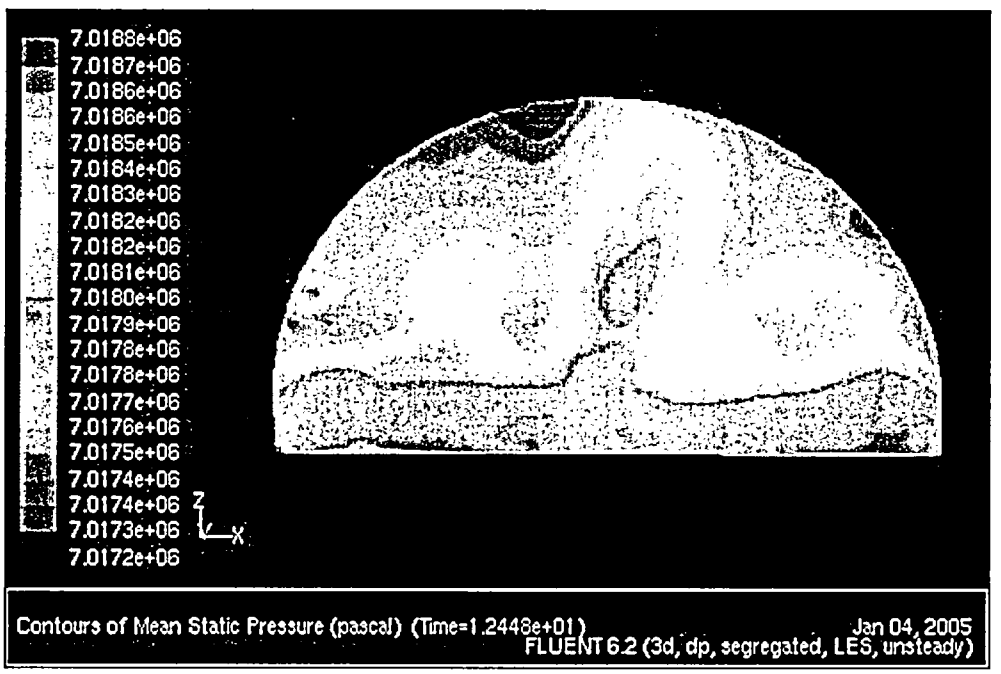

Figure 13. Mean static pressure contours along mesh interface derived from LES model on coarse mesh.

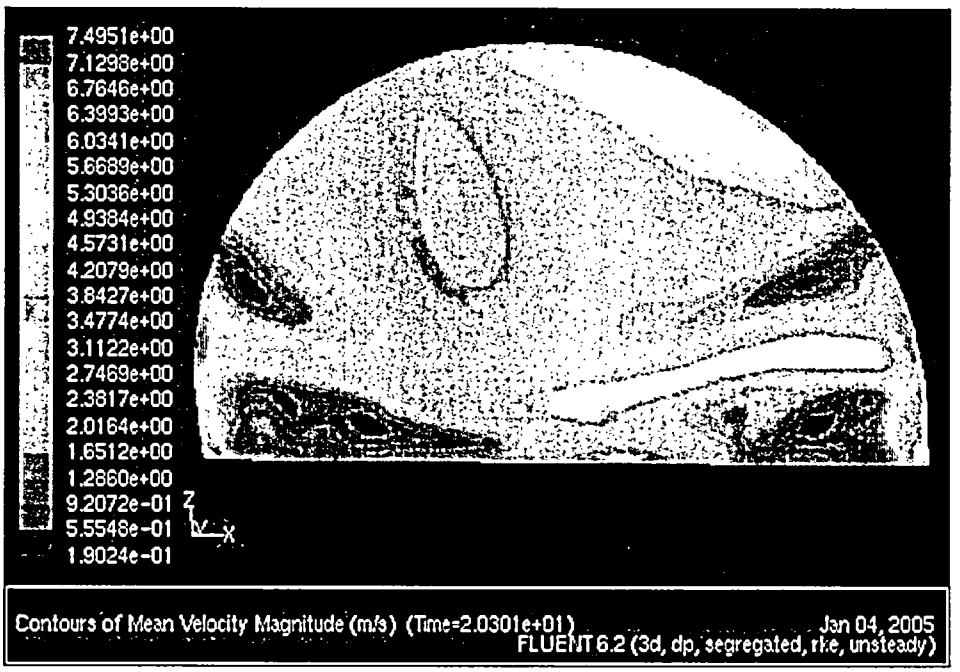

Figure 14. Mean velocity magnitude contours along mesh interface derived from URANS model on coarse mesh.

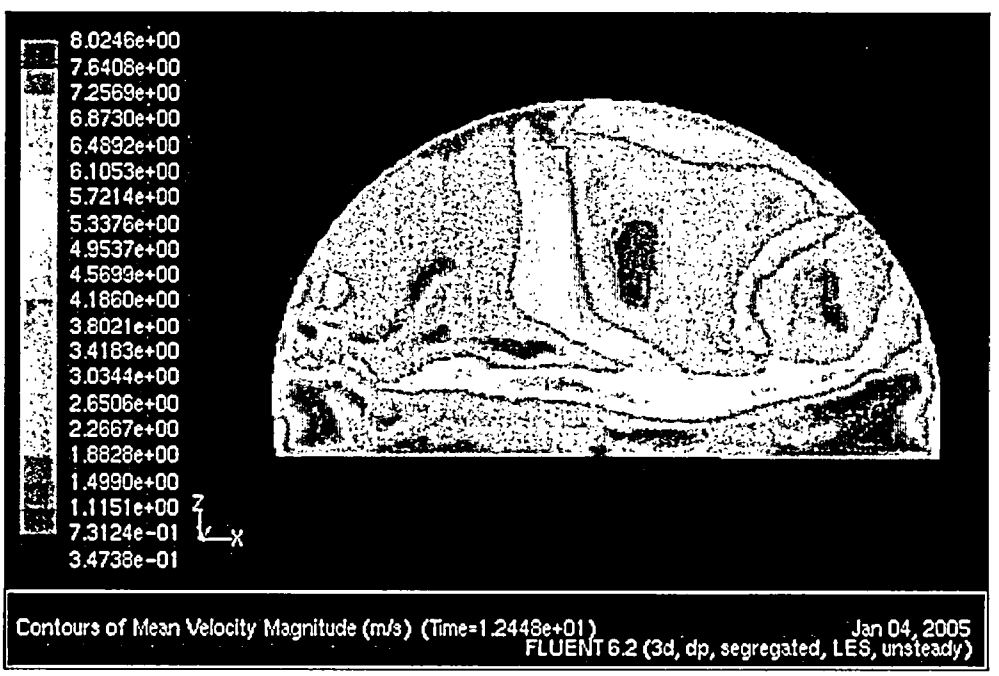

Figure 15. Mean velocity magnitude contours along mesh interface derived from LES model on coarse mesh.

4.2 LES Solution on Hybrid Mesh for 100% Load

4.2.1 Observations on the Flow Field in the Vessel Head for 100% Load

The changes in the model used in the Phase II work improve the accuracy of the simulations over that of the Phase I work. These modifications involved improvements to the geometrical representation of the steam pipes and steam dams and account for flow compressibility. In addition, the hybrid mesh allowed the flow field in one of the plenums to be resolved using the LES model while still accounting for the system wide flow transients associated with the jet flow in the dome. These improvements to accuracy are specific to the region that is resolved using the LES-appropriate mesh, though the solutions still provide considerable insight into the flow field in the entire model. A review of the results supports the findings of the Phase I work that the upper vessel of the power plant hosts a complex, three-dimensional flow system. Observations of the results of the Phase II studies show numerous local flow features. For the 100% load case, velocity and pressure distributions of the 17 full data sets were reviewed (see Appendix A.2). Findings from a selection of these data sets are discussed below.

As with the Phase I studies, the Phase II work shows a transient behavior in which the steam jets entering the dome interact with each other and the dome wall in a transient fashion. Figures 16a - 16d show the velocity jets in velocity magnitude contour plots along the x=+50 in. plane at four different simulation times, t=3.20 sec, 4.95 sec, 5.98 sec, and 6.20 sec (these times coincide with four distinct vertical face plate pressure patterns to be discussed later). In this view, the LES mesh is on the left. The dryer is noted to introduce a greater mass flow rate into the dome region in two of the four quadrants (each quadrant being loosely identified with a corresponding steam line). This is due to the asymmetrical design of the dryer which has, in two of the four quadrants, a greater inlet surface area relative to the other two quadrants. The higher mass flow from the two quadrants tends to draw flow in from the adjacent lower mass flow quadrants. The cumulative jet can be observed to impinge the dome wall near the top and diverge outwards towards one or both of the outlet plenums. Figures 16c and 16d show the bulk of the jet flow headed towards the left plenum. Figure 16b shows the bulk of the jet flow in this plane is roughly divided between both plenums. As the flow returns down towards the outlet plenums, it can be observed to interact with the two outermost jets. The right most jet in Figure 16c is likely washed to the left from redirected flow off the dome wall. It is possible that this interaction causes the outer most jets to oscillate back and forth as noted in the Phase I work, thereby affecting the oscillations of the central jets. These oscillations appear to occur at a low frequency, on the order of 1 Hz. Figure 17 shows a similar velocity magnitude contour plot at the x=-50 in. plane at t=5.98 sec. A comparison with Figure 16c shows that the entrained jet is directed towards the other plenum.

Considering velocity vector plots along similar planes further highlights the variability of the flow within the dryer. Figures 18 and 19 respectively show velocity vector plots at x=0 and x=50 in at t=5.98 sec. Both plots show that the flow entering the plenum is, in general, directed from above. At x=0, the flow is also seen to impinge on top of the dryer and diverge towards both the plenum and the 6 inch dam. The portion of the flow that is directed towards the dam sets up a small recirculation zone. At x=50 in, the downward flow produces interference with the jet opposite the 6 inch dam. The recirculation zone, though less clearly defined, still exists.

As with the Phase I LES and URANS studies, the flow is observed to form vortical structures as it exits the outlet plenums through the steam pipe nozzles. This is evident in Figures 20 and 21 which respectively show pathlines exiting the right and left steam pipe nozzles on the LES-mesh side of the model. The pathlines originated from a plane just downstream of the 6 inch dam and

were generated from a fixed flow field at t=5.98 sec. Superimposed in this figures are pressure contour plots along the vertical face plate. Similar to the Phase I findings, the pathlines are observed to circulate about the low pressure region on the vertical face plate. Figure 20 clearly shows that the flow feeding the vortical structure not only comes from the top, but also from the 2 inch gap on the bottom and side.

The pressure contours along the vertical face plate for times t=3.20 sec, 4.95 sec, 5.98 sec, and 6.20 sec are shown in Figures 22a-22d. The LES-mesh side is in the foreground. The pressure contours show that during the course of the simulation, the vortices can, over time, appear stronger at either inlet or at both inlets. Furthermore, Figure 22b shows that the vortices can be relatively weak compared to other times (all plots use the same scale). Though not evident in these figures, vortices of similar magnitude were evident at other times on the other vertical face plate (coarse mesh). Different from the Phase I results are the newly predicted strength and location of the vortices. The Phase I LES solutions showed the vortices to be more in line with the vertical position of the outlet steam pipes. The locations of the vortices predicted from the current simulation are much closer to the horizontal cover plate (consistent with the Phase I URANS studies). The strengths of the vortices are also weaker than predicted in Phase I. The minimum and maximum pressures indicated by the scale limits provide a good indication of the relative vortex strength. Here, the vortex core is roughly 120 kPa or 17.5 psi lower than the surrounding pressure. A 40 psi pressure differential was calculated in the Phase I analyses. This difference is likely to be attributable to compressibility effects. The centrifugal forces are directly balanced by the radial pressure gradient for an incompressible flow. Compressibility relaxes the local pressure gradient and the overall pressure differential becomes less severe.

For one-and-a-half seconds of the simulation, the mass flow rates in each of the steamlines at the strain gages were recorded over time. A plot of the mass flow rates at strain gages 1 through 4 (identified as sg1 - sg4) is given in Figure 23. It is noted that strain gages 1 and 2 (2 being on the left when viewing the plenum from the outside) are associated with the steamlines shared by one plenum, and strain gages 3 and 4 are associated with the other plenum (see Figure 3). Of interest are two apparent dominant frequencies, a higher ~20 Hz signal superimposed on a lower ~ 3 Hz signal (Figure 24).

The pressure in the dryer at 100% load was calculated to be 7.22 MPa (1047 psia), roughly 20 psi or 2% higher than the operating pressure of 1025 psia. This difference was the result of maintaining the constant outlet pressure boundary at 1009 psia. The ~40 psi pressure drop between the dryer inlet and throttle steam valve was maintained in the model. The higher absolute pressure results in a higher density and in turn, lower average flow velocities (by 2%). The net effect of this deviation on the observed flow features is assumed to be negligible. Turbulent kinetic energies typically scale with the dynamic head of the flow. The dynamic head in this case is about 2% lower than with the correct operating pressure. Thus, the energy associated with turbulent eddies can be expected to be underestimated by 2%.

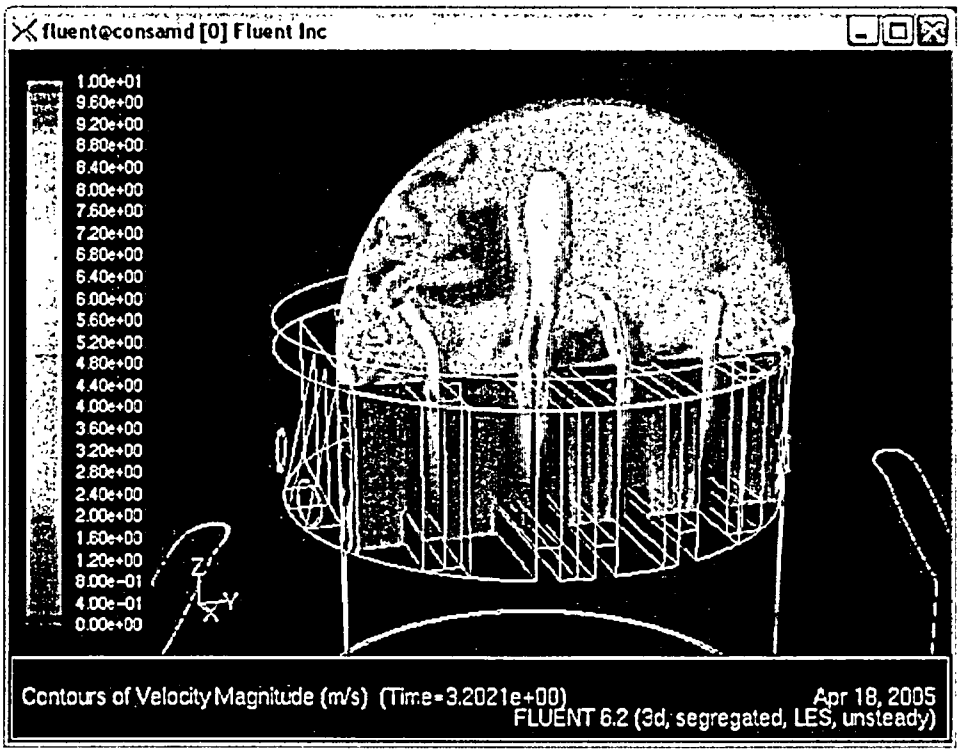

Figure 16a. Velocity magnitude contours at x=50 in at t=3.20 sec.

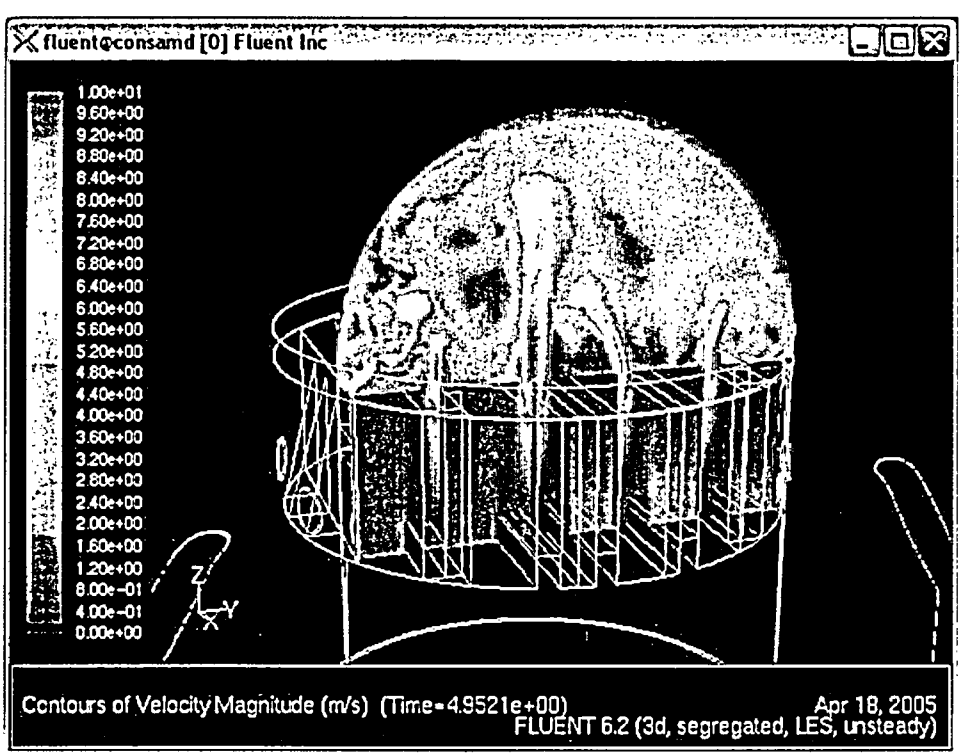

Figure 16b. Velocity magnitude contours at x=50 in at t=4.95 sec.

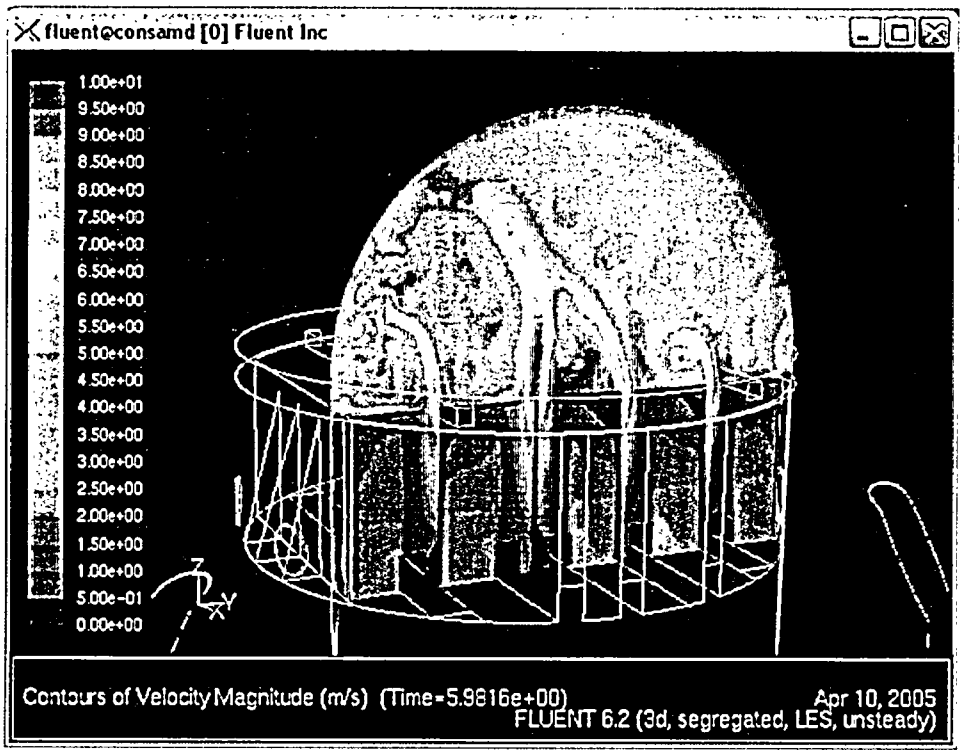

Figure 16c. Velocity magnitude contours at x=50 in at t=5.98 sec.

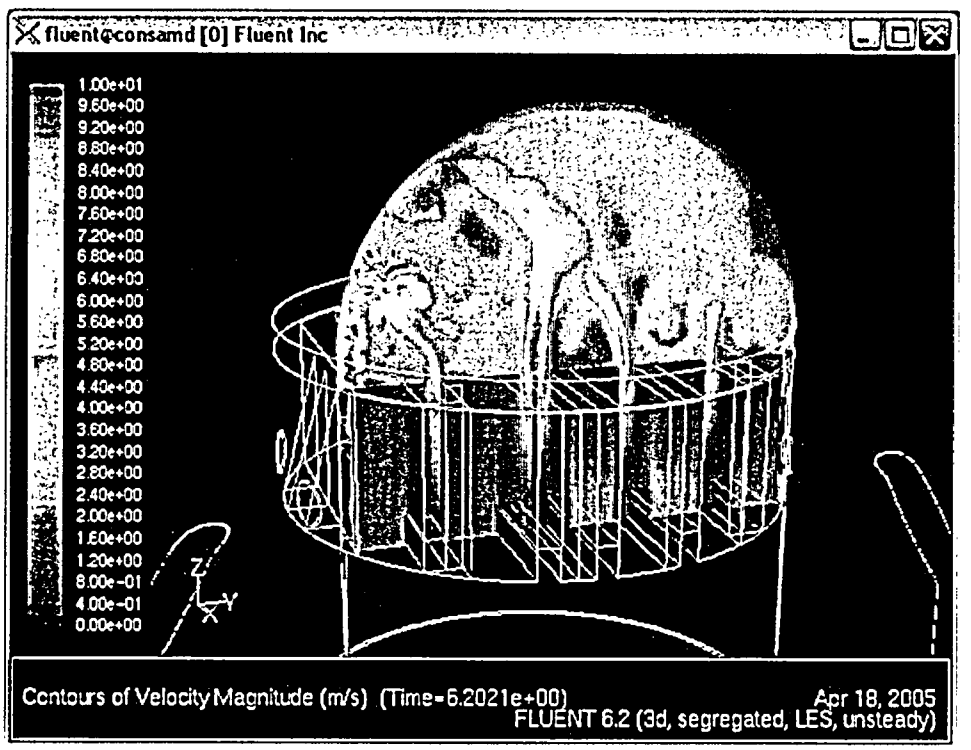

Figure 16d. Velocity magnitude contours at x=50 in at t=6.20 sec.

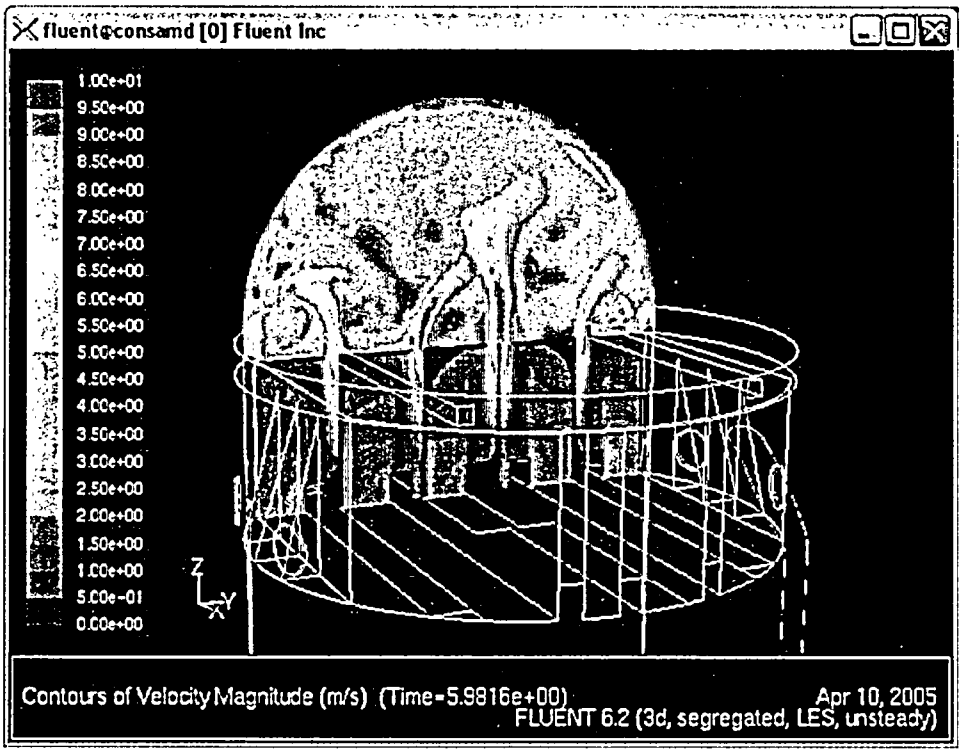

Figure 17. Velocity magnitude contours at x=-50 in at t=5.98 sec.

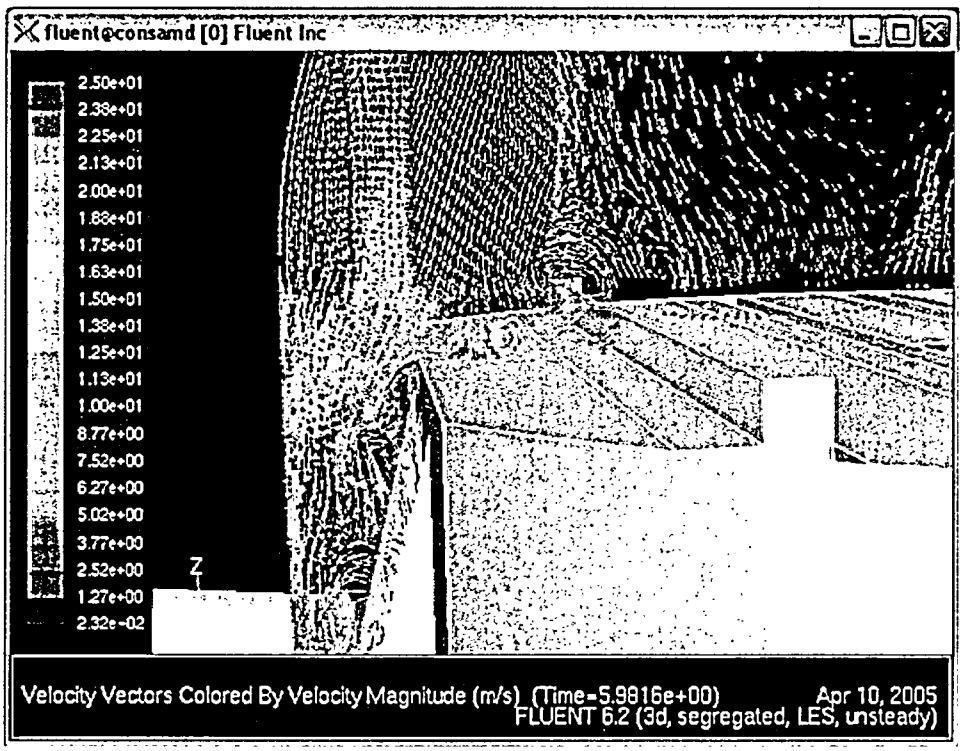

Figure 18. Velocity vectors near 6" dam at x=0 inches and t=5.98 sec.

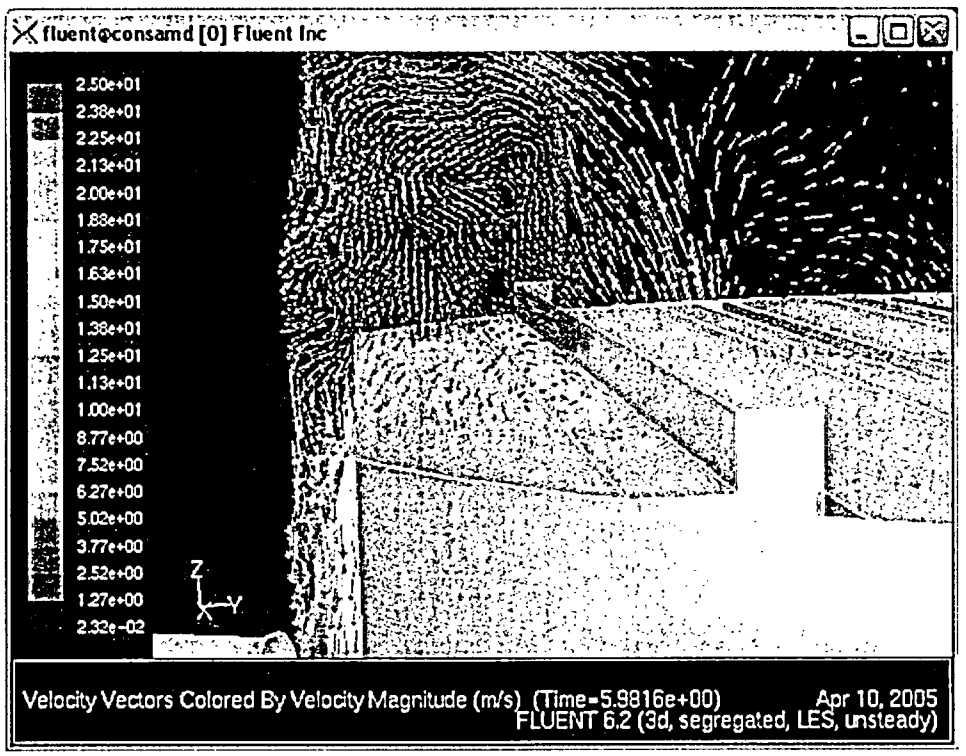

Figure 19. Velocity vectors near 6" dam at x=50 inches and t=5.98 sec.

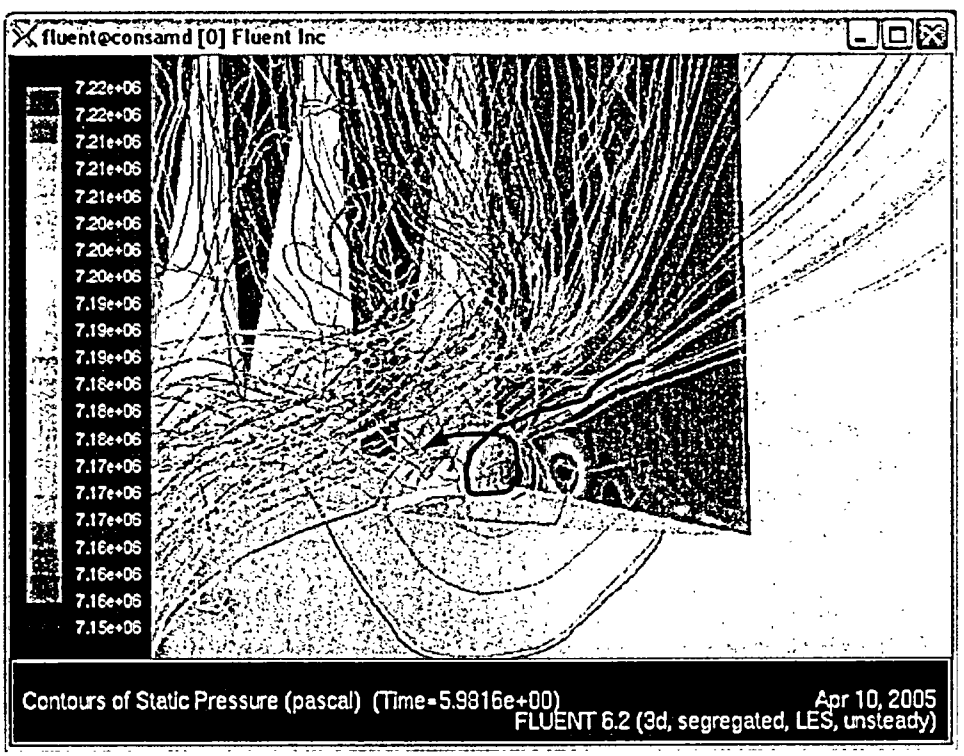

Figure 20. Pathlines through right steam line.

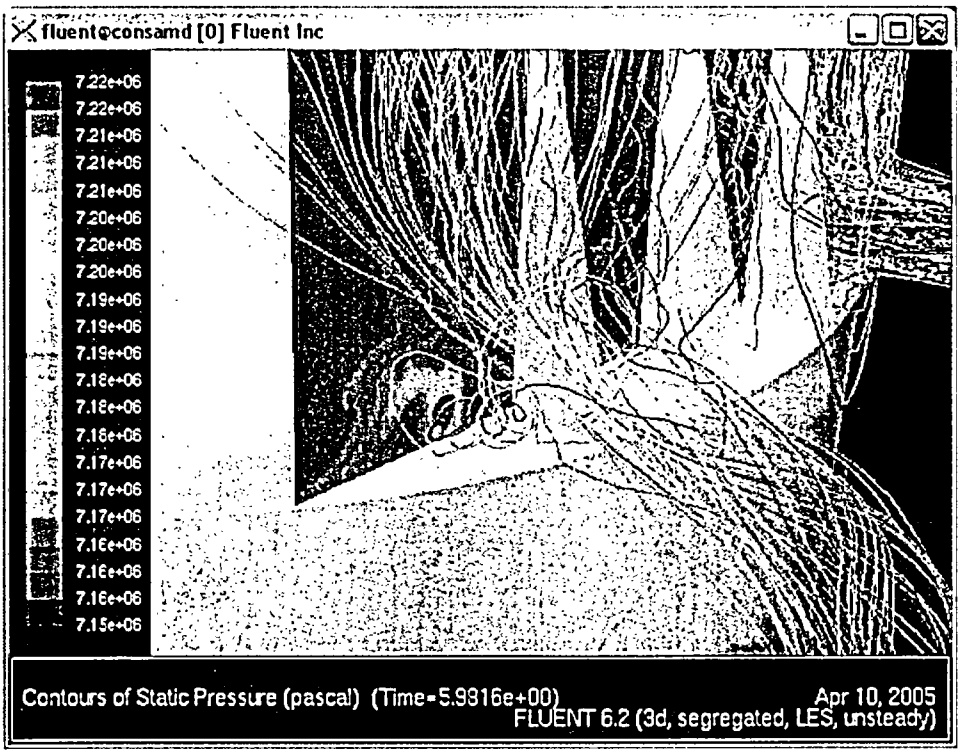

Figure 21. Pathlines through left steam line.

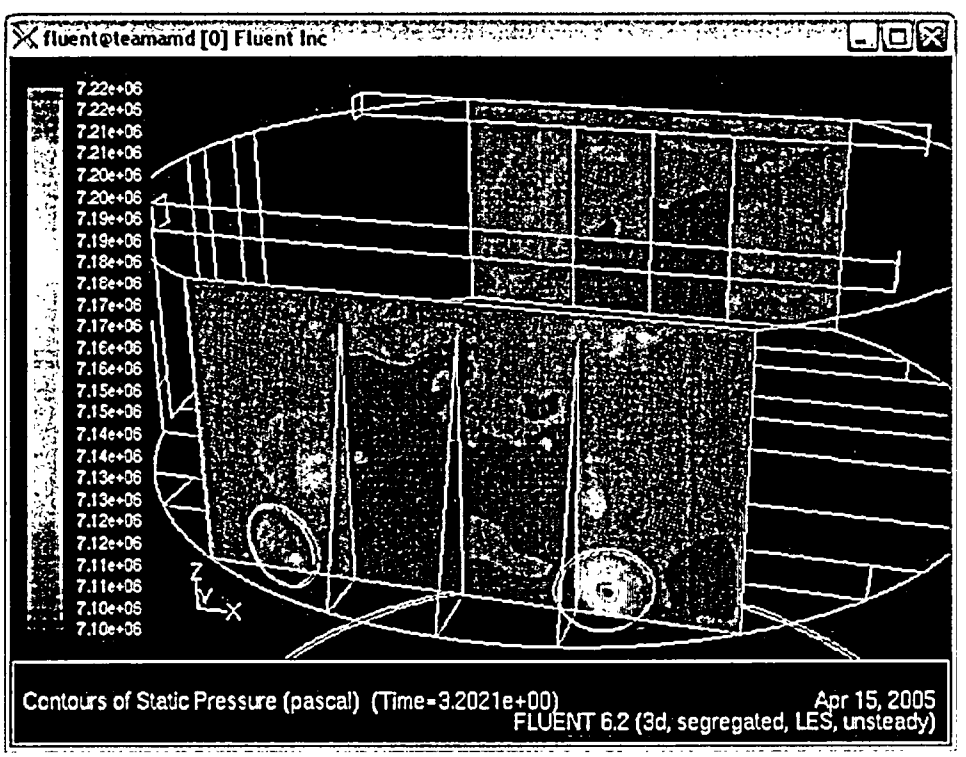

Figure 22a. Static pressure contour at 100% load at t=3.20 sec

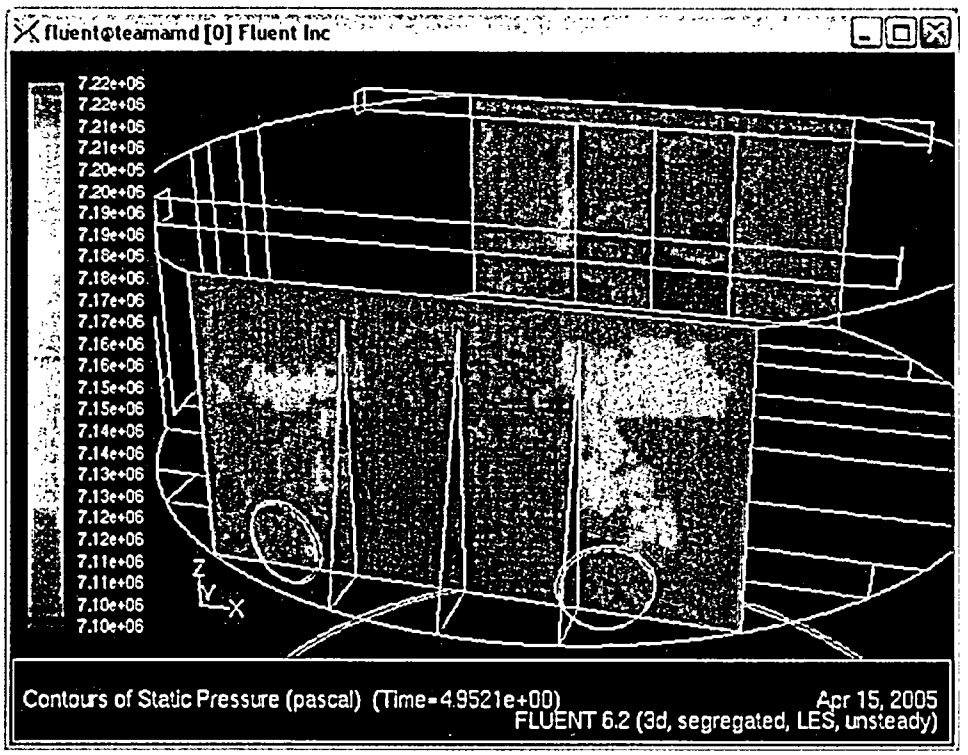

Figure 22b. Static pressure contour at 100% load at t=4.95 sec

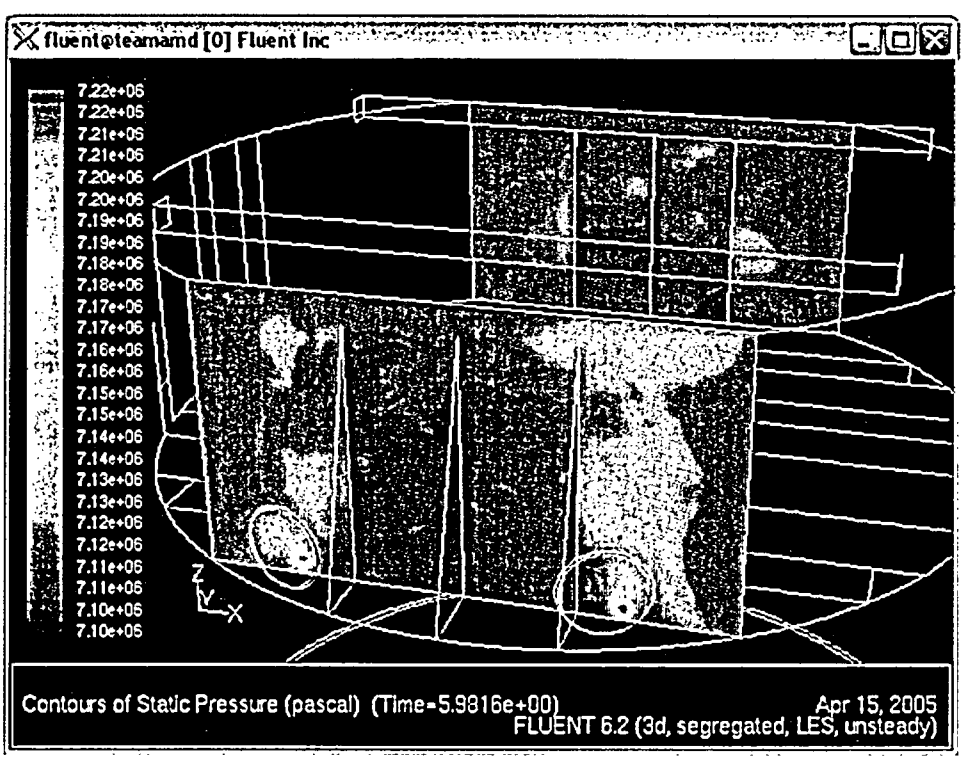

Figure 22c. Static pressure contour at 100% load at t=5.98 sec

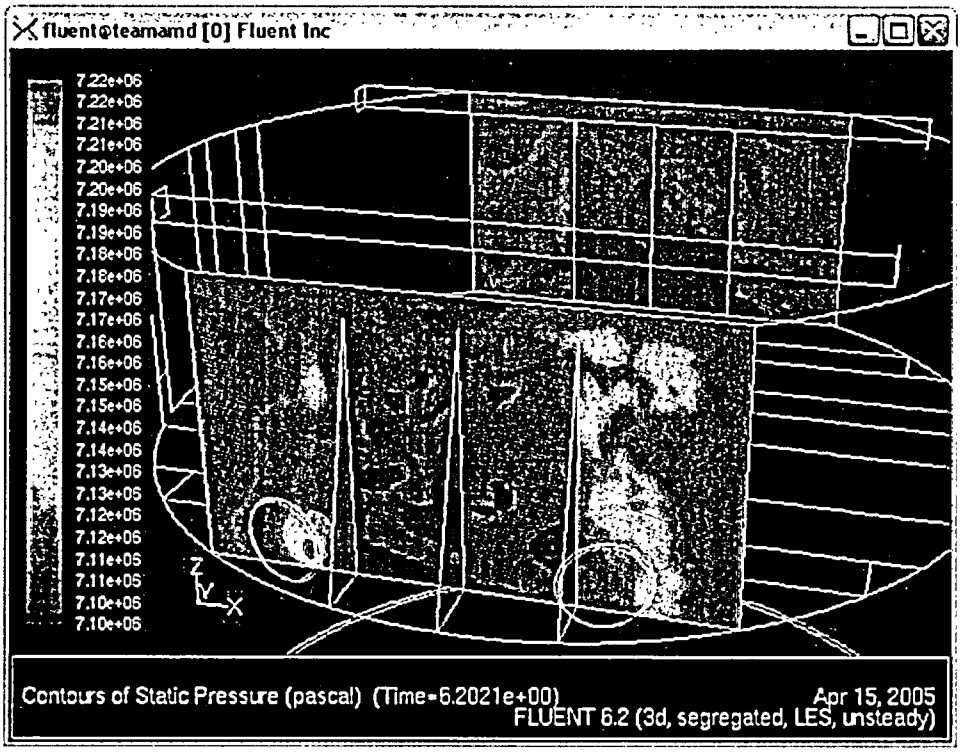

Figure 22d. Static pressure contour at 100% load at t=6.20 sec

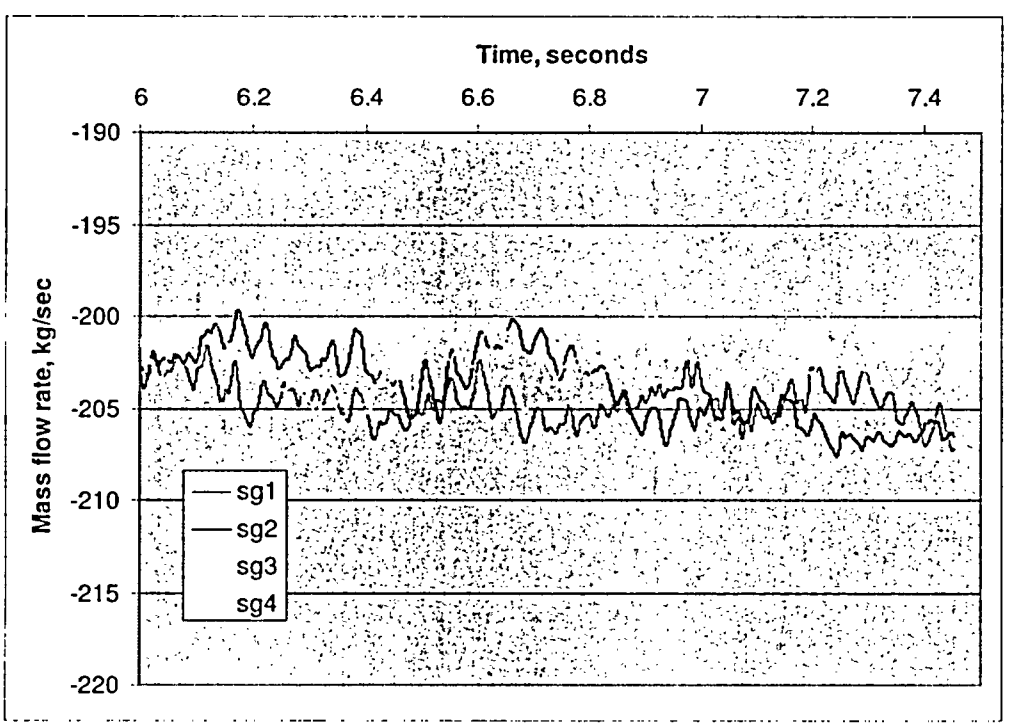

Figure 23. Mass flow in the steamlines at the strain gages versus time

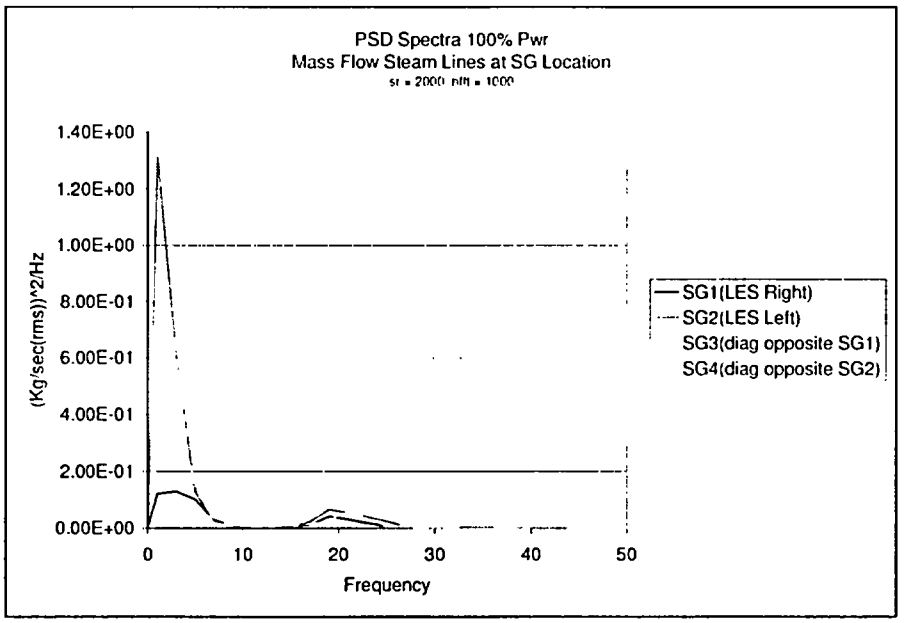

Figure 24. PSD of mass flow recorded at strain gages

4.2.2 Pressure Data Analysis for 100% Load

Though full data sets were recorded roughly every 0.25 seconds, pressure data at the point 6 monitor and along the dryer walls were recorded at a sampling rate of 0.0005 seconds and 0.001 seconds, respectively. The pressure history at point L6 was used to monitor the progress of the solution (Figure 25). The signal shows a high frequency response to turbulent eddies superimposed on lower frequency oscillations likely associated with the transient flow in the dome. These lower frequency oscillations are evidence of the improved boundary conditions employed in the Phase II work. The vertical lines in this figure mark the times used for post-processing in the previous section.

Differential pressure data at all computation cell locations across the walls of the dryer were recorded from approximately t=5.25 sec through t=7.5 sec in 0.001 sec intervals. Contours of differential pressure (Pa) on the dryer walls are shown for t=3.20 sec, 4.95 sec, 5.98 sec, and 6.20 sec in Figures 26a-26d. These contours reflect trends similar to those shown in the pressure contour plots of Figures 22a-22d. The ΔP dryer wall surface data were provided to Entergy for use as the applied load for evaluating the structural stresses.

Pressure signals at two points were extracted from the larger, surface pressure history file. Figure 27 shows ΔP data from t=5.25 sec through t=7.5 sec near point-2 and point-6. The surface pressure data was also averaged spatially using an area-weighted averaging scheme over the regions shown in Figure 28. Figure 29a shows the time signals of the averaged pressure for the four vertical quadrants of the face plate, DP-1-4. A breakdown of the averaged pressure histories of the first quadrant into octants is shown in Figure 29b. In this figure, the average pressure at the bottom of the face plate (DP-41) is observed to increase significantly for roughly one second. This behavior is a reflection of the varying strength of the vortex attached to this section of the face plate.

For a 0.75 second simulated duration, mass-weighted average pressures were recorded at the strain gage and the inlet to the corresponding steam pipe (Figure 30). The mass weighted averaged pressure is given as, $\bar{p} = \frac{1}{\dot{m}} \sum p_i \dot{m}_i$, where the summation is over all the individual faces that make up the region over which the pressure is averaged. The average pressure produced by this method is influenced more by the regions in which the mass flow is greatest, and best represents the average pressure at the location involved. This data was provided to Entergy (Figure 31).

The pressure data provided to Entergy are derived from the calculated pressure field. The pressure field results from the simultaneous solution of the conservation equations of mass, momentum, and energy. The flow is modeled as compressible; the density is evaluated using the ideal gas equation of state. A compressibility factor is used to provide the correct density for the given operating pressures and temperatures. The flow is considered as only mildly compressible as the maximum Mach number observed appears to be of the order of 0.15 (speed of sound ~ 489 m/sec).

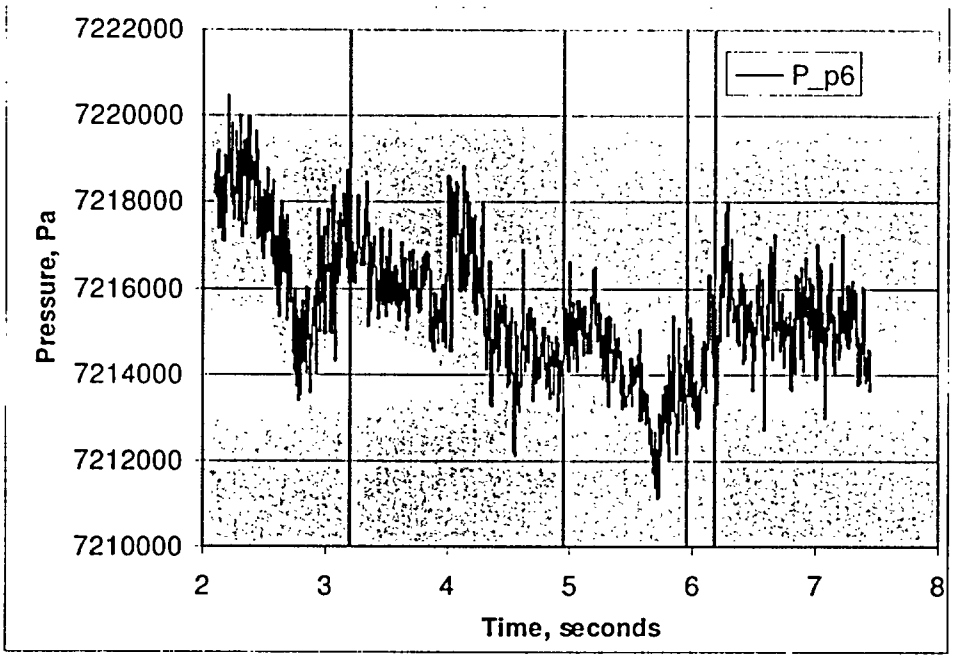

Figure 25. Pressure data at point monitor L6 (point L6 and p6 identified in graph are identical).

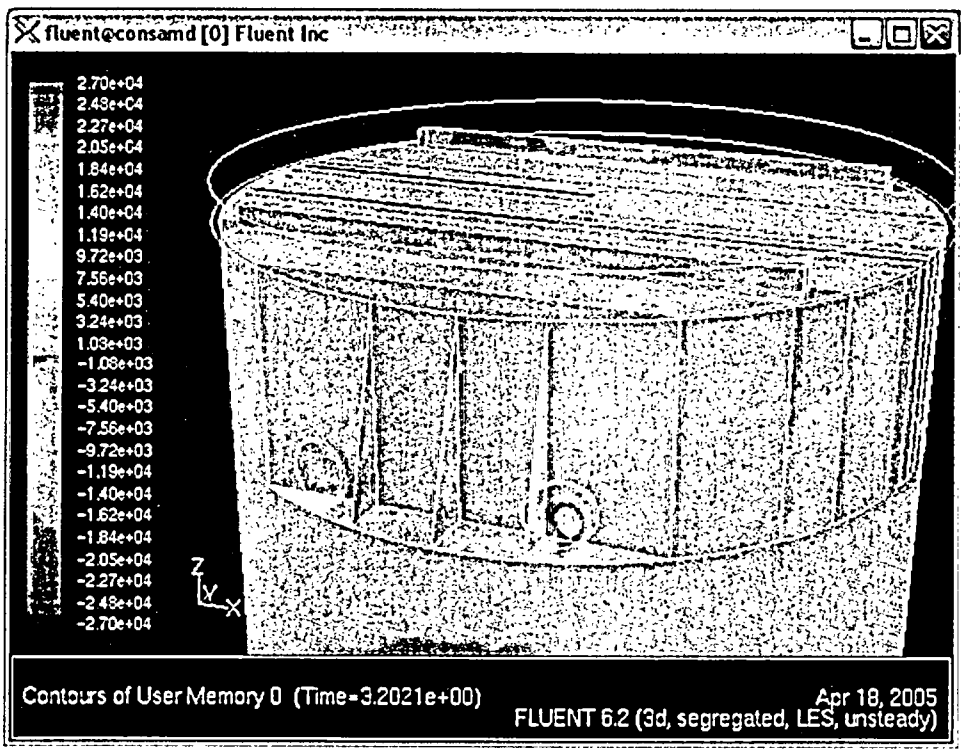

Figure 26a. ΔP contours along dryer walls at t=3.20 sec.

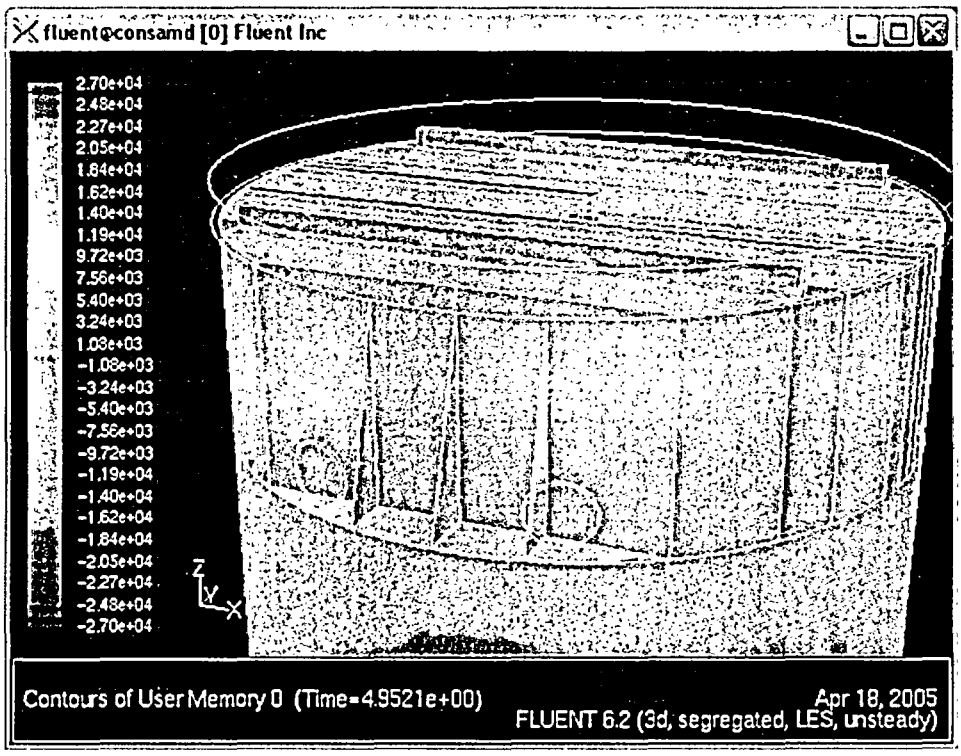

Figure 26b. ΔP contours along dryer walls at t=4.95 sec.

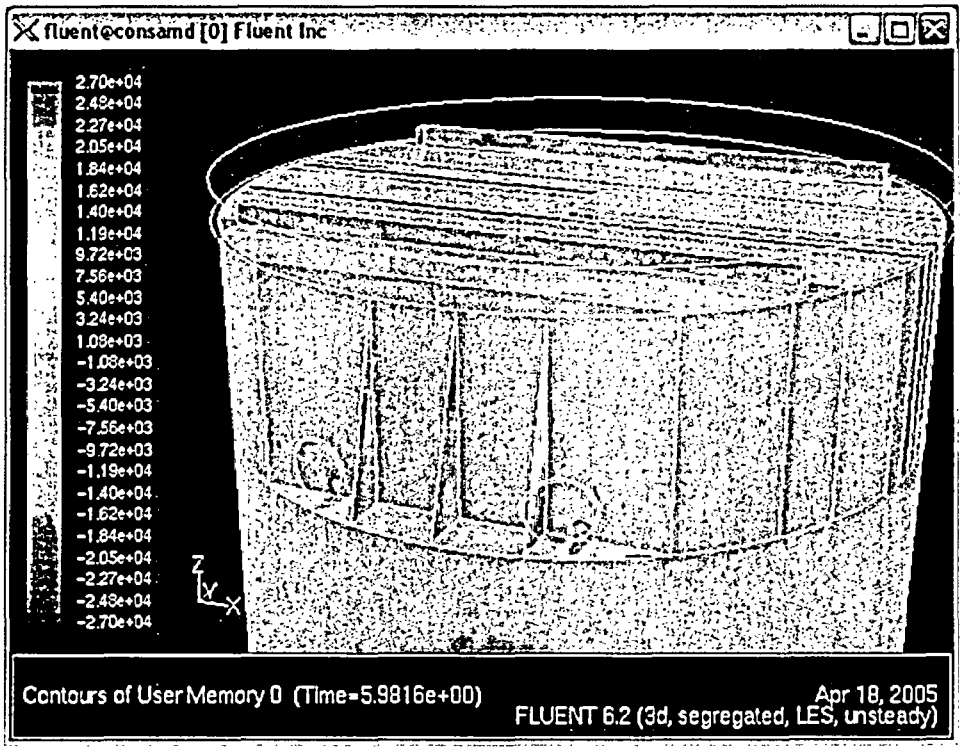

Figure 26c. ΔP contours along dryer walls at t=5.98 sec.

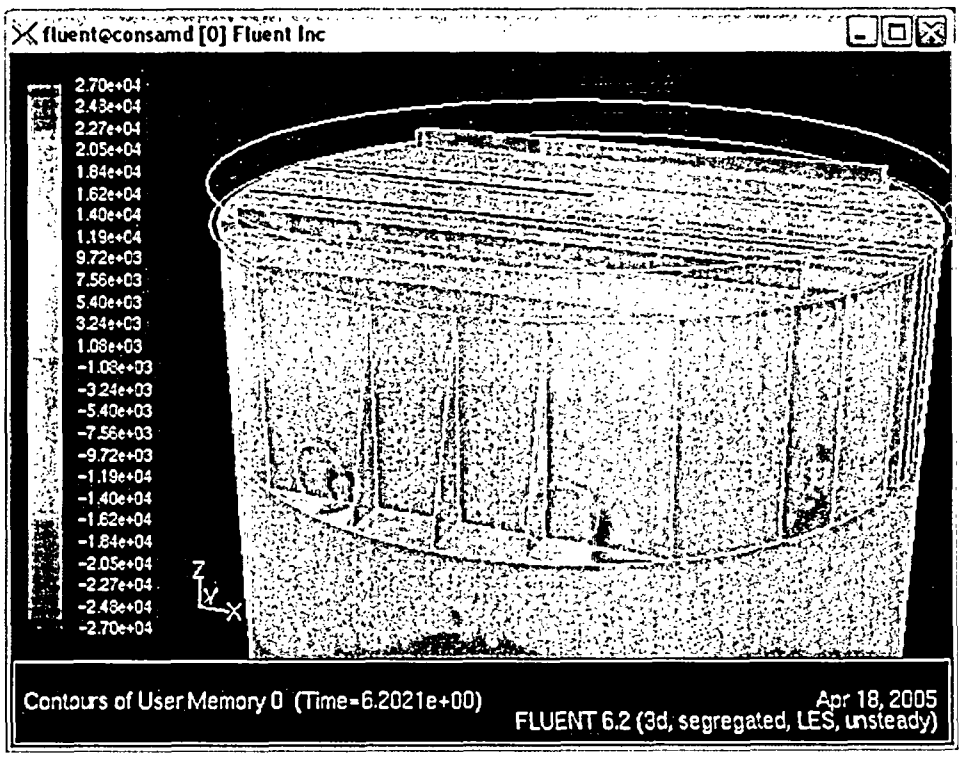

Figure 26d. ΔP contours along dryer walls at t=6.20 sec.

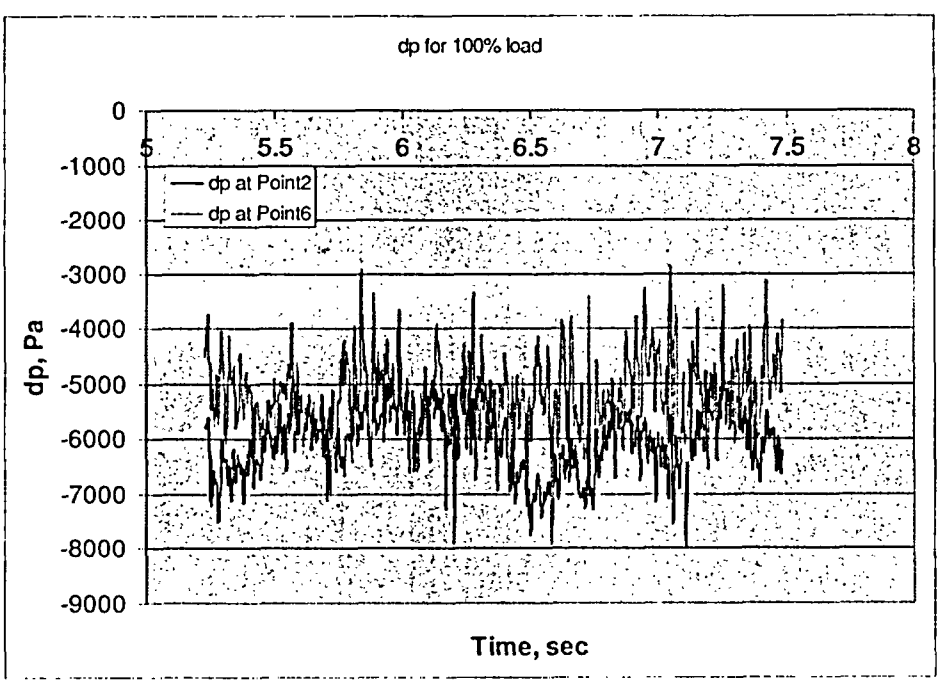

Figure 27. ΔP data at points 2 and 6 for 100% load.

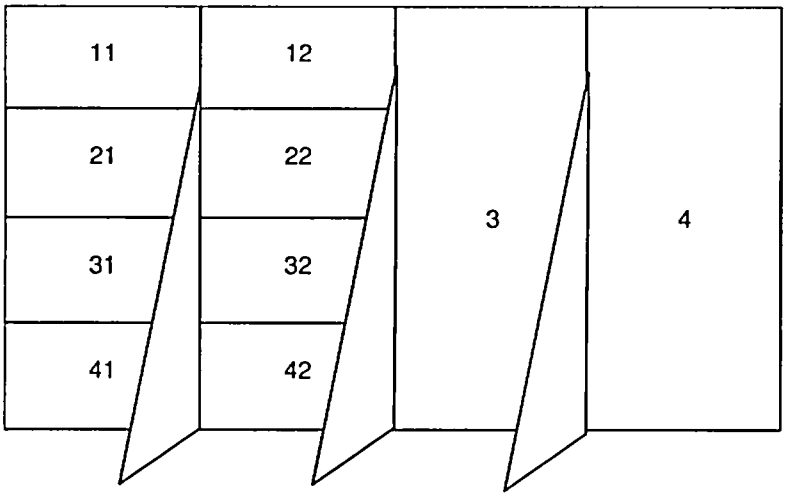

Figure 28. Breakdown of vertical face plate for spatial averaging

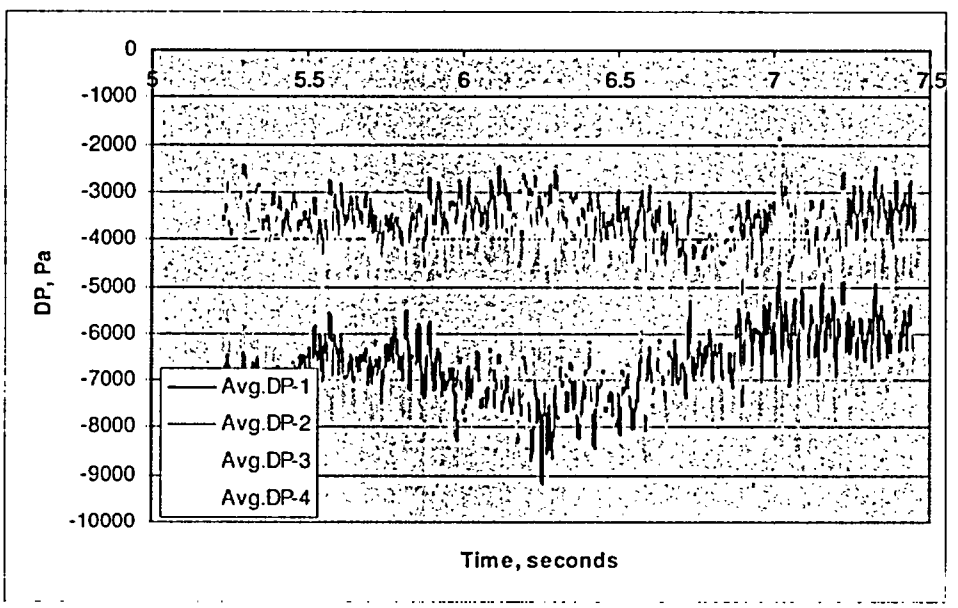

Figure 29a. DP time history for vertical column quadrants 1-4, 100% case

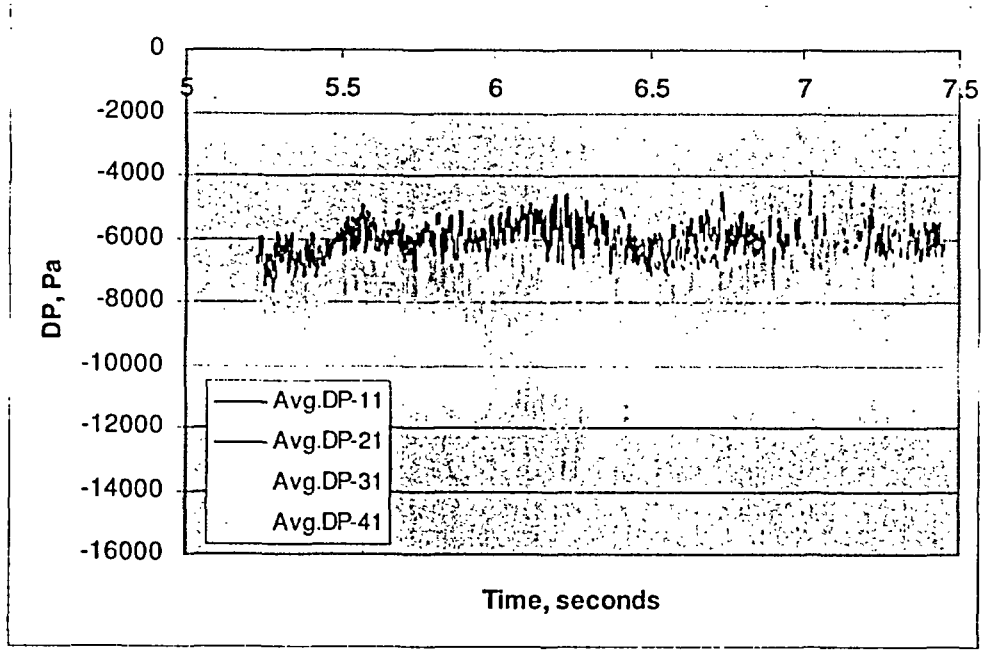

Figure 29b. DP time history for Octants 11-41, 100% case

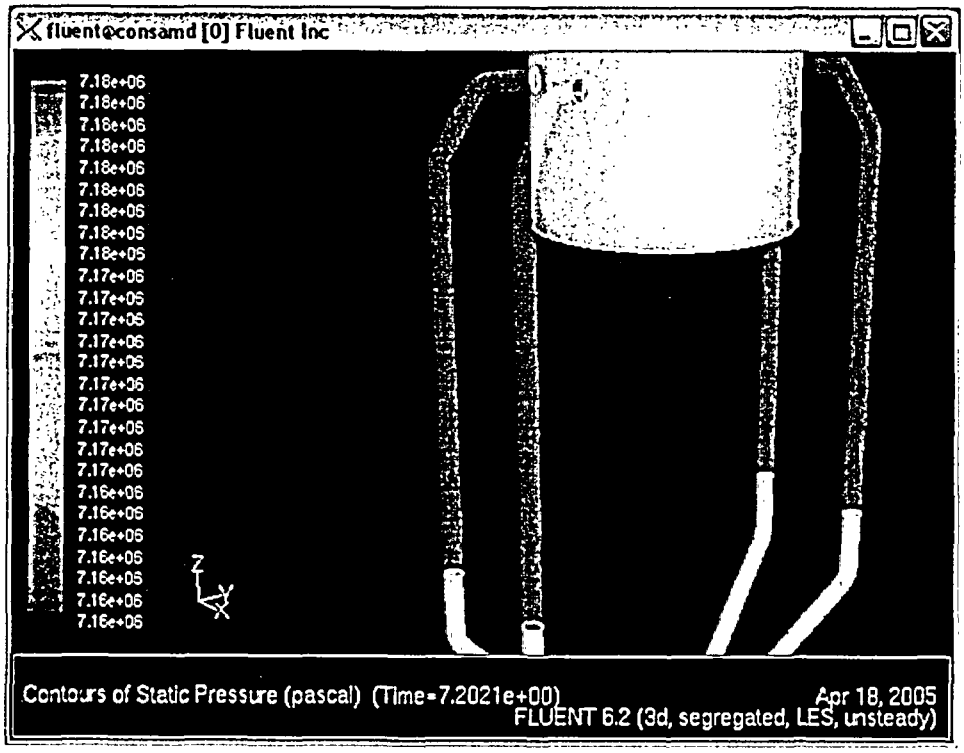

Figure 30. Pressure contours at strain-gage-1 and the inlet to the corresponding pipe.

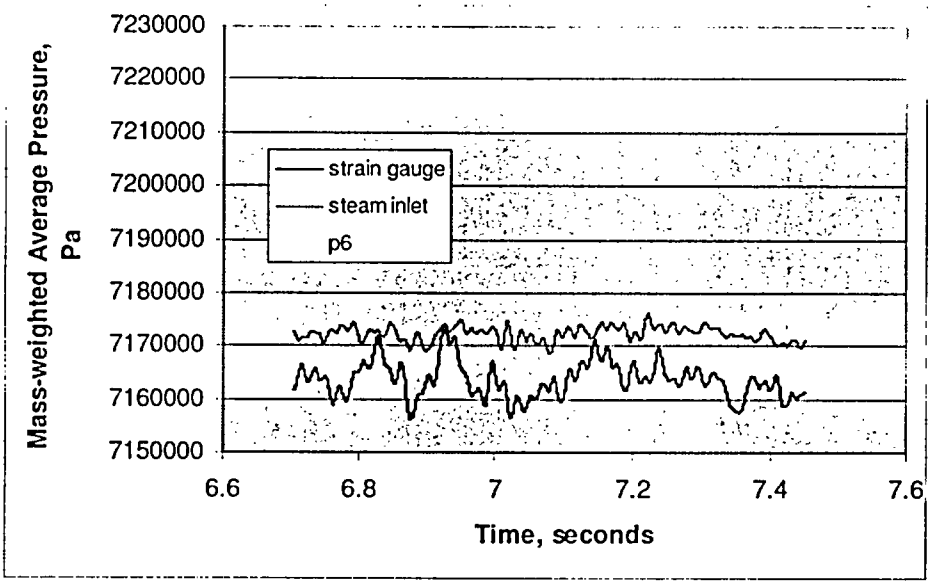

Figure 31. Mass-weighted average pressures at point L6, strain-gage-1 and the inlet to the corresponding pipe (point L6 and p6 identified in graph are identical).

4.3 LES Solution on Hybrid Mesh for 120% Load

4.3.1 Observations on the Flow Field in the Vessel Head for 120% Load

For the 120% load case, a review of the 18 full data sets showed a similar response in the flow field (see Appendix A.3). Findings from a selection of these data sets are discussed below.

Figures 32a – 32c show the velocity magnitude contour plots along the x=+50 in. plane at three different simulation times, t=5.17 sec, 5.77 sec, and 6.77 sec (again, these times coincide with three distinct vertical face plate pressure patterns). The view and the scale in these figures are the same as that discussed for the 100% load case. Evident are the velocity jets, again shown to interact with the dome wall and with each other. The peak velocities at the base of these jets are higher than that observed in the 100% case and as such are clipped from the contour plots.

Figures 33 and 34 respectively show velocity vector plots at x=0 and x=50 in at t=6.77 sec. Both plots show that the flow entering the plenum is, in general, directed from above, though a lateral flow component exists. A closer examination of the vortical structures downstream of the 6" dams show that the vortices span across the width of the reactor (parallel with the dam).

The pathlines of Figure 35 again highlight the vortical structure that feeds the steam pipes. The pathlines in this figure were created in an identical manner as for the 100% presentation. The pathlines again show that the flow feeding the vortical structure not only comes from the top, but also from the 2 inch gap on the bottom and side. Figure 36 shows pressure contours on a surface defined by a constant, relatively high value of vorticity (isosurface of vorticity). Since vorticity is related to the rotation of the flow, the vorticity is observed to be high wherever high velocity gradients appear. High velocity gradients are observed within the boundary layer along a wall, and this is evident as the entire vertical face plate is blanketed by the isosurface. The high shear flow off the leftmost gusset generates a portion of the isosurface that is observed to become entrained into the left steamline (not unlike the vortical structure observed to become entrained in the drain of a bathtub). The color of the isosurface shows the pressure decrease as the flow accelerates into the steamline from the high pressure plenum. A second portion of the isosurface is associated with the vortical structure that generates the low pressure spot on the vertical face plate. A possible third structure is shown being generated off the lower lip of the steam line nozzle. These swirling flows likely interact with each other as the steam flows down the line. Though not shown, similar structures appear for the 100% load case.

The pressure contours along the vertical face plate for times t=5.17 sec, 5.77 sec, and 6.77 sec are shown in Figures 37a-37c. Though the pressure levels are higher for the 120% load case than the 100% case, the color scale in these plots use the same range as that of the100% load plots. Interestingly, it appears that the strength of the vortices appear weaker than that observed with the 100% load case (based on the depth of color of vortices). As with the 100% load case, however, the pressure contours still show that during the course of the simulation, the vortices can, over time, appear stronger at either inlet or at both inlets.

Similar to the 100% load case, mass flow rates in each of the steamlines at the strain gages were recorded during the last ~2 seconds of simulated time. A plot of the mass flow rates at strain gages 1 through 4 (identified as sg1 - sg4) is given in Figure 38. As with the 100% load case, two apparent dominant frequencies, a higher ~20 Hz signal superimposed on a lower ~ 3 Hz signal can be observed (Figure 39).

The pressure in the dryer at 120% load was calculated to be 7.33 MPa (1063 psia) roughly 40 psi or 4% higher than intended. Similar to the 100% load case, it can be argued that the differences are small and therefore negligible. The energy associated with turbulent eddies can be expected to be underestimated by 4%.

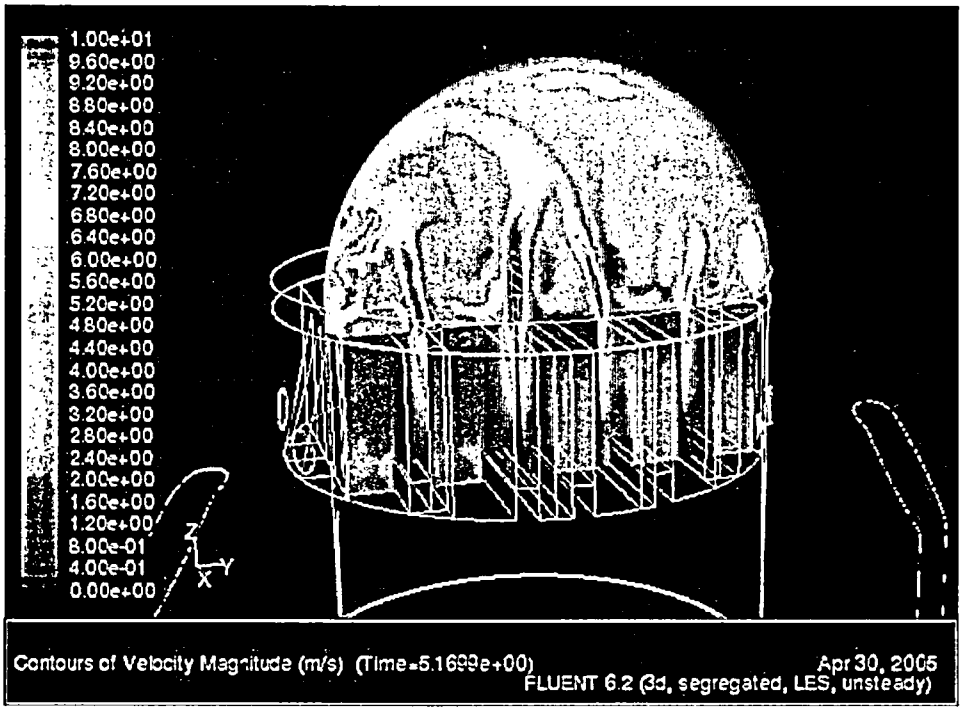

Figure 32a. Velocity magnitude contours at x=50 in at t=5.17 sec

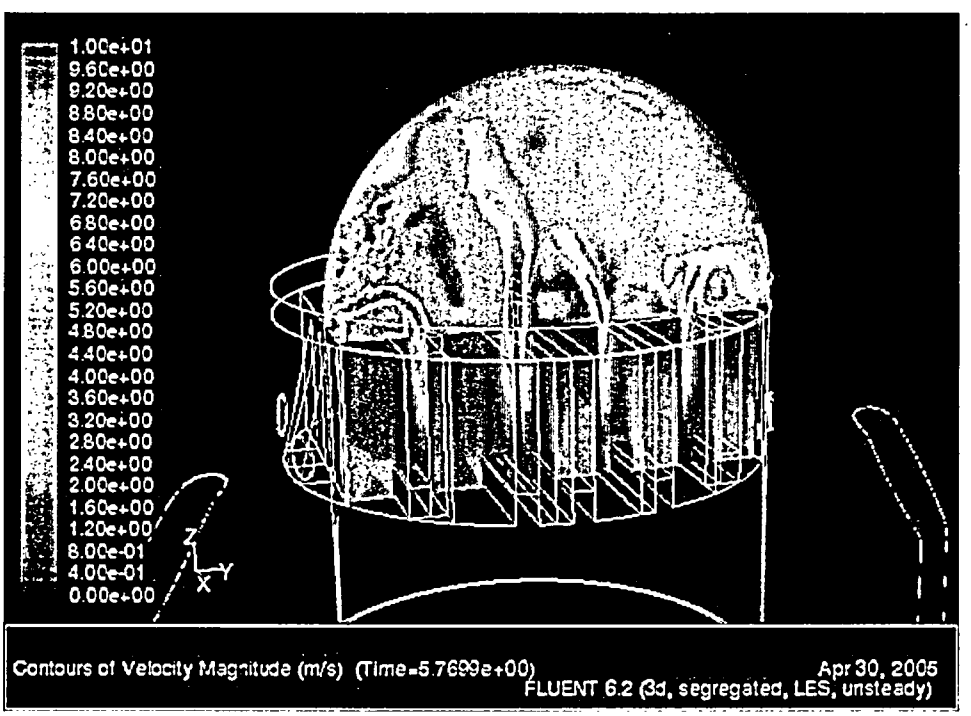

Figure 32b. Velocity magnitude contours at x=50 in at t=5.77 sec

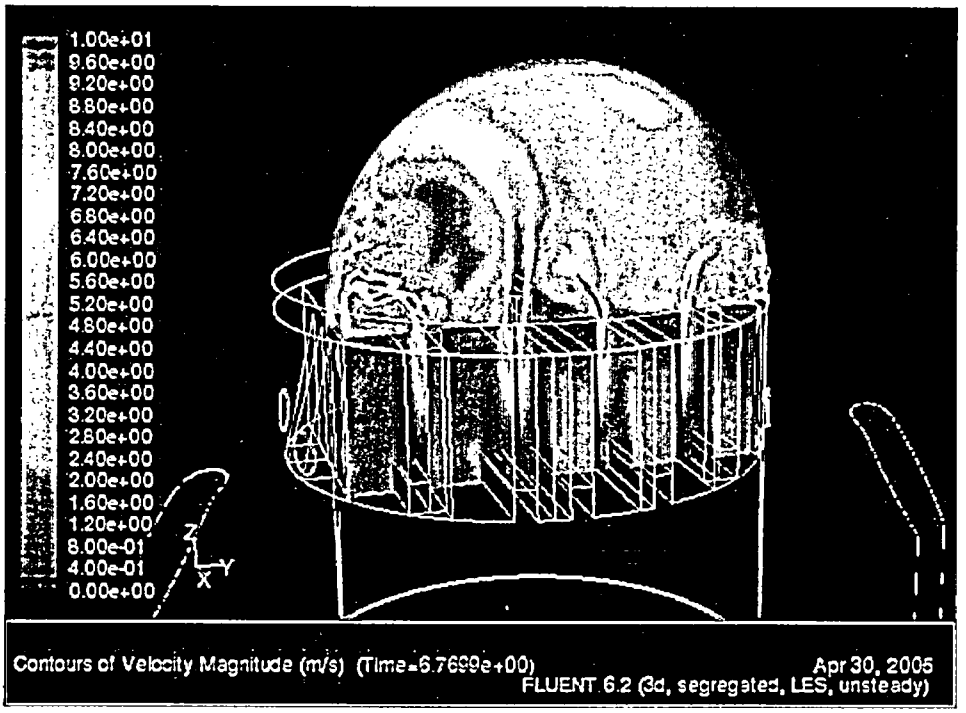

Figure 32c. Velocity magnitude contours at x=50 in at t=6.77 sec

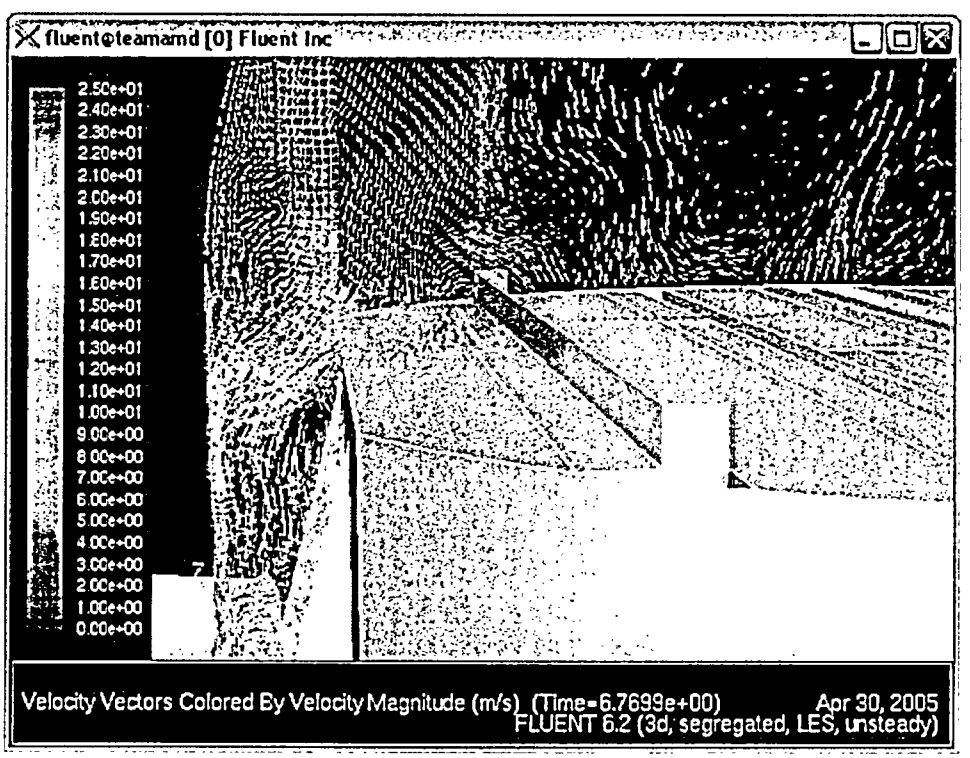

Figure 33. Velocity vectors near 6" dam at x=50 inches and t=6.77 s.

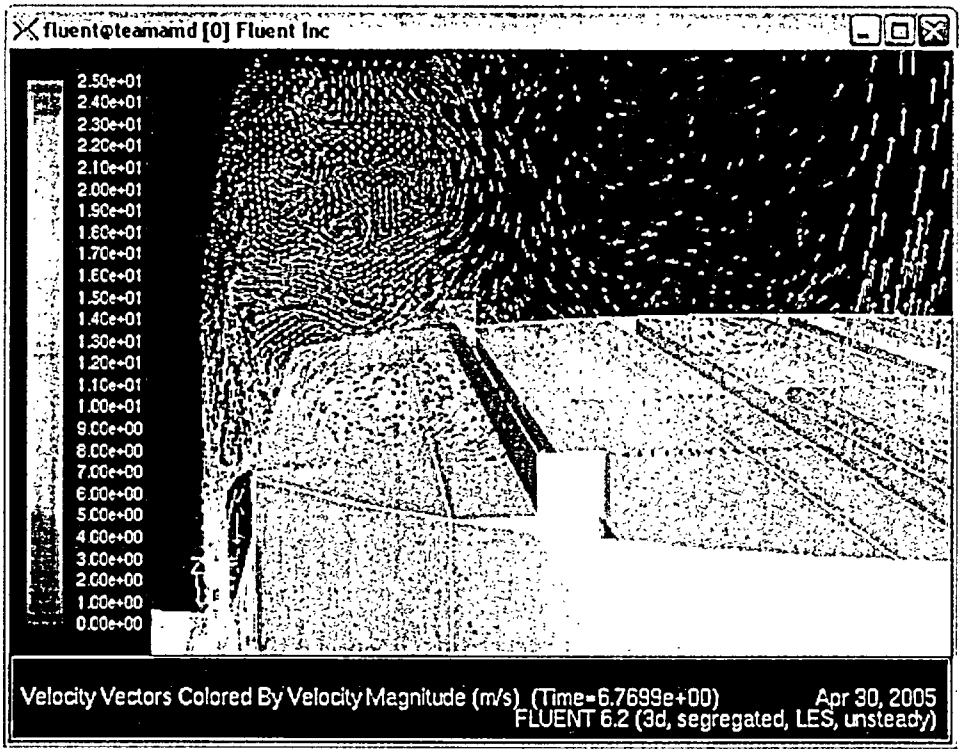

Figure 34. Velocity vectors near 6" dam at x=50 inches and t=6.77 s.

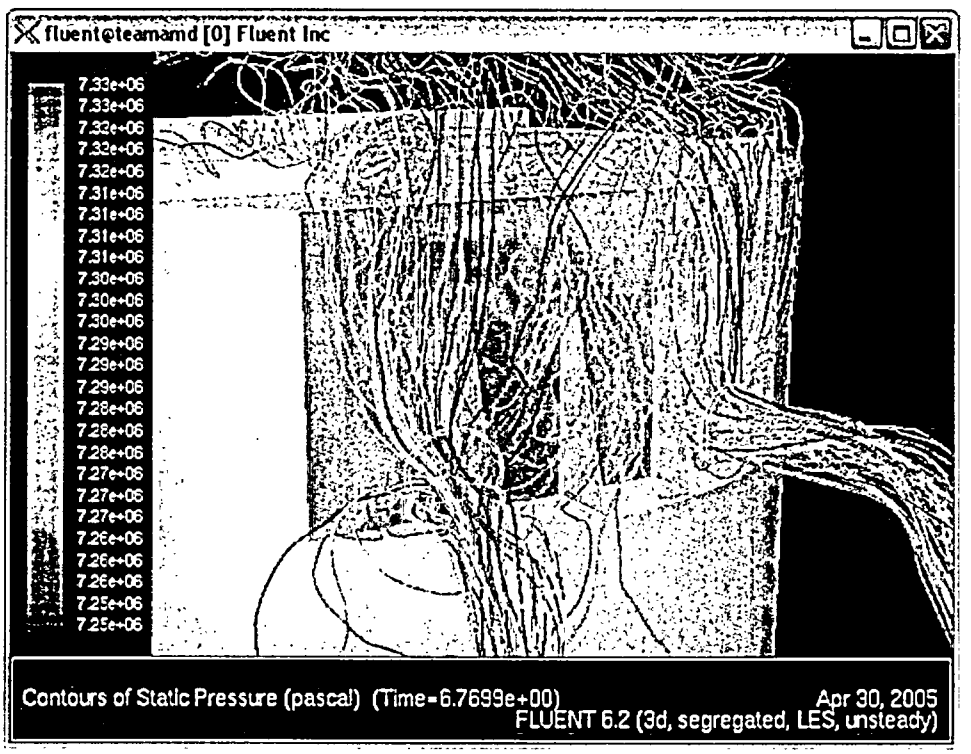

Figure 35. Pathlines through steamlines for 120% load.

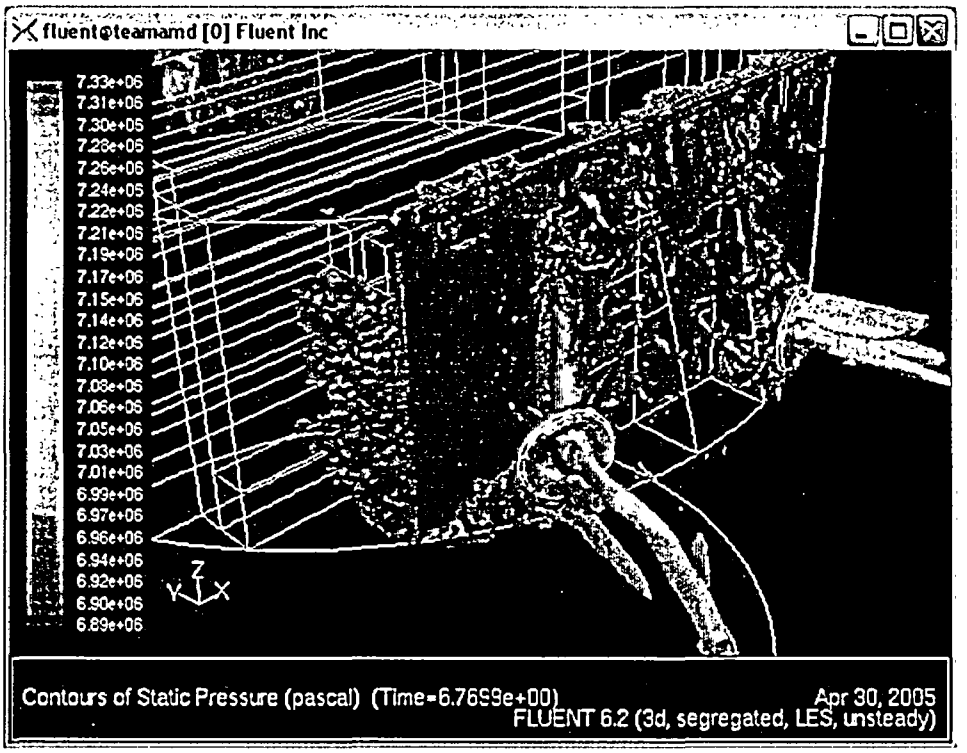

Figure 36. Contours of static pressure isosurface of vorticity magnitude.

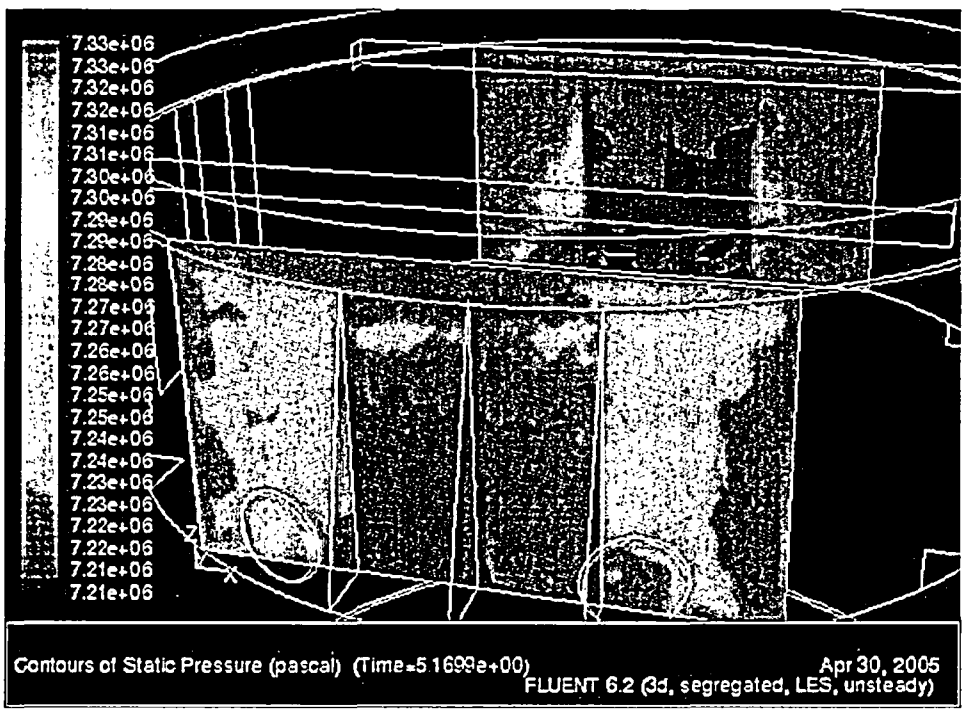

Figure 37a. Static pressure contour at 120% load at t=5.17 sec

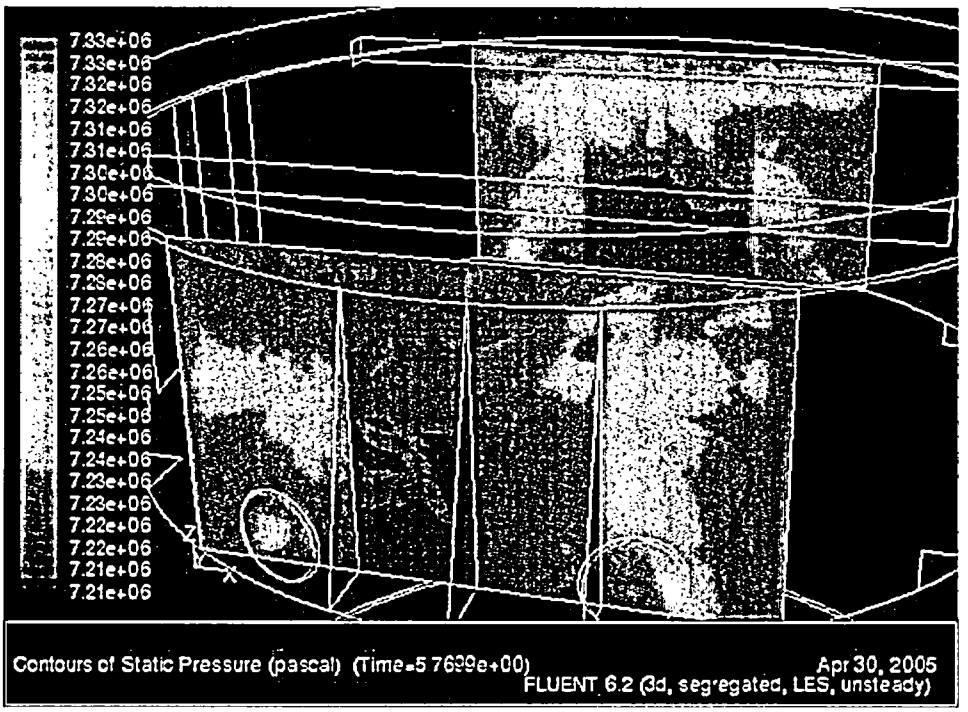

Figure 37b. Static pressure contour at 120% load at t=5.77 sec

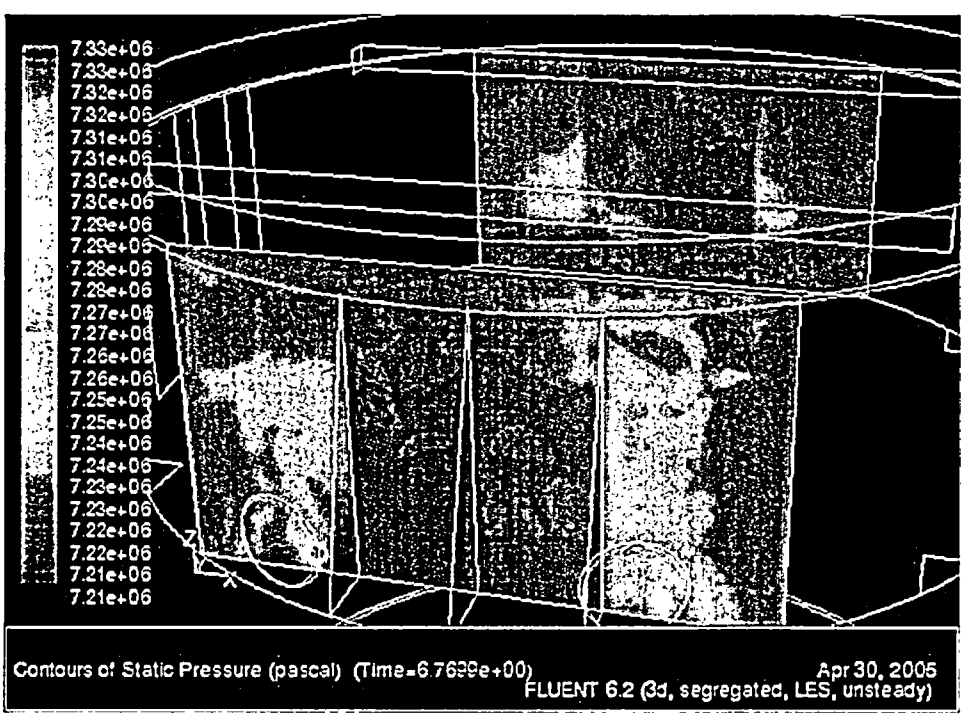

Figure 37c. Static pressure contour at 120% load at t=6.77 sec

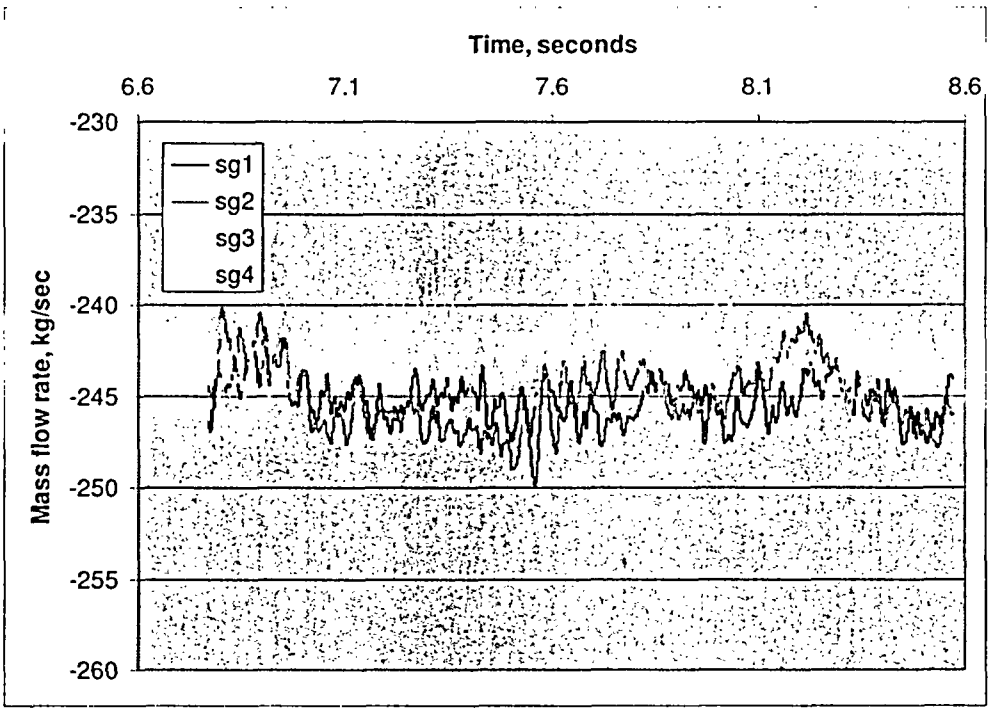

Figure 38. Mass flow in the steamlines at the strain gages versus time for 120% load

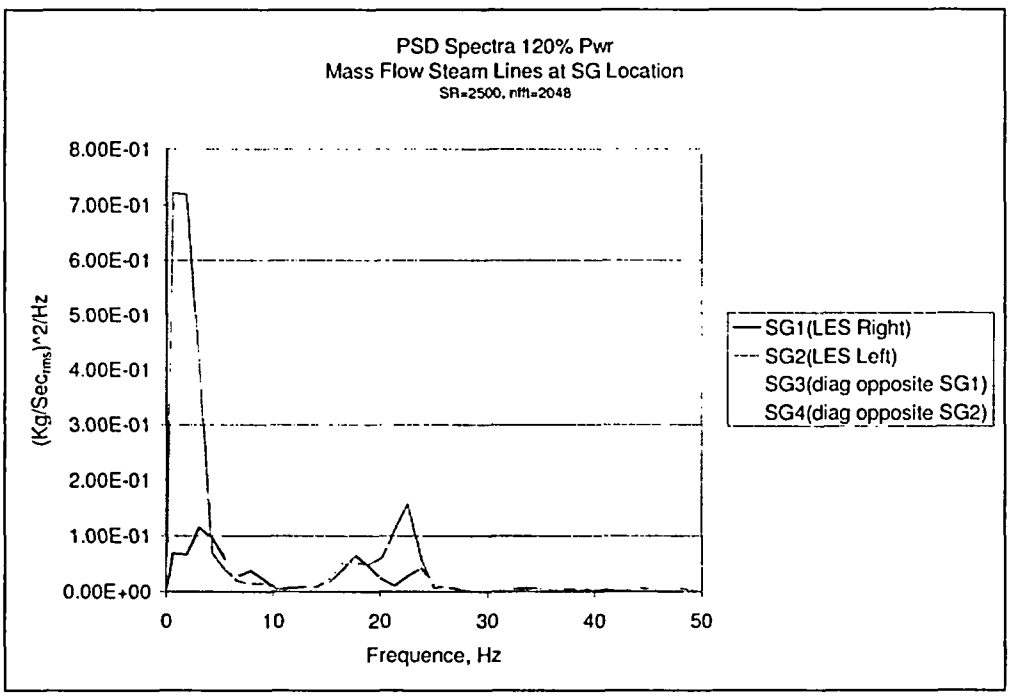

Figure 39. PSD of mass flow signals at strain gages

4.3.2 Pressure Data Analysis for 120% Load

For the 120% case, full data sets were recorded every 0.2 seconds. Pressure data at the point 2 monitor and along the dryer walls were recorded at a sampling rate of 0.0004 seconds and 0.0008 seconds, respectively. The pressure history at point L2 was used to monitor the progress of the solution (Figure 40). The red lines in this figure identify the times used for post-processing in the previous section.

The UDF used for the 100% load data was also employed to record ΔP data at all cell face locations (140,517 points) on all dryer walls at 0.0008 second intervals from approximately t=6.8 sec through t=8.6 sec. As before, the UDF was also used manually to establish ΔP distributions from the 18 full data sets. Contours of differential pressure (Pa) on the dryer walls are shown for t=5.17 sec, 5.77 sec, and 6.77 sec in Figures 41a-41c. These contours reflect trends similar to those shown in the pressure contour plots of Figures 37a-37c. The scales for these plots are the same as the corresponding plots for the100% load case. The contour plots show the relatively weaker vortices on the vertical face plate. The ΔP dryer wall surface data were provided to Entergy for use as boundary conditions for evaluating the structural stresses.

Figure 42 shows the dryer wall ΔP data from t=6.8 sec through t=8.6 sec near point-2 and point-6. Figures 43a and 43b show the averaged pressure signals for quadrants 1-4 and octants 11-41, respectively (see Figure 28 for region identification). As was observed for the 100% load case, the average pressure for octant DP-41 is observed to increase in magnitude, again reflecting the varying strength of the vortex in this region.

For a 1.8 second simulated duration, mass-weighted average pressures were recorded at the strain gage and the inlet to the corresponding steam pipe (Figure 44).

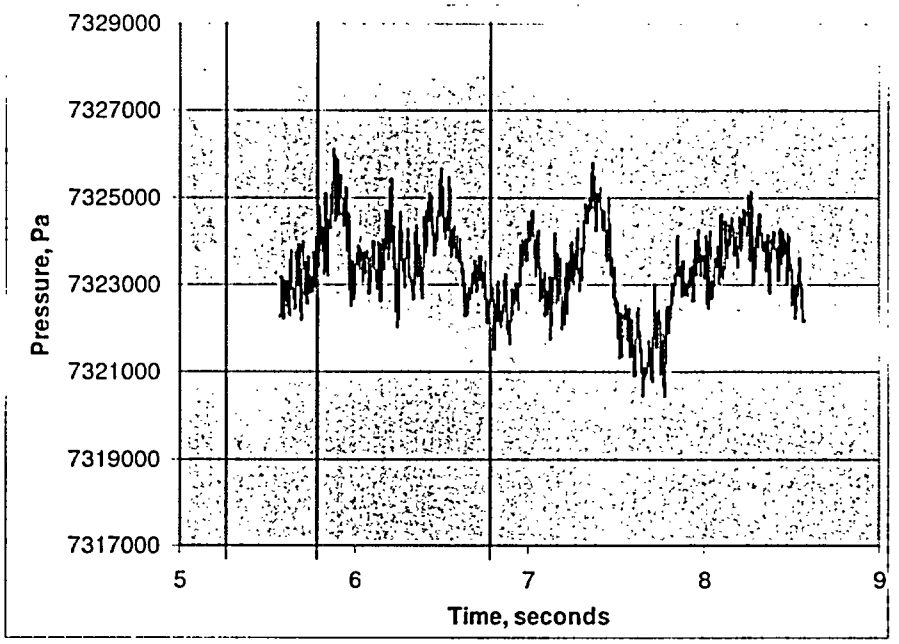

Figure 40. Pressure data at point monitor L2

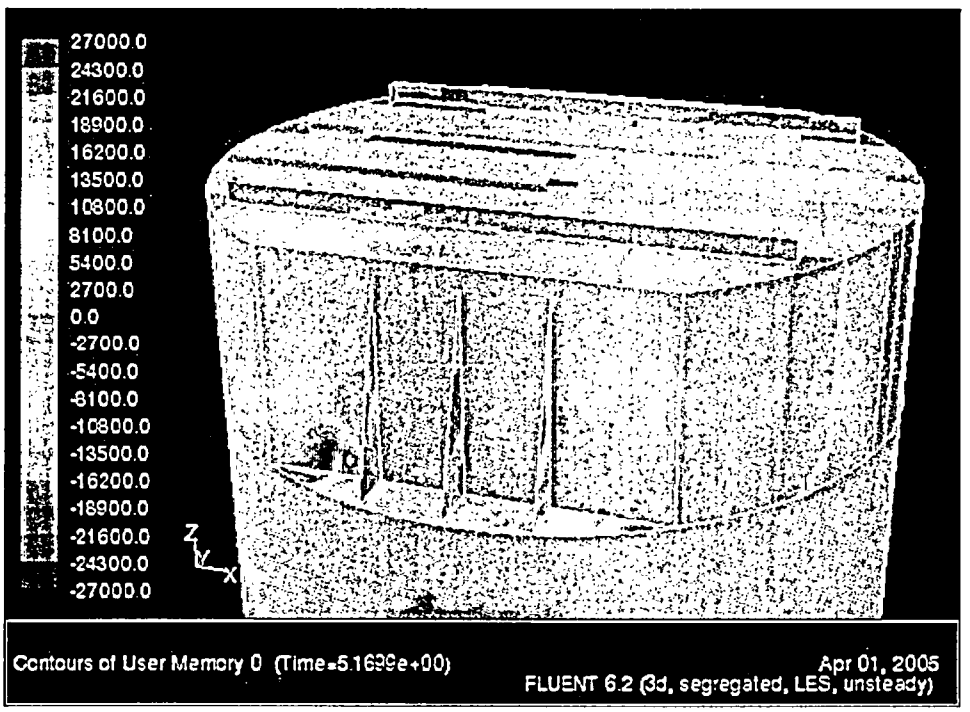

Figure 41a. ΔP contours along dryer walls at t=5.17 sec.

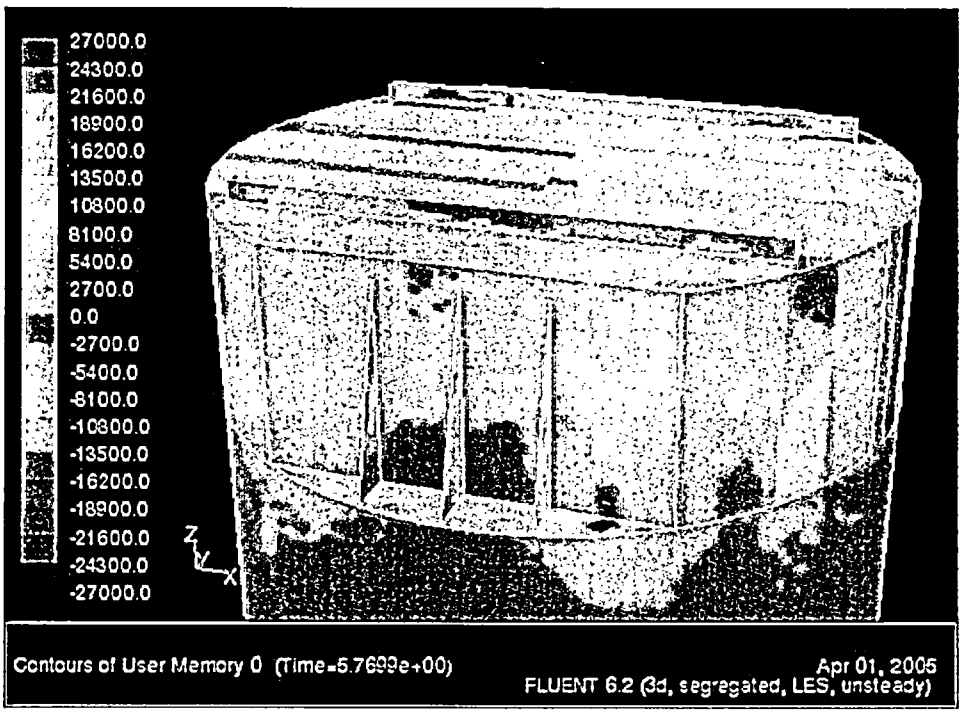

Figure 41b. ΔP contours along dryer walls at t=5.77 sec.

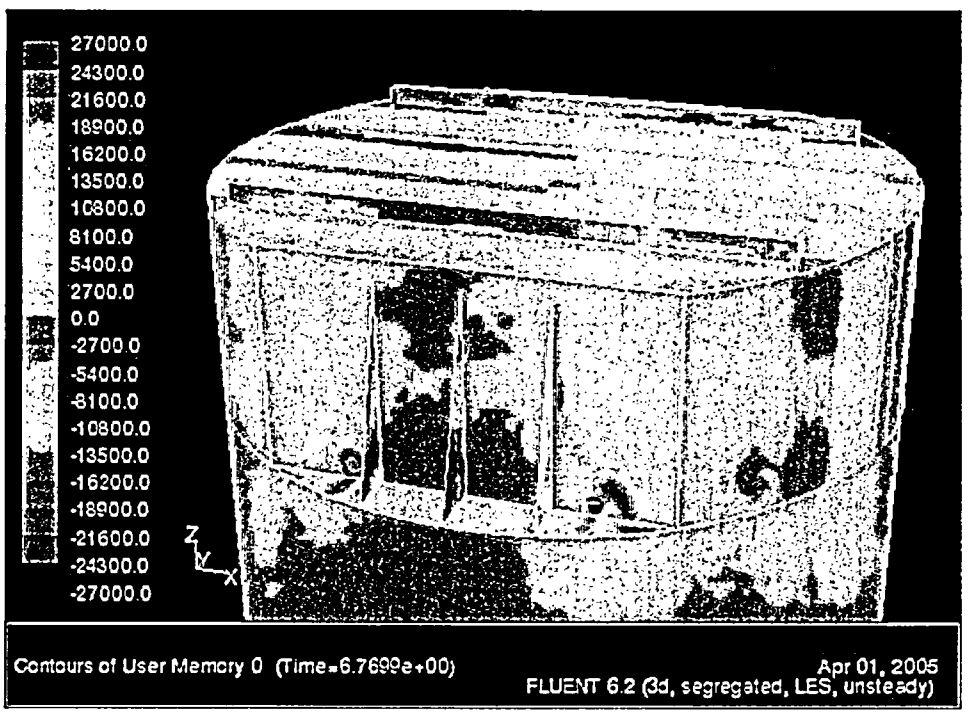

Figure 41c. ΔP contours along dryer walls at t=6.77 sec.

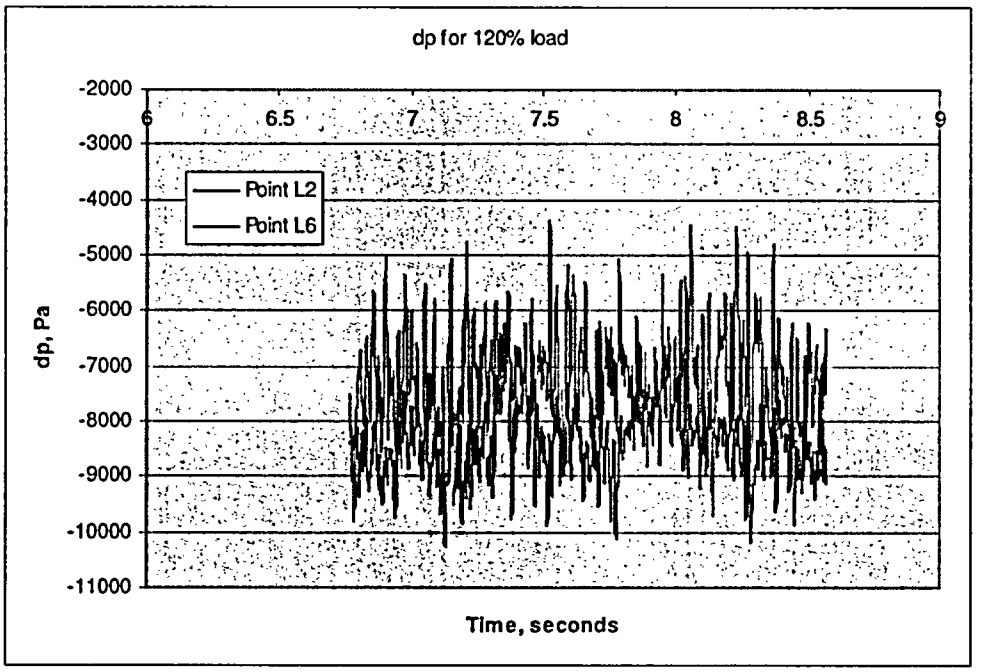

Figure 42. ΔP data at points 2 and 6 for 120% load

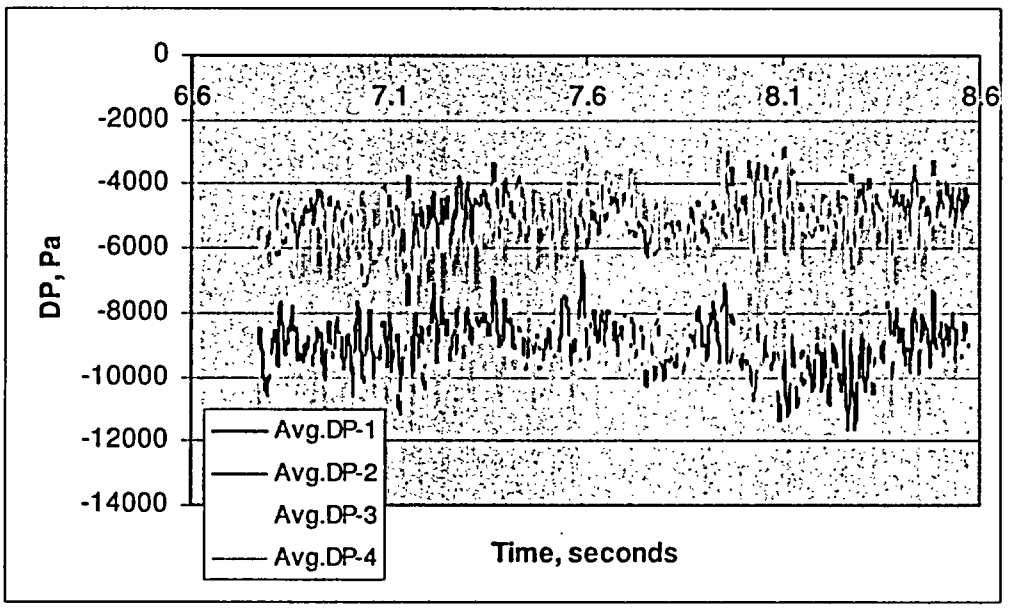

Figure 43a. DP signals for quadrants 1-4 of face plate, 120% case.

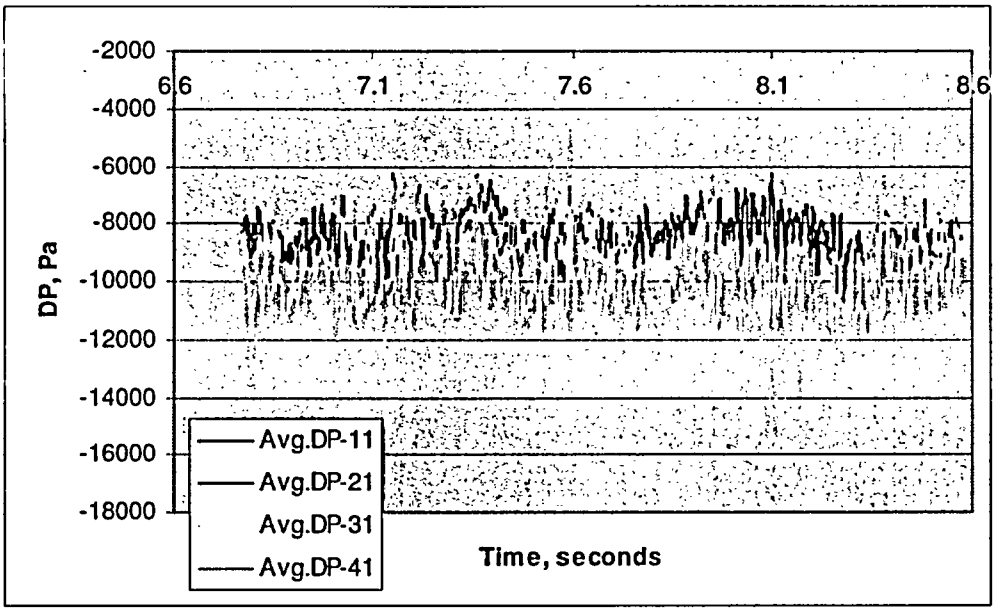

Figure 43b. DP signals for octants 11-41 of face plate, 120% case.

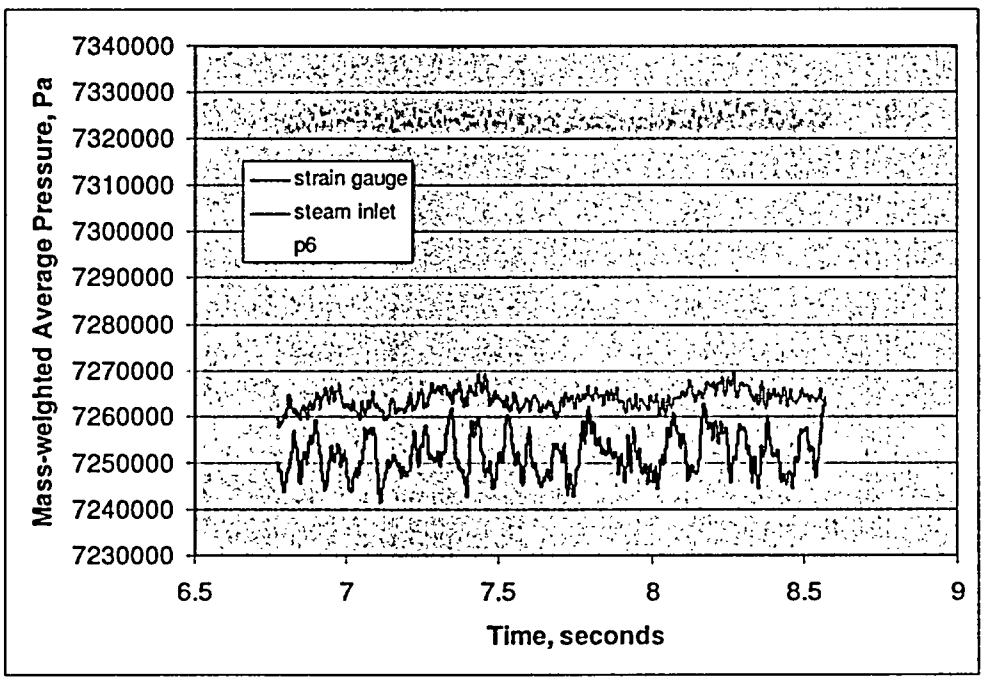

Figure 44. Mass-weighted average pressure at strain-gage-1, point L6, and the inlet to the corresponding pipe (point L6 and p6 identified in graph are identical)

4.3.3 Comparison of 100% and 120% Load Data

Global flow features for both the 100% and 120% load conditions were readily obtained by post-processing the full data sets, which represented snapshots of the flow field at roughly 0.2 second intervals. The global flow features for both the 100% and 120% load cases were observed to be similar.

A study of higher frequency phenomena was made possible by an examination of the high resolution (~0.001 second sampling rate) pressure data across the dryer walls and in the steam lines. Mass flow histories at points in the steam lines were also archived.

Power spectral density (PSD) plots of the dryer wall surface ΔP, steam line pressure, and mass flow data were generated for both the 100% and 120% load cases and compared. Figures 45a-45d show PSD plots of spatially averaged ΔP for the four quadrants of the face plate for both the 100% and 120% loads. Comparing the two curves within one figure highlights the variations associated with the change in mass flow. Comparing the curves between Figures 45a-45d highlights the variations along the plate from one side to the other (left to right). Figures 46a-46d show similar (PSD) plots for the four octants that are vertically aligned with the left-most quadrant. A comparison of the curves among these figures highlights the variations along the left quadrant in the vertical direction. Figure 46e shows the PSD plot comparison between 100% and 120% for point L2. This point compares well with the top octant shown in Figure 46a. Figure 47 provides a PSD plot of the ΔP across the left-most gusset. Figure 48 provides a PSD plot of the averaged pressure at the steam nozzle and strain gage for 100% and 120% load.

From an inspection of Figures 45 through 48, it is noted that:

- The amplitudes of the signals are typically stronger for the 120% case than for the 100% case.
- For a given mass flow, little variation in the PSD plots from the left-most quadrant to the right-most quadrant is observed across the face plate.
- In the left quadrant, the pressure signals are stronger at the bottom than on the top.
- The average gusset pressure shows little response above 20 Hz.
- No significant shift of the frequencies of the peak signals above 30 Hz accompanies the shift from 100% load to120% load.

The frequency of flow-induced oscillations typically varies with the freestream velocity. As a result, one would expect an increase in the velocity (resulting from an increase in mass flow rate) to be accompanied by a proportional increase in the oscillating frequency. The fact that the peak signals are observed at nearly the same frequencies (> 30 Hz) for both load conditions implies that other modes of excitation are present. This invariance to the changes in flow conditions is characteristic of acoustically generated resonance – a condition governed solely by the geometry of the structure and properties of the compressible fluid. Here, it is assumed that a driving mechanism is always present as a result of the broadband noise spectrum generated by turbulent flows. Thus the pressure signals contain both hydrodynamic and acoustically generated components.

Other observations also support this conclusion:

- A visual inspection of the ΔP signals in the time spectrum indicates a strong correlation between signals at different positions on the dryer. There is little observed phase shift between these signals from different locations, implying that the communication of these signals throughout the dryer are occurring rapidly (likely consistent with the local speed of sound). Had the source of the pressure perturbations been convected with the mean flow, a noticeable time lag would have been observed between corresponding peaks.

- If the fluid was assumed to be incompressible, the mechanism by which acoustic waves travel is removed, and the model would be incapable of resolving acoustically generated resonance. The signals, presumed to be acoustically generated, disappear if the fluid is modeled as incompressible. This was seen from the PSD plots generated at point L2 (consistent with octant DP-11) from the incompressible analysis of Phase I, which show almost no excitation above 30 Hz.

- The gusset is subjected to very strong hydrodynamic loads as it imposes a resistance to the flow directed toward the steam nozzle. Yet the PSD plots indicate that the associated frequencies of these loads are relatively low. The lack of higher frequency responses implies that the pressure load is occurring on both sides at the same time. This would be the case if the pressure waves were directed parallel to the gusset.

The accuracy to which these acoustic features are resolved is limited in this model by the choice of solver and the time step size. The CFD model was developed to focus on resolving the hydrodynamic loads associated with the turbulent flow. A segregated solver was used to solve for the flow field because of its efficiency and applicability for low-compressibility, transient flows. The time step size was chosen to resolve the smaller, turbulent eddies. The time step size required for resolving acoustic waves would have to have been based on the local speed of sound, i.e., an order of magnitude smaller than currently used.

The impact of using the segregated solver and a large time step size (relative to the requirements for the resolution acoustics) is that the acoustic waves are numerically dissipated as it travels through the domain. The waves still propagate at the local speed of sound, but the magnitude becomes reduced. Since the speed of sound is preserved, the solution is expected to correctly predict the position and frequency of wave interference. Since the strength of the waves are reduced as it travels, only the effects of stronger waves can be resolved.

The magnitudes of the signals in Figures 45 - 48 result from both hydrodynamic and acoustic pressures. The higher frequency signals are assumed to originate from acoustic effects because of the reasons described above. Significant hydrodynamic activity is observed in the solutions at lower frequencies, and the hydrodynamic portion of the load at lower frequencies is assumed to be higher. Overall, the signals are observed to be higher for the 120% case.

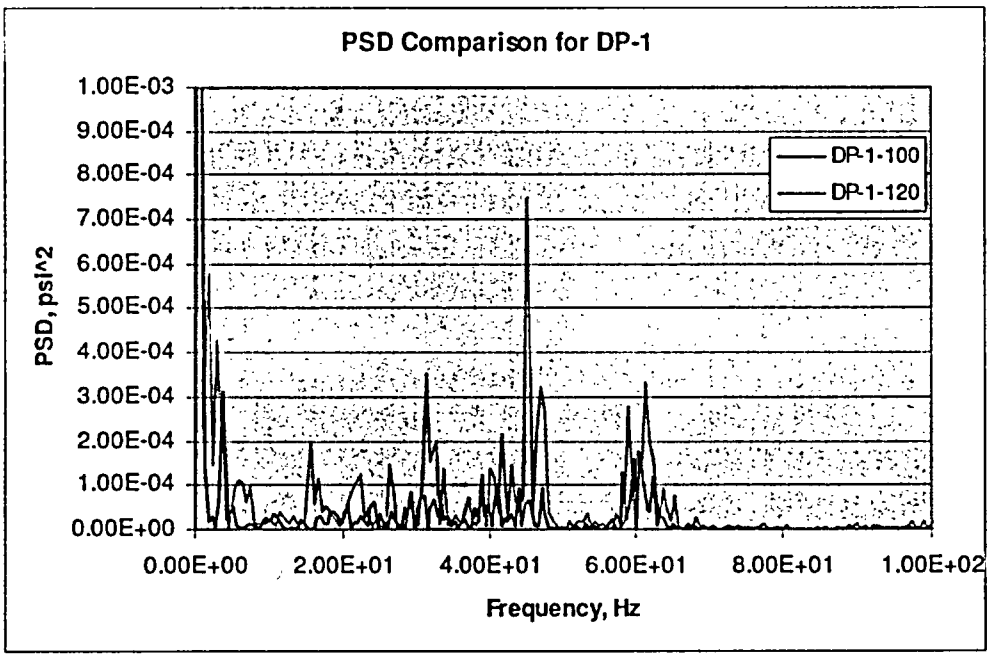

Figure 45a. PSD plot of DP-1 for 100% and 120% load

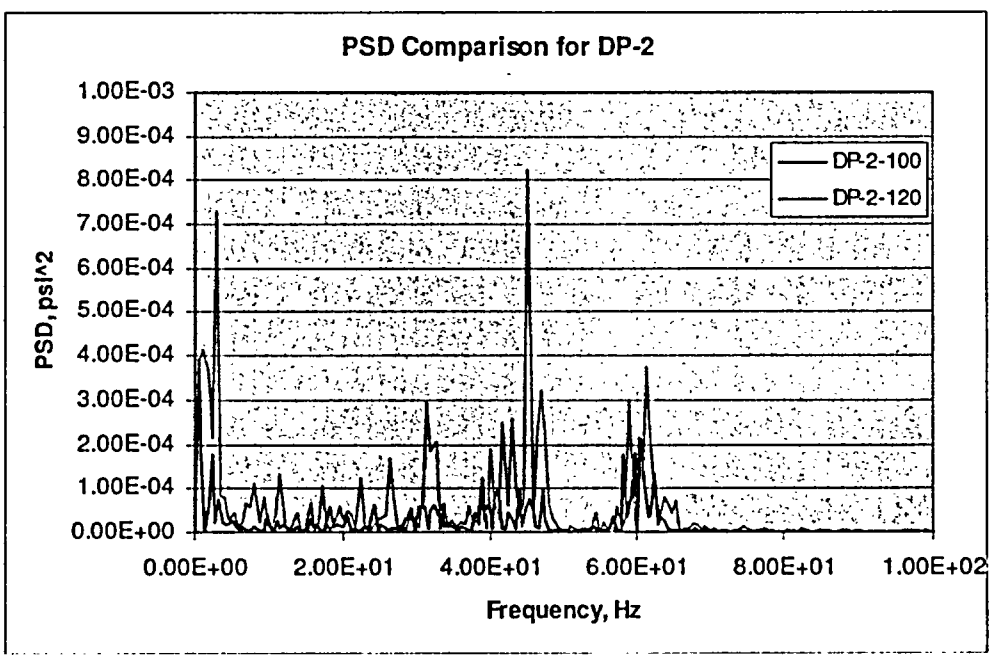

Figure 45b. PSD plot of DP-2 for 100% and 120% load

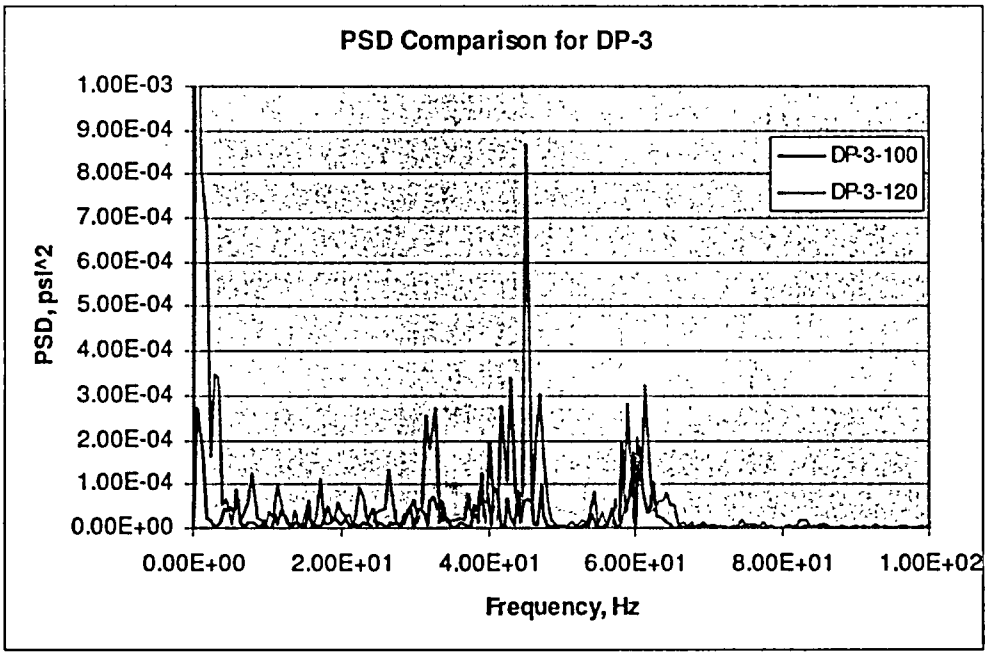

Figure 45c. PSD plot of DP-3 for 100% and 120% load

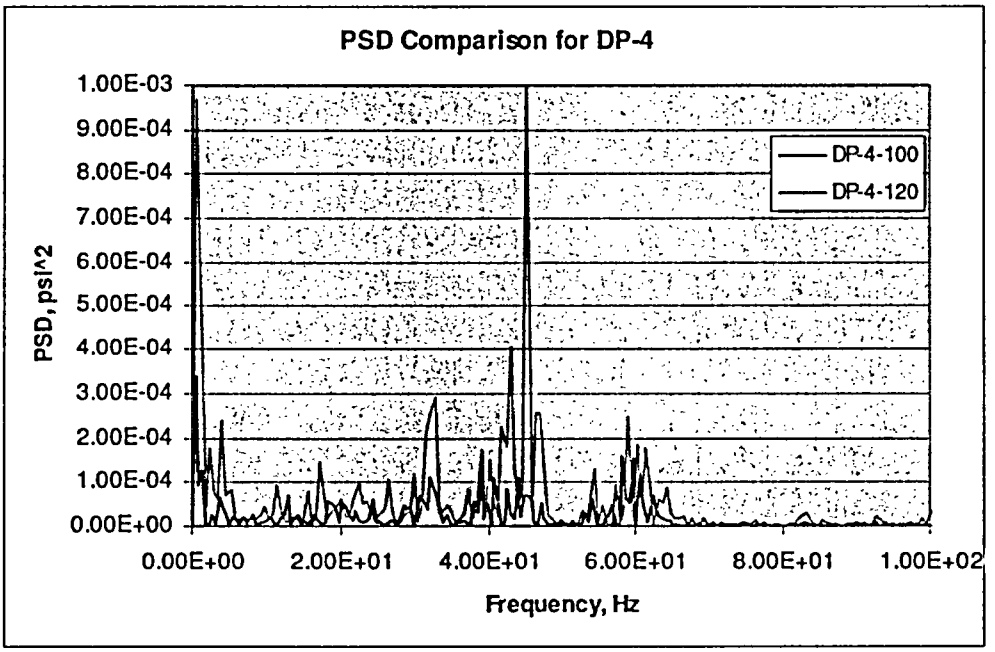

Figure 45d. PSD plot of DP-4 for 100% and 120% load

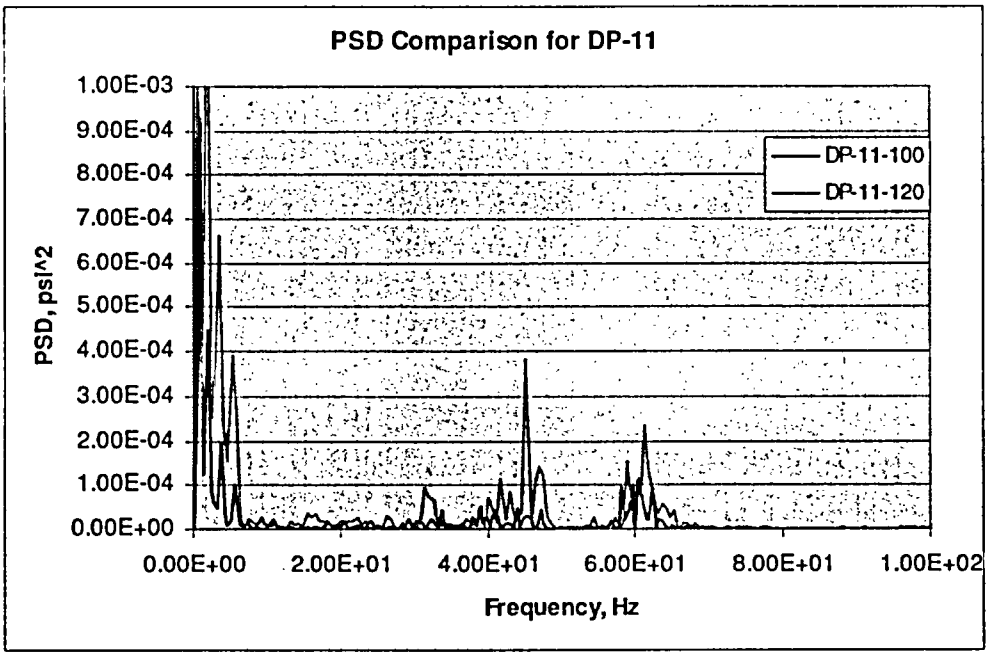

Figure 46a. PSD plot for DP-11 for 100% and 120% load

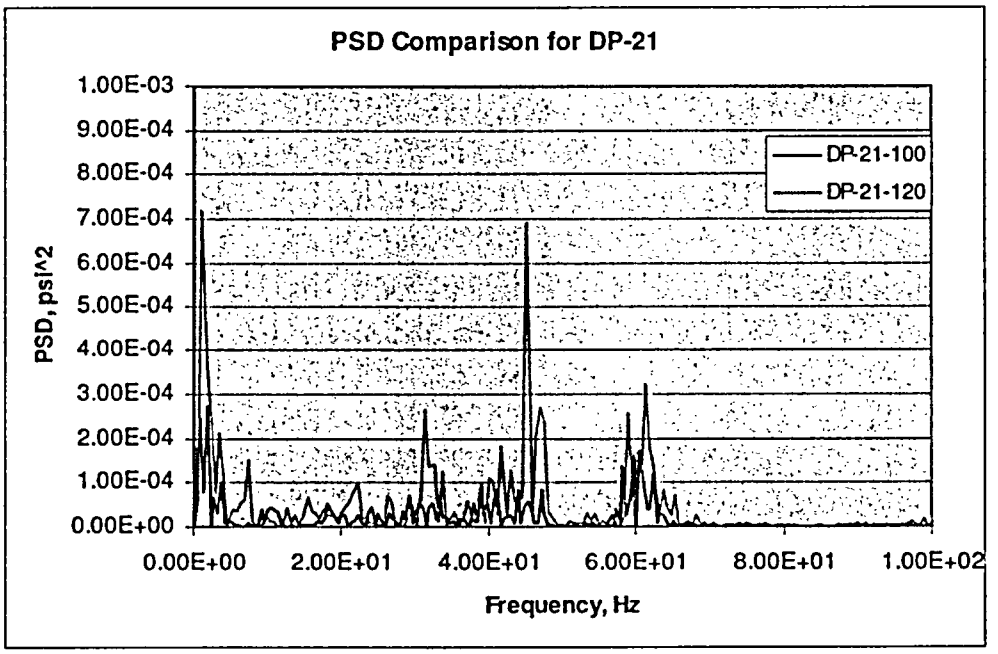

Figure 46b. PSD plot for DP-21 for 100% and 120% load

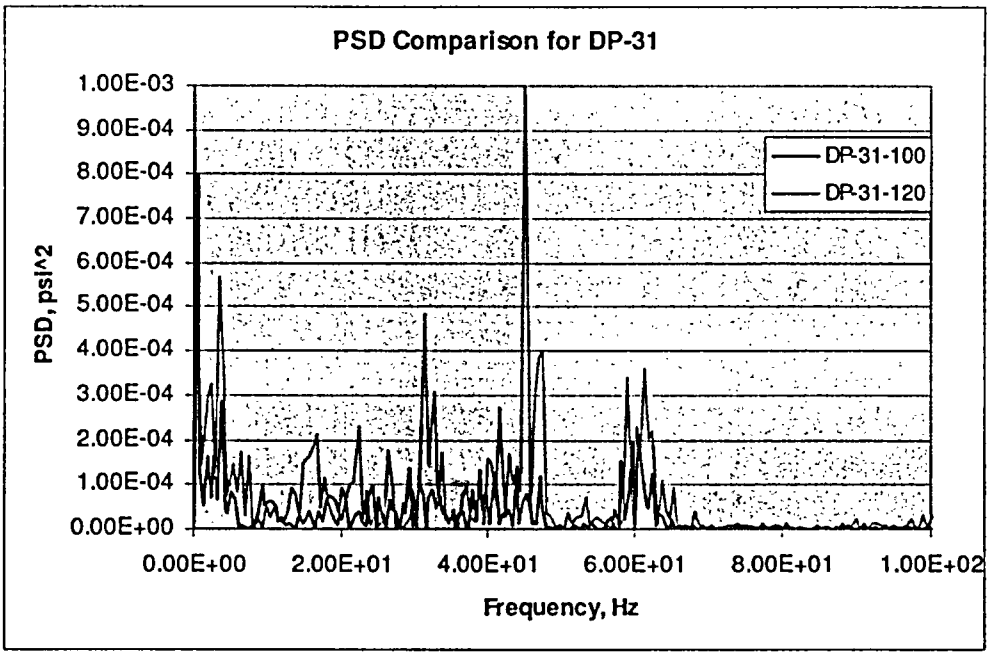

Figure 46c. PSD plot of DP-31 for 100% and 120% load

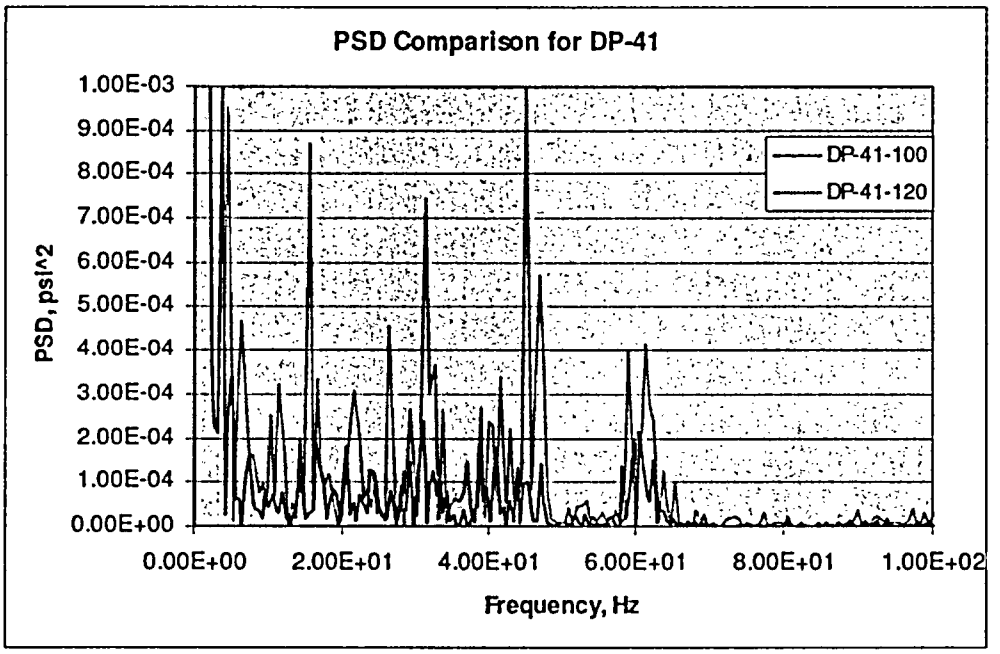

Figure 46d. PSD plot of DP-41 for 100% and 120% load

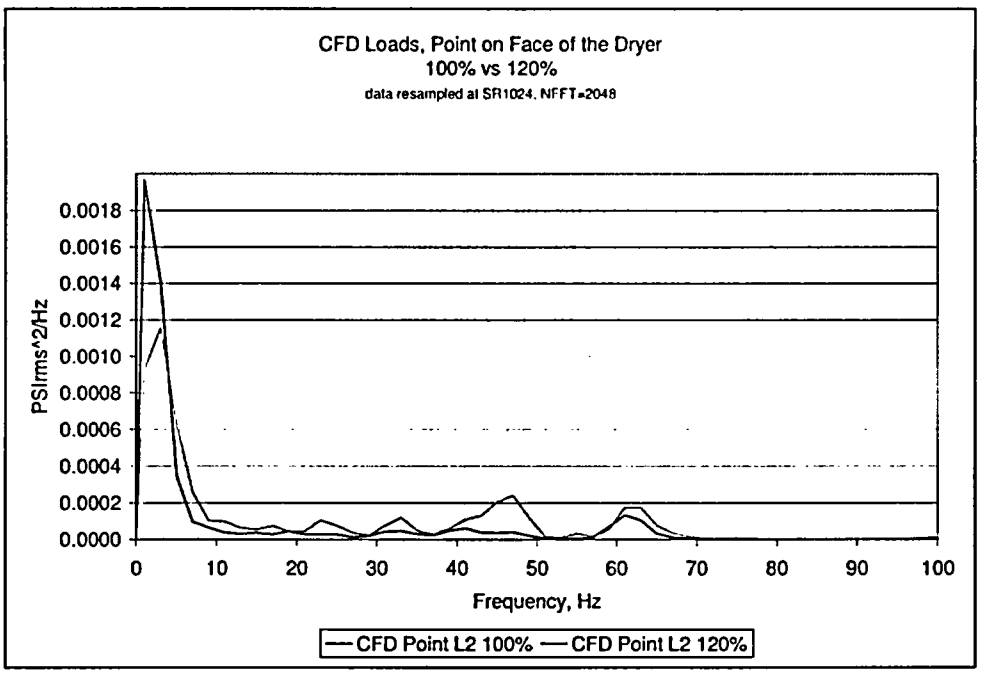

Figure 46e. PSD plot of Point L2 for 100% and 120% load

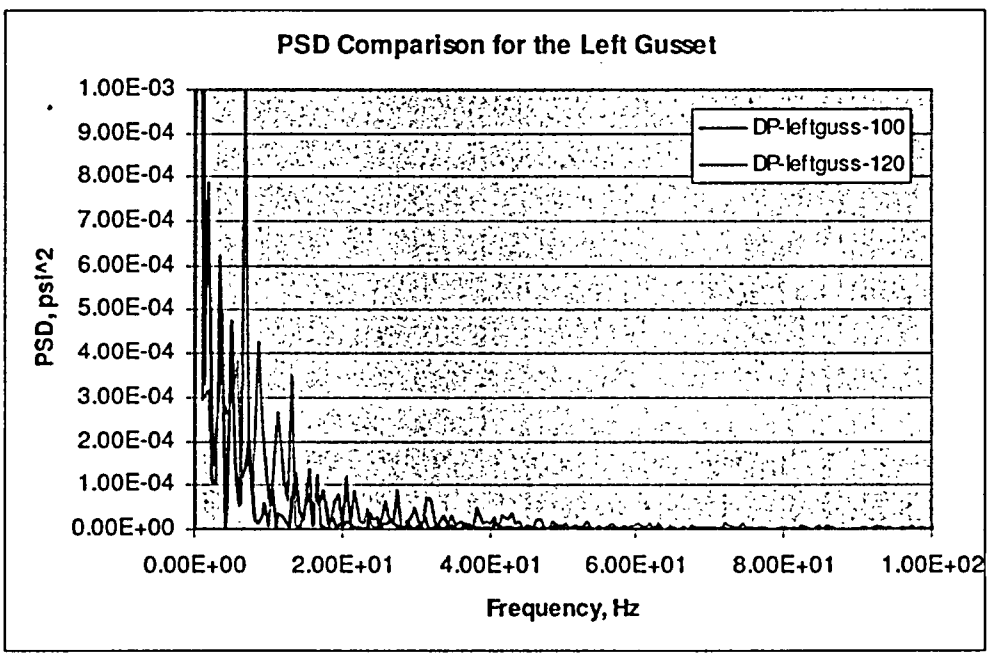

Figure 47. PSD plot of DP on the left gusset for 100% and 120% load.

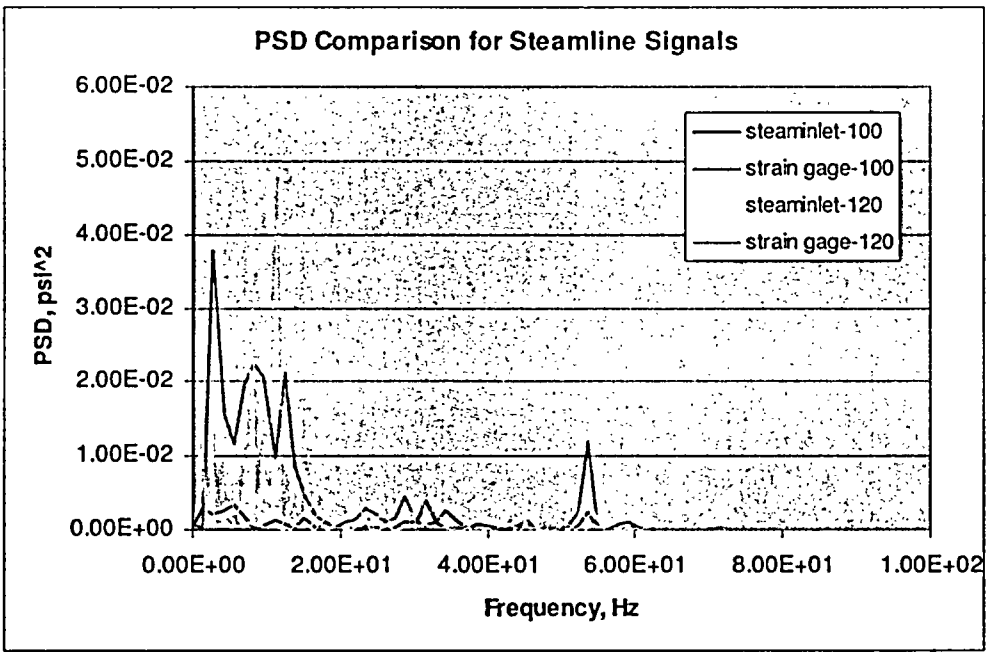

Figure 48. PSD plot of averaged pressure in steamline for 100% and 120% load

4.3.4 Evaluation of Results

An accurate assessment of the structural response of the dryer to flow-induced loads requires an accurate assessment of the flow conditions. The flow-induced loads can include both hydrodynamic and acoustically generated components. The current model approach focused mainly on predicting the hydrodynamic loads.

The LES model is a state-of-the-art turbulence model that is used when predictions with a high degree of accuracy and fidelity are needed. The LES model is an inherently transient approach. The accuracy of the LES method has been demonstrated for a variety of flow conditions through a comparison with measured flow data. Comparisons of mean values of flow variables, fluctuations and frequencies can be found in the literature. The use of the LES model for industrial applications has been limited in the past because of the high cost and high computational demands. The LES simulation presented in this report were made possible due to recent advances of computational speed and improvements of numerical algorithms. The project discussed in this report is considered to be at the cutting edge of the current state of the technology and required 10 months to complete.

The main parameters that influence the accuracy of the flow field predictions based on the LES turbulence model are the mesh resolution and the time step size. The grid and time scale requirements stem from the underlying turbulence modeling approach in the LES model and are based on characteristic turbulence integral length and time scales of the flow under consideration. The integral length and time scales in the area of the face plate have been estimated in Phase I from predicted turbulent kinetic energy and dissipation rate fields.

The integral length scale has been used to define suitable meshing criterion for the plenum around the face plate. The plenum has been meshed with a uniform mesh size of 0.65 inches according to the meshing criterion. A coarser mesh has been applied elsewhere. Therefore, the mesh in the plenum at the face plate meets LES requirements. The use of a coarser mesh outside of the plenum has been justified by the assumption that fluctuations of hydrodynamic loads are related to vortex shedding and unsteady phenomena that occur within the plenum are only weakly coupled to the upstream flow. The hydrodynamic loads on the face plate are generated locally in the plenum rather than upstream. A flow field simulation on a coarser mesh still yields reasonable results of the overall flow pattern, even if some details in the flow structure are under resolved. The flow entering the plenum is considered as sufficiently well represented.

The mesh in the plenum is of a high quality and distributed uniformly. The mesh structure was targeted to focus on free shear layers in the flow rather than on boundary layer phenomena because boundary layer effects were deemed to be less important in this case. A typical case that requires a highly refined near-wall mesh is the flow over an airfoil. The flow in the plenum is dictated mostly by the shape of the geometry rather than by losses in the boundary layer. For example, the flow that enters the plenum is forced to separate similar to a backward facing step scenario. The mesh structure therefore is appropriate for the flow pattern in the plenum.

The time step size was chosen such that in most parts of the plenum the Courant number does not become larger than 1. The Courant number definition used is based on the local flow velocity and does not include the speed of sound. The choice of this time step is consistent with the integral time scale criterion mentioned above. In some areas, such as near the vortex in the lower left and right corner, the Courant could be larger than 1. The time step is 5e-4 seconds for the 100% case and 4e-4 seconds for the 120% case. The dominant observed flow frequencies are not larger than

100 Hz and are well in the range of the used time step. The magnitude of fluctuations decreases considerably above 100 Hz. The used time step is deemed suitable for the flow pattern and frequencies in the plenum.

The accuracy of the solutions was checked by considering both the mean flow and transient data. The mean pressure load on the face plate is due to the static pressure differential across the plate. In general, this mean pressure differential arises from a combination of losses in the dryer, dome, and plenum, and from the acceleration of flow through the plenum. Local flow features can also contribute to the mean loads. The mean pressure differential across the plate for the 100% load case is approximately 5500 Pa (0.8 psi). For the 120% load case, the mean pressure differential is approximately 7500 Pa (1.1 psi). Approximately 40% of the mean pressure difference is accounted for by the losses in the dryer vane assembly. 30% is associated with the acceleration of the flow into the plenum. This is consistent with a simple calculation of the change in dynamic head from the dryer inlet to the plenum. The remaining pressure differential is due to the strong vortices attached to the lower left and right corners of the face plate. The vortices generate a low-pressure region that contributes a total of 2000 Pa (0.3 psi) averaged over the face plate. The mean pressure load is seen as reasonable because it is consistent with simple engineering calculations.

It is known from simulations of vortex shedding behind cylinders that frequency predictions are less sensitive to mesh resolution. The frequency analysis on the opposite face plate (coarse mesh) shows consistent results (Figure 49).

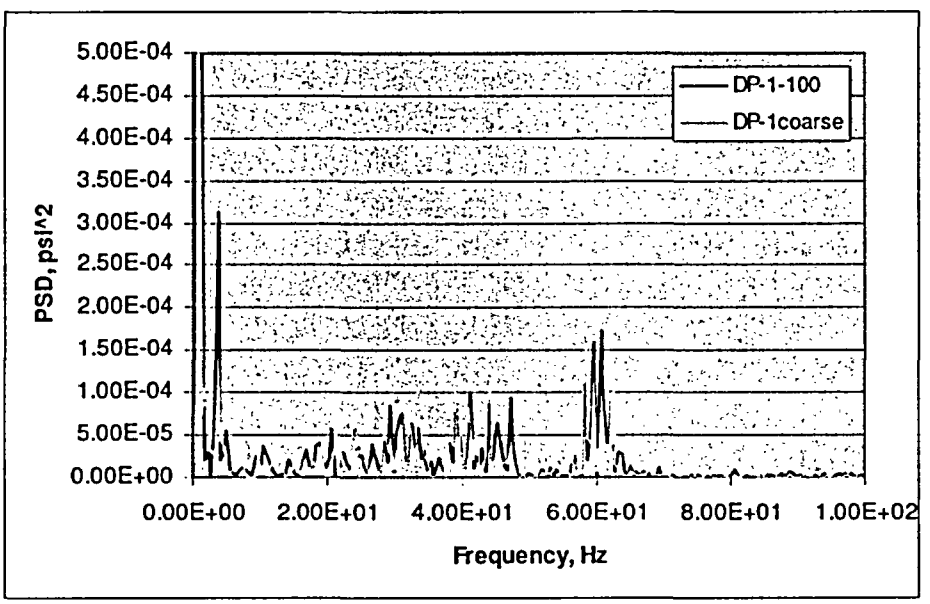

Figure 49. Comparison of PSD plots between coarse mesh and fine mesh.

5. Conclusions

CFD simulations have been performed for the 100% and 120% load cases. Transient pressure loads on the dryer walls have been extracted and delivered to Entergy for use in additional structural analyses. The loads on the face plate can be characterized as follows:

- The mean pressure loads on the face plate are 0.8 psi for 100% and 1.1 psi for 120%
- The mean pressure loads scale with square of velocity.
- Significant pressure fluctuations on the face plate originating from hydrodynamic effects have a frequency lower than 30 Hz. Complex flow structures and vortices in the plenum are responsible for these pressure fluctuations.
- Some pressure fluctuations on the face plate with frequencies higher than 30 Hz have been identified and are associated with acoustic modes. The mean frequencies of the pressure bands are around 40 Hz and 60 Hz.
- The time averaged load on the left gusset is 0.8 psi for the 100% case and 1.04 psi for the 120% case.
- Signals at the strain gage location are considerably stronger than at the face plate.
- The CFD model time step and modeling parameters were developed to accurately simulate hydrodynamic effects. Because the LES simulation included compressibility, acoustic effects are also captured. Accurate depiction of acoustic loads amplitude would require a much smaller time step and result in an order of magnitude increase in the solution time.

Appendix

Appendix A.1. Zone ID information used for ΔP data writes.

Zone ID	Zone Name	Add'l Description	Zone Type	# Cell Faces	Face Type	use?	
17	wall_dryer		wall	21525	quadrilateral	1	21525
19	dam2	6" dams	wall	456	quadrilateral	1	456
20	dam1	6" dams	wall	456	quadrilateral	1	456
21	wall-face-plate2	vertical face plate (nonLES)	wall	3034	quadrilateral	1	3034
22	wall-face-plate1	vertical face plate (LES)	wall	17722	mixed	1	17722
23	wall-enforce2	3 gussets (nonLES)	wall	1260	triangular	1	1260
24	wall-slope2	horizontal face plate (nonLES	wall	1280	triangular	1	1280
26	wall_middle		wall	451	quadrilateral	1	451
28	wall_hook_hole_end		wall	285	quadrilateral	1	285
29	wall_dryer_top		wall	3230	quadrilateral	1	3230
33	wall_enforce1	3 gussets (LES)	wall	3812	triangular	1	3812
34	wall_slope1	horizontal face plate (LES)	wall	3335	mixed	1	3335
35	wall_inner_cylinder		wall	17778	mixed	1	17778
45	wall_dryer:045		wall	14032	mixed	1	14032
46	wall_dryer:046		wall	660	quadrilateral	1	660
47	wall_dryer:047		wall	3230	quadrilateral	1	3230
48	wall_middle:048		wall	330	quadrilateral	1	330
49	wall_middle:049		wall	80	quadrilateral	1	80
50	wall_dryer_top:050		wall	8769	quadrilateral	1	8769
51	wall_inner_cylinder:051		wall	37670	quadrilateral	1	37670
52	wall_inner_cylinder:052		wall	1122	quadrilateral	1	1122
							140517

Appendix A.2. Pressure contour plots from the 17 full data sets for 100% Load.

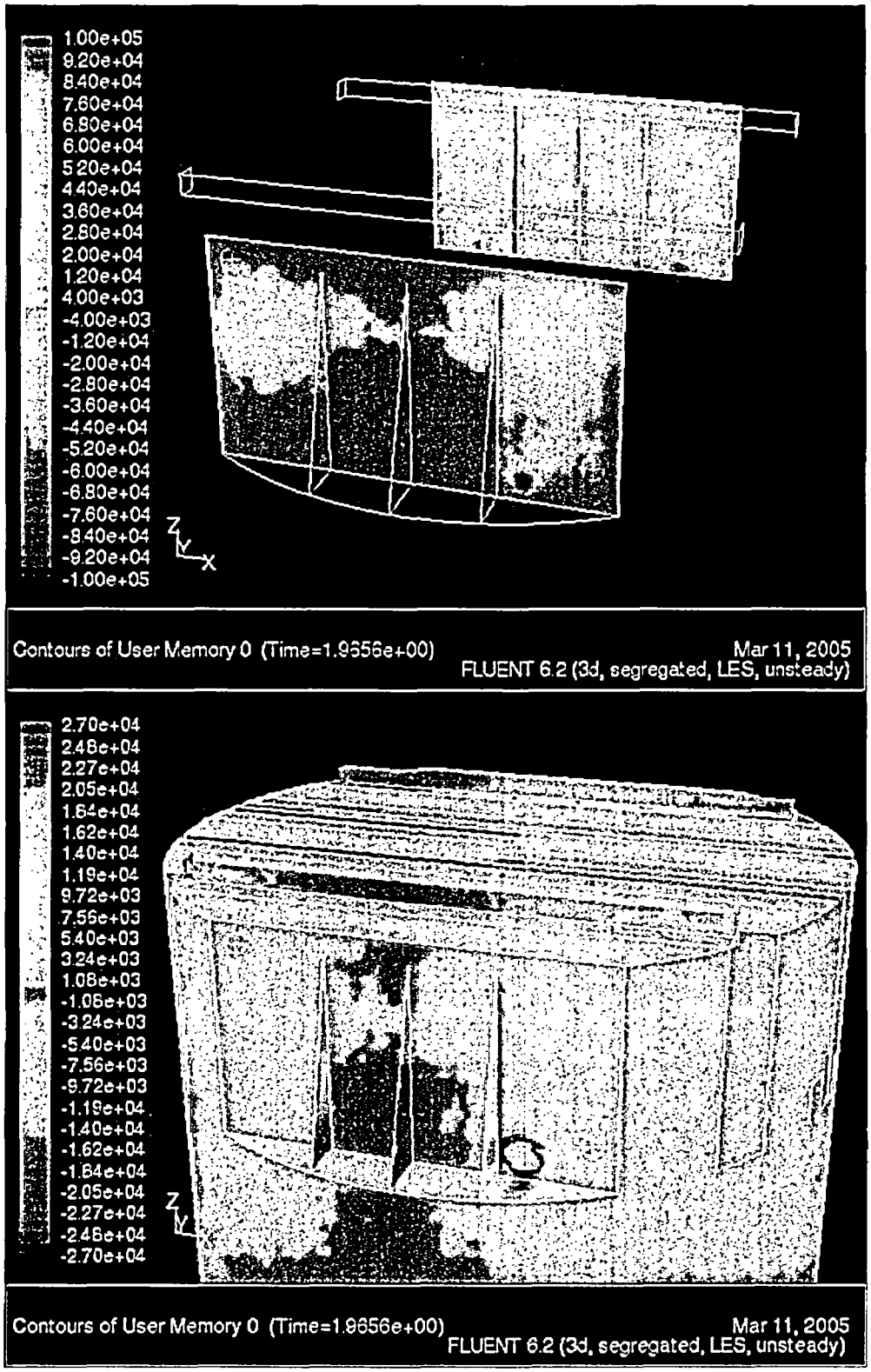
1.00e+05
9.20e+04
8.40e+04
7.60e+04
6.80e+04
6.00e+04
5.20e+04
4.40e+04
3.60e+04
2.80e+04
2.00e+04
1.20e+04
4.00e+03
-4.00e+03
-1.20e+04
-2.00e+04
-2.80e+04
-3.60e+04
-4.40e+04
-5.20e+04
-6.00e+04
-6.80e+04
-7.60e+04
-8.40e+04
-9.20e+04
-1.00e+05
Z
Y
X
Contours of User Memory 0 (Time=1.9556e+00)
Mar 11, 2005
FLUENT 6.2 (3d, segregated, LES, unsteady)
2.70e+04
2.48e+04
2.27e+04
2.05e+04
1.84e+04
1.62e+04
1.40e+04
1.19e+04
9.72e+03
7.56e+03
5.40e+03
3.24e+03
1.08e+03
-1.08e+03
-3.24e+03
-5.40e+03
-7.56e+03
-9.72e+03
-1.19e+04
-1.40e+04
-1.62e+04
-1.84e+04
-2.05e+04
-2.27e+04
-2.48e+04
-2.70e+04
Z
Y
Contours of User Memory 0 (Time=1.9656e+00)
Mar 11, 2005
FLUENT 6.2 (3d, segregated, LES, unsteady)

Time 1.96

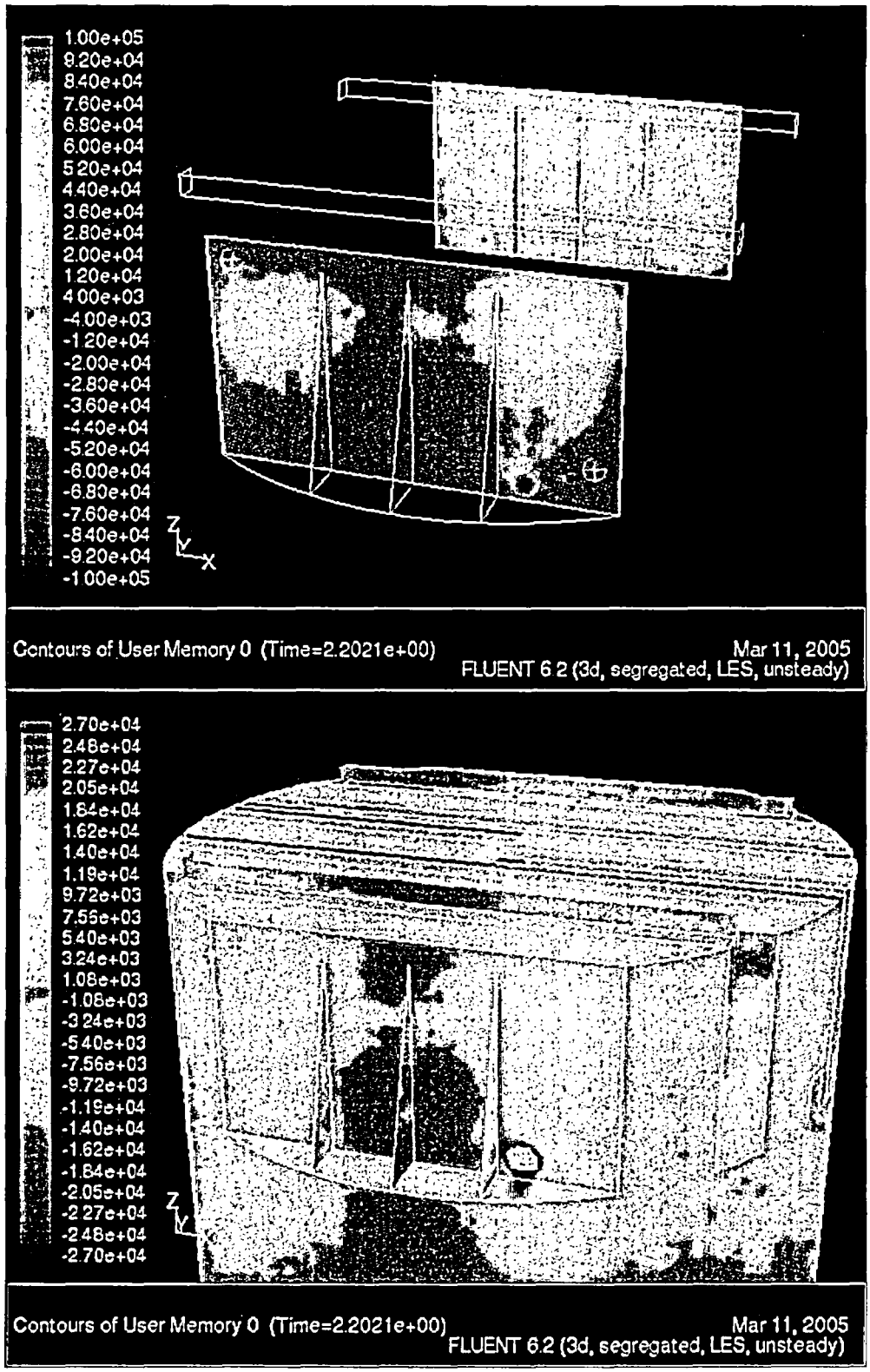

Time 2.20 Seconds

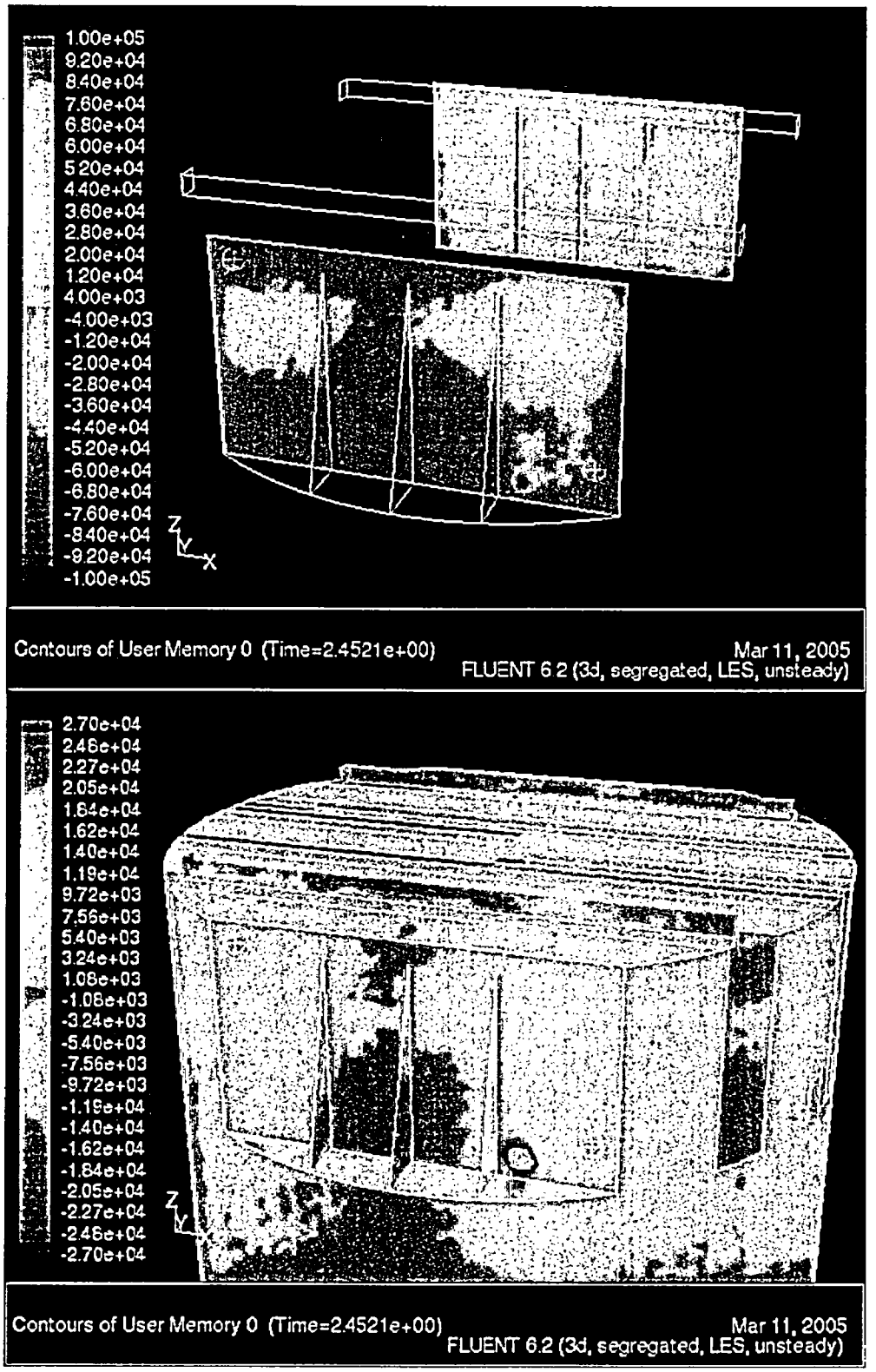

Time 2.45 Seconds

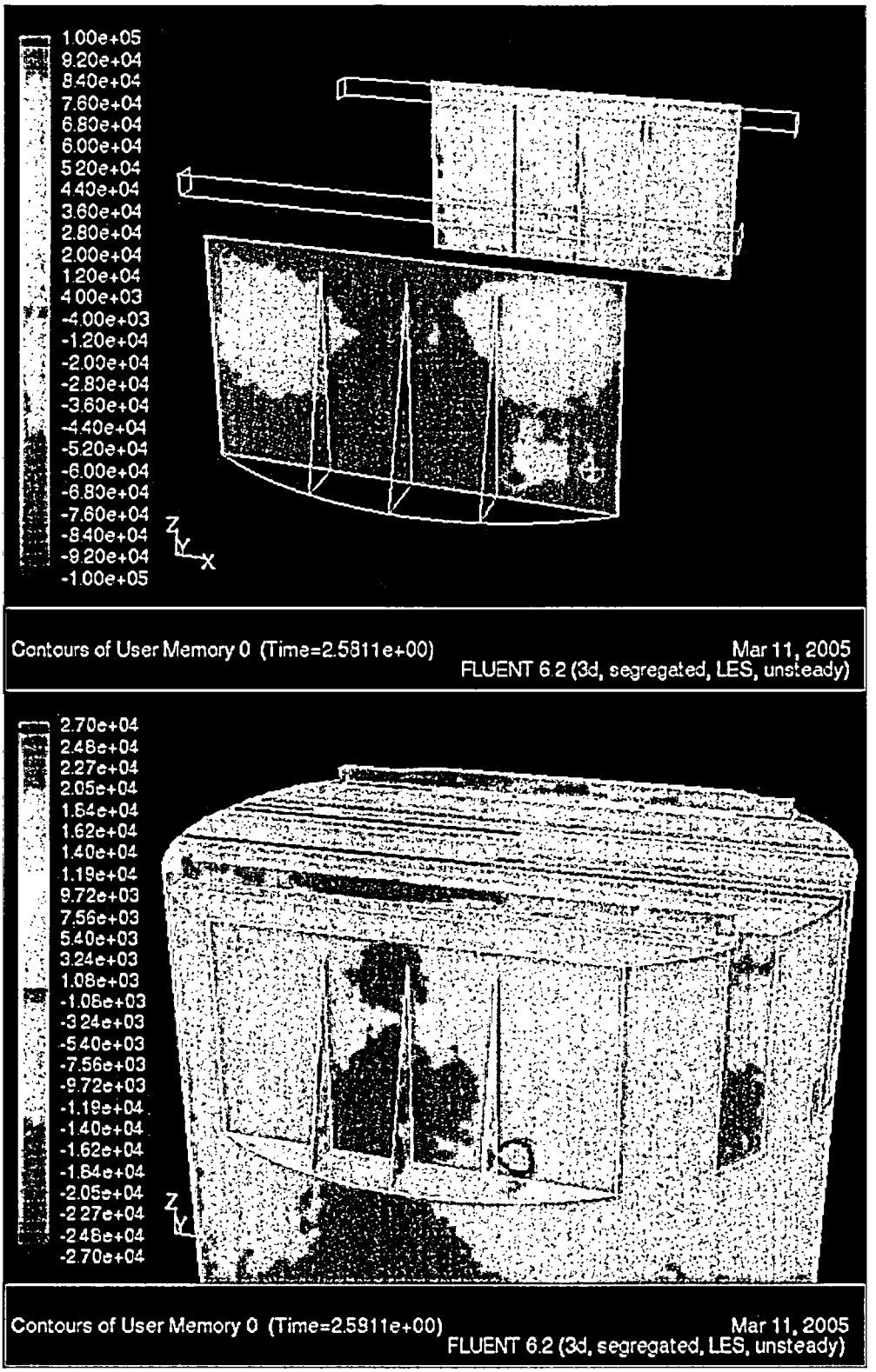

Time 2.58 Seconds

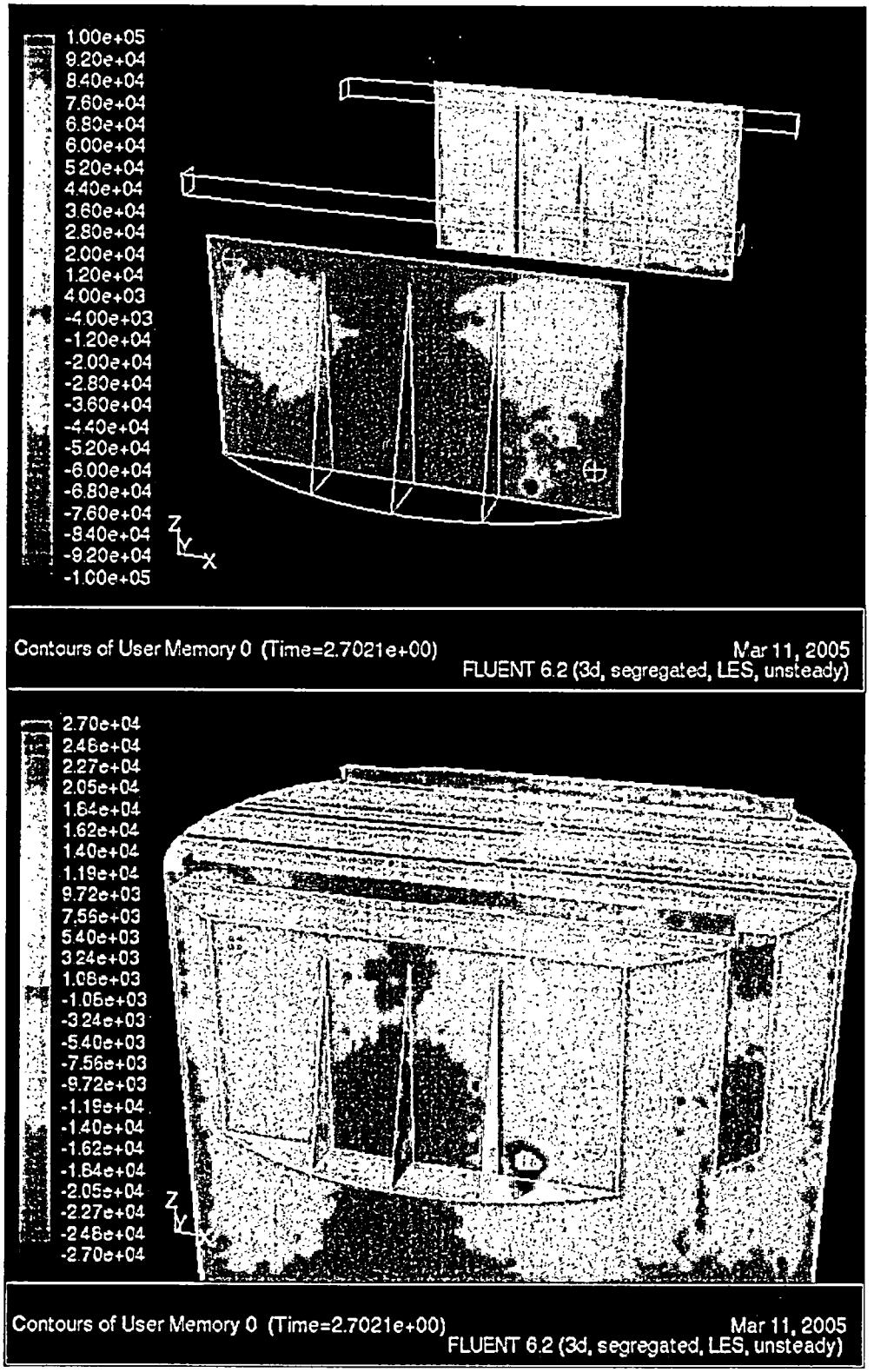

Time 2.70 Seconds

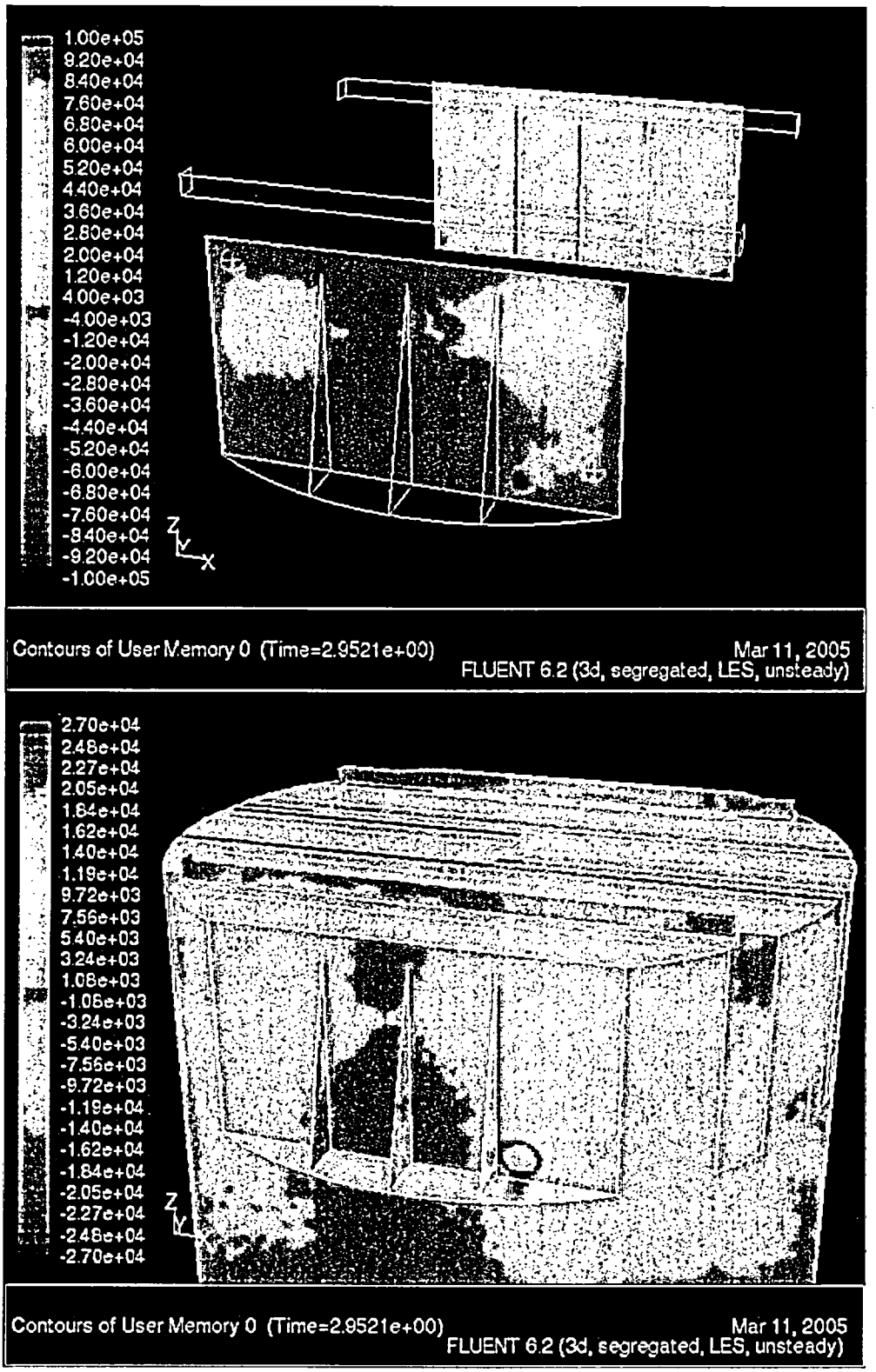

Time 2.95 Seconds

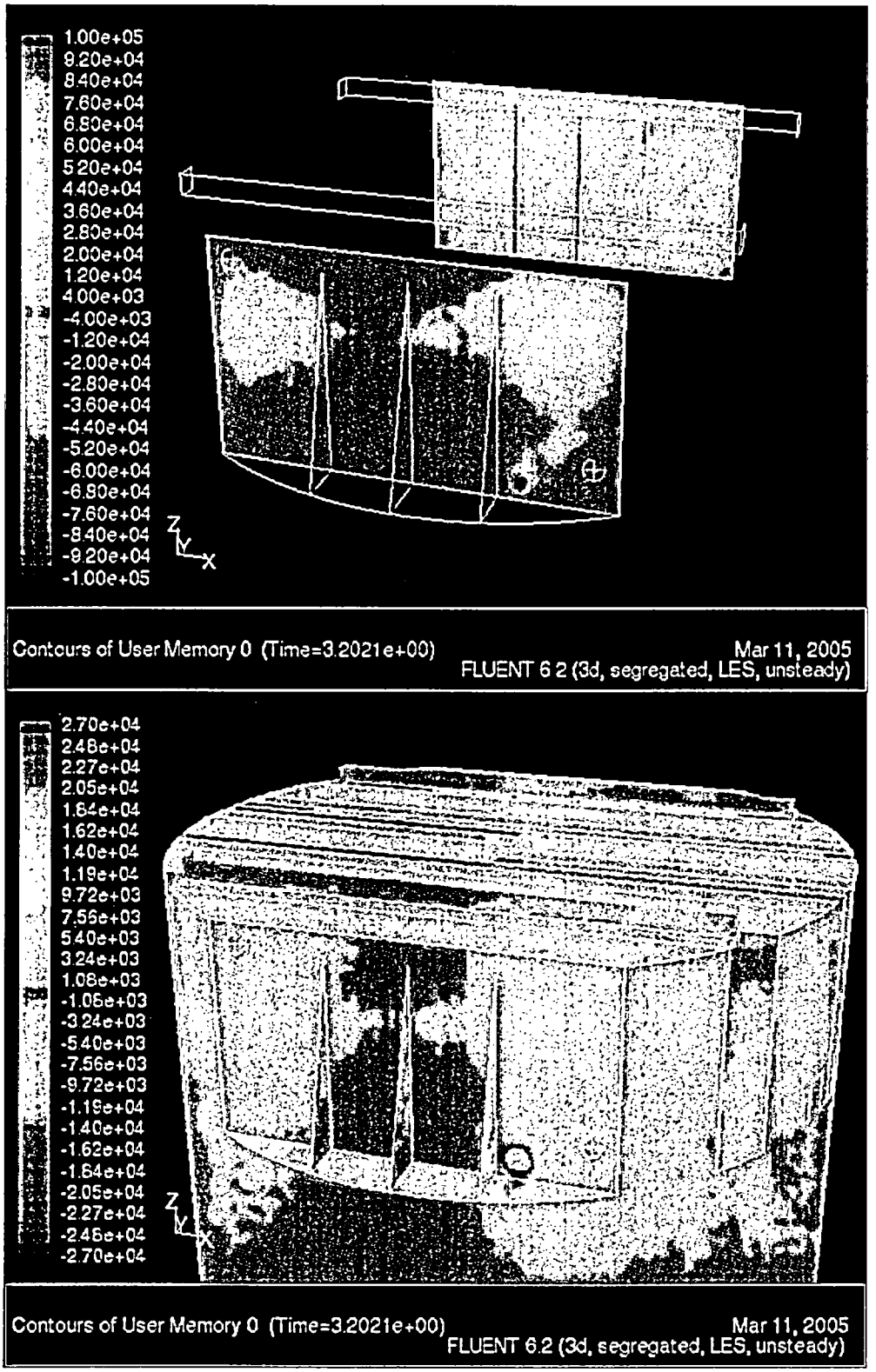

Time 3.20 Seconds

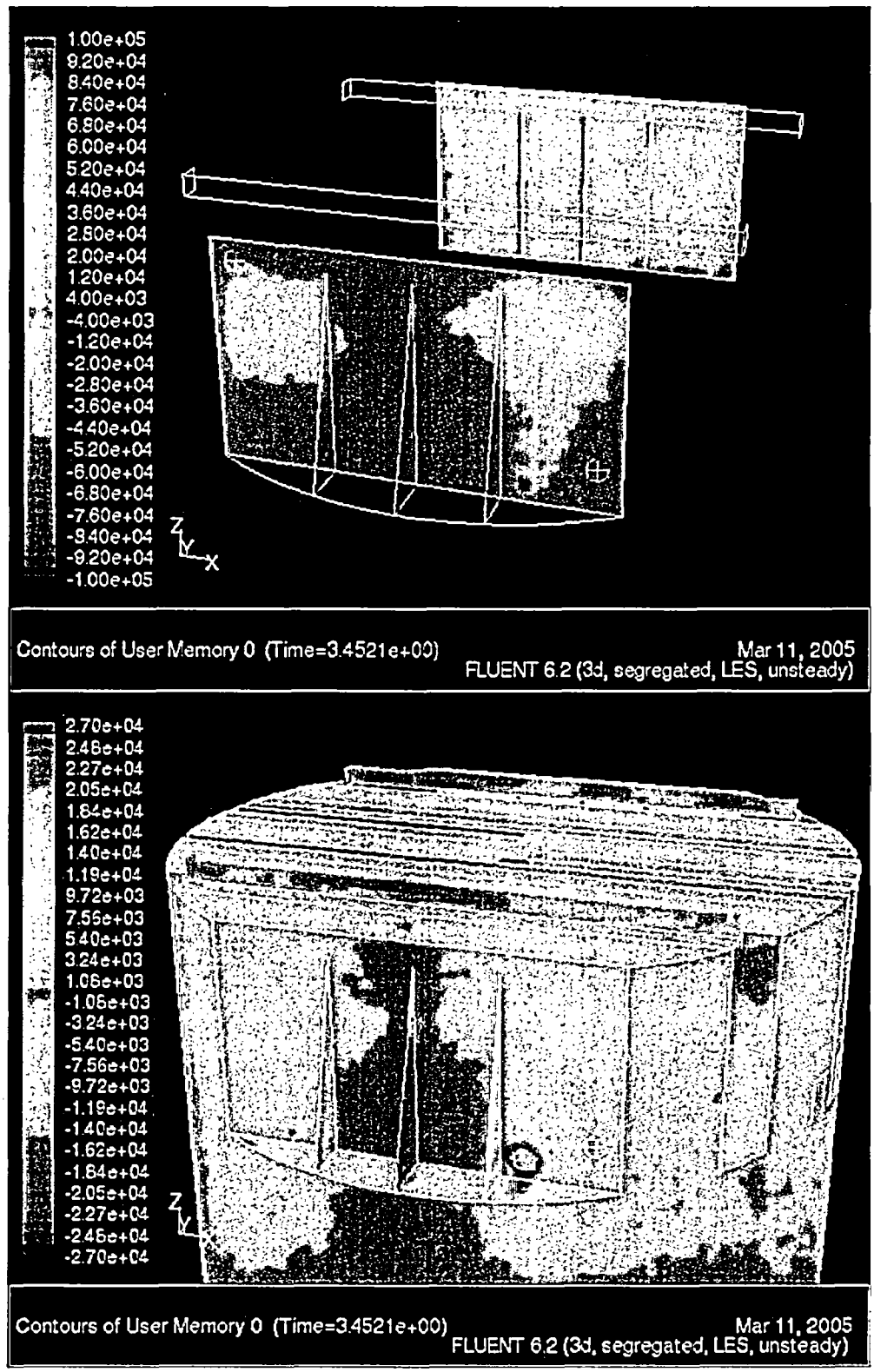

Time 3.45 Seconds

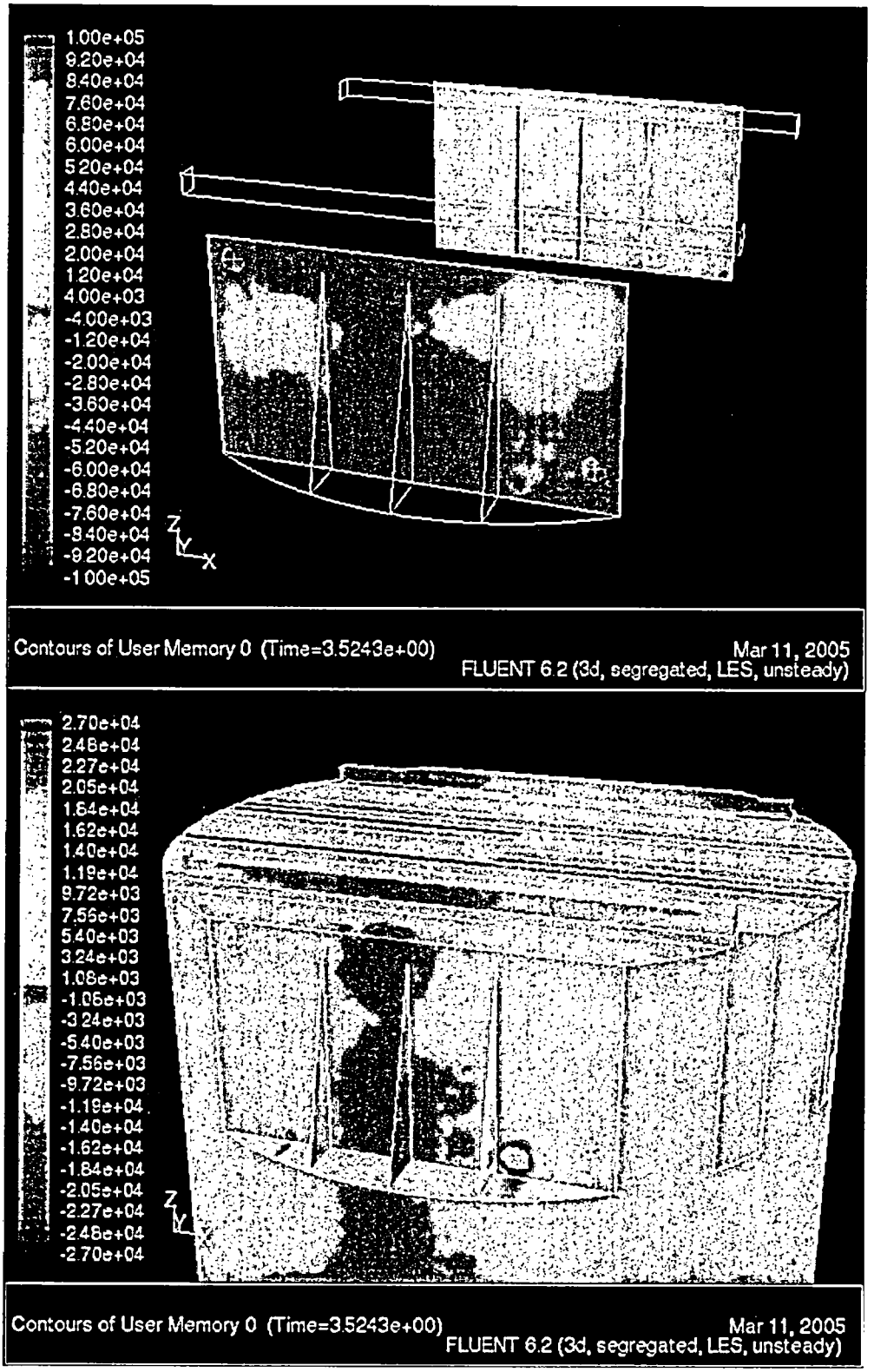

Time 3.52 Seconds

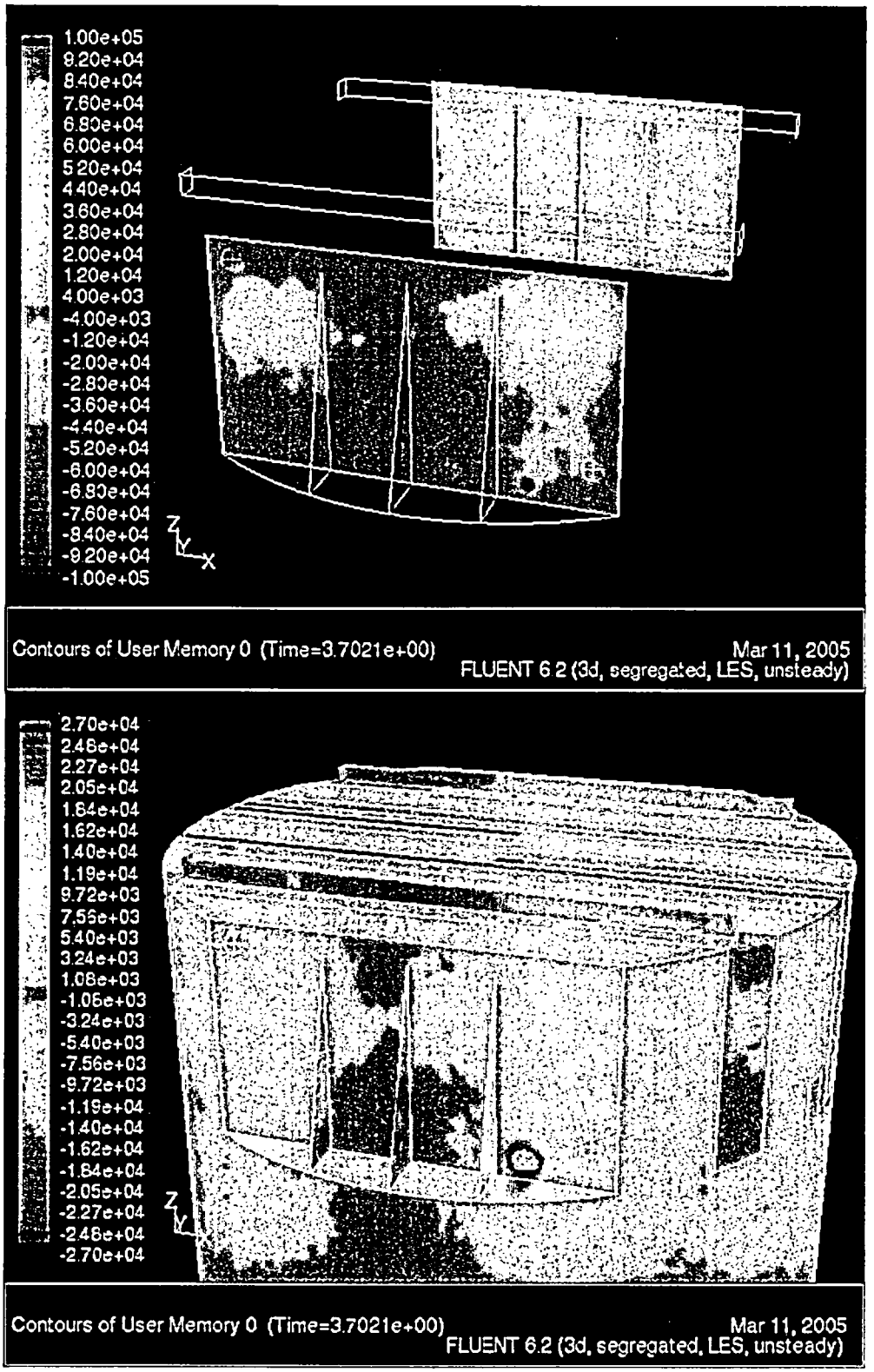

Time 3.70 Seconds

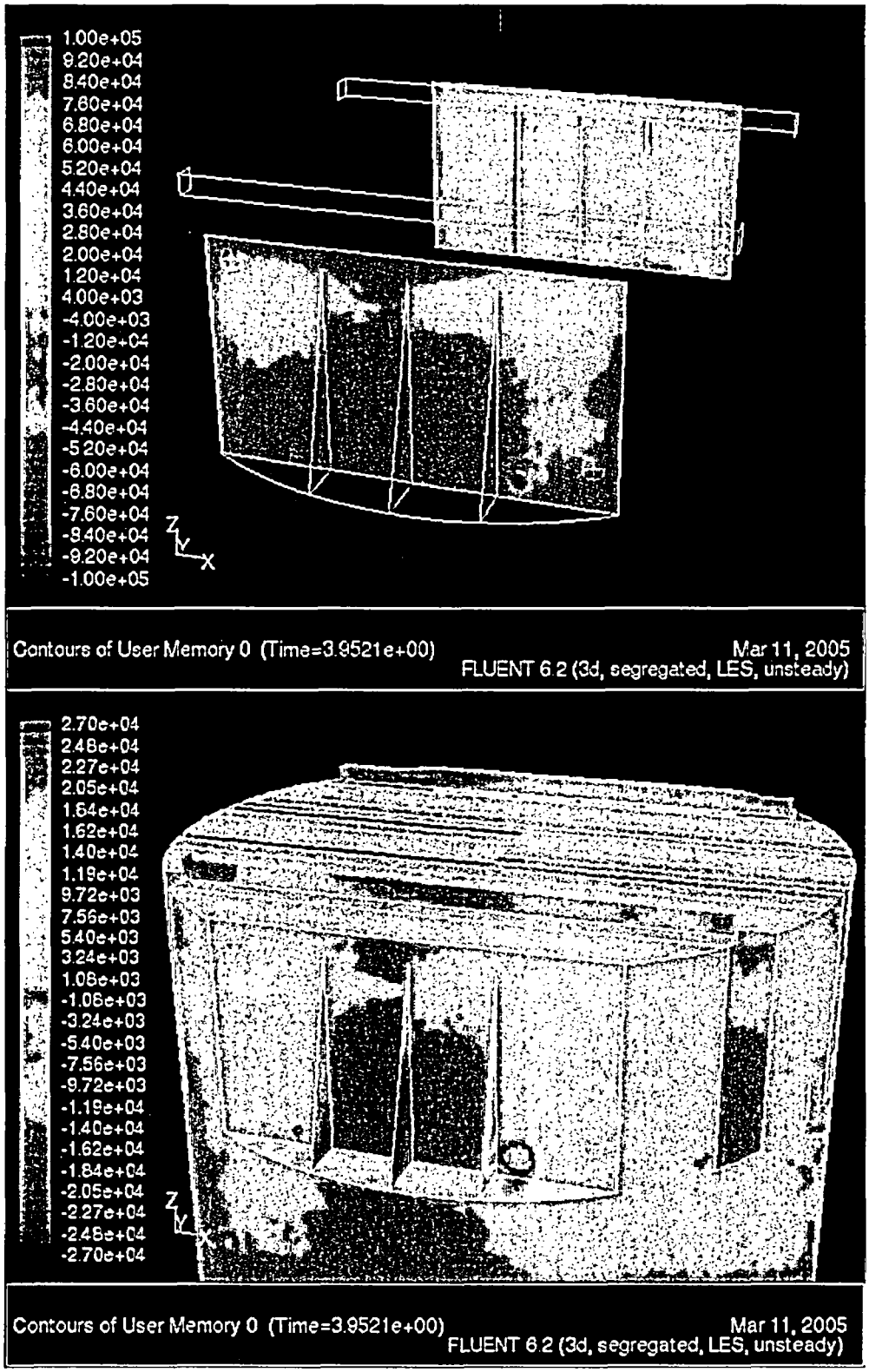

Time 3.95 Seconds

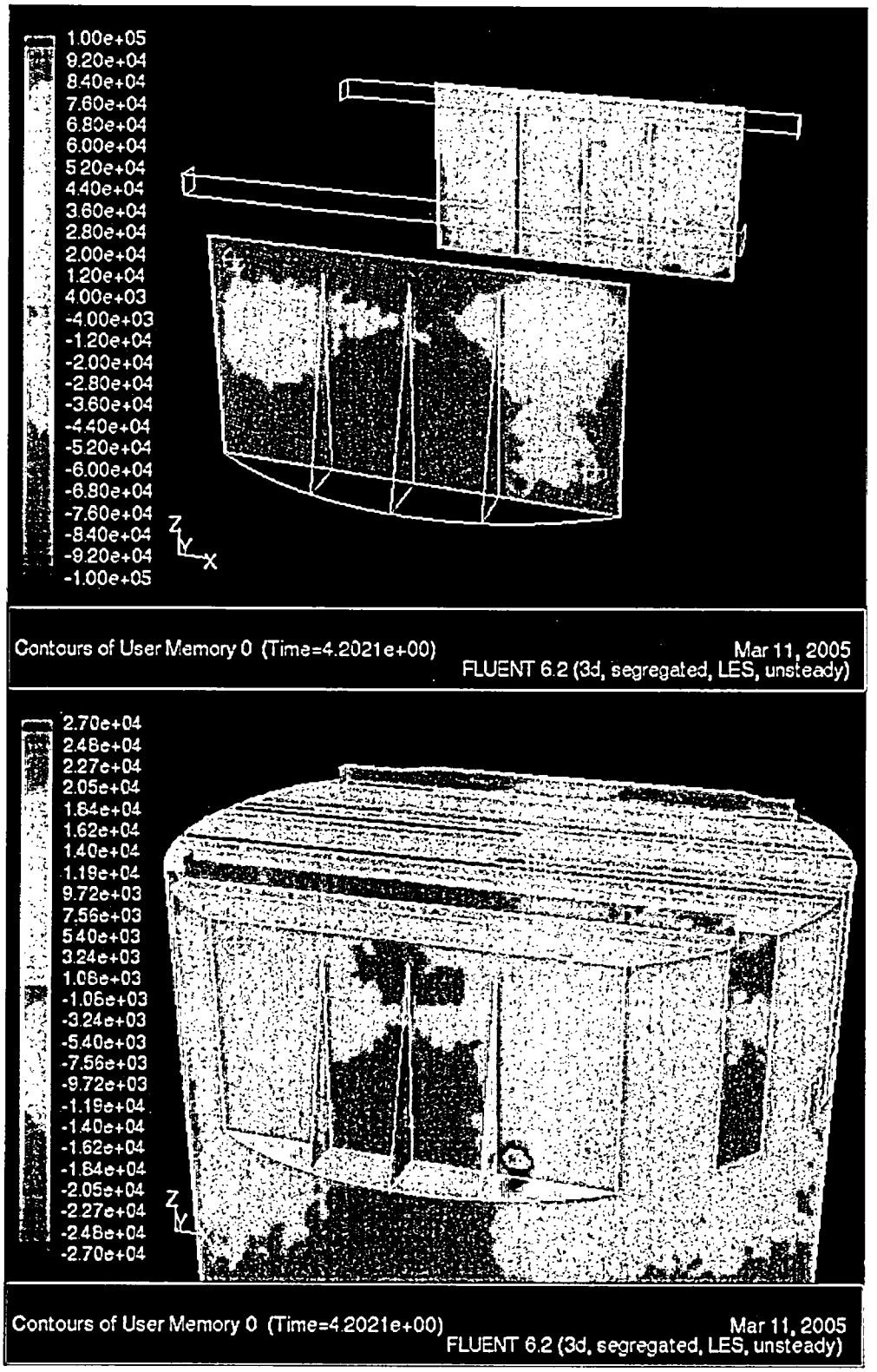

Time 4.20 Seconds

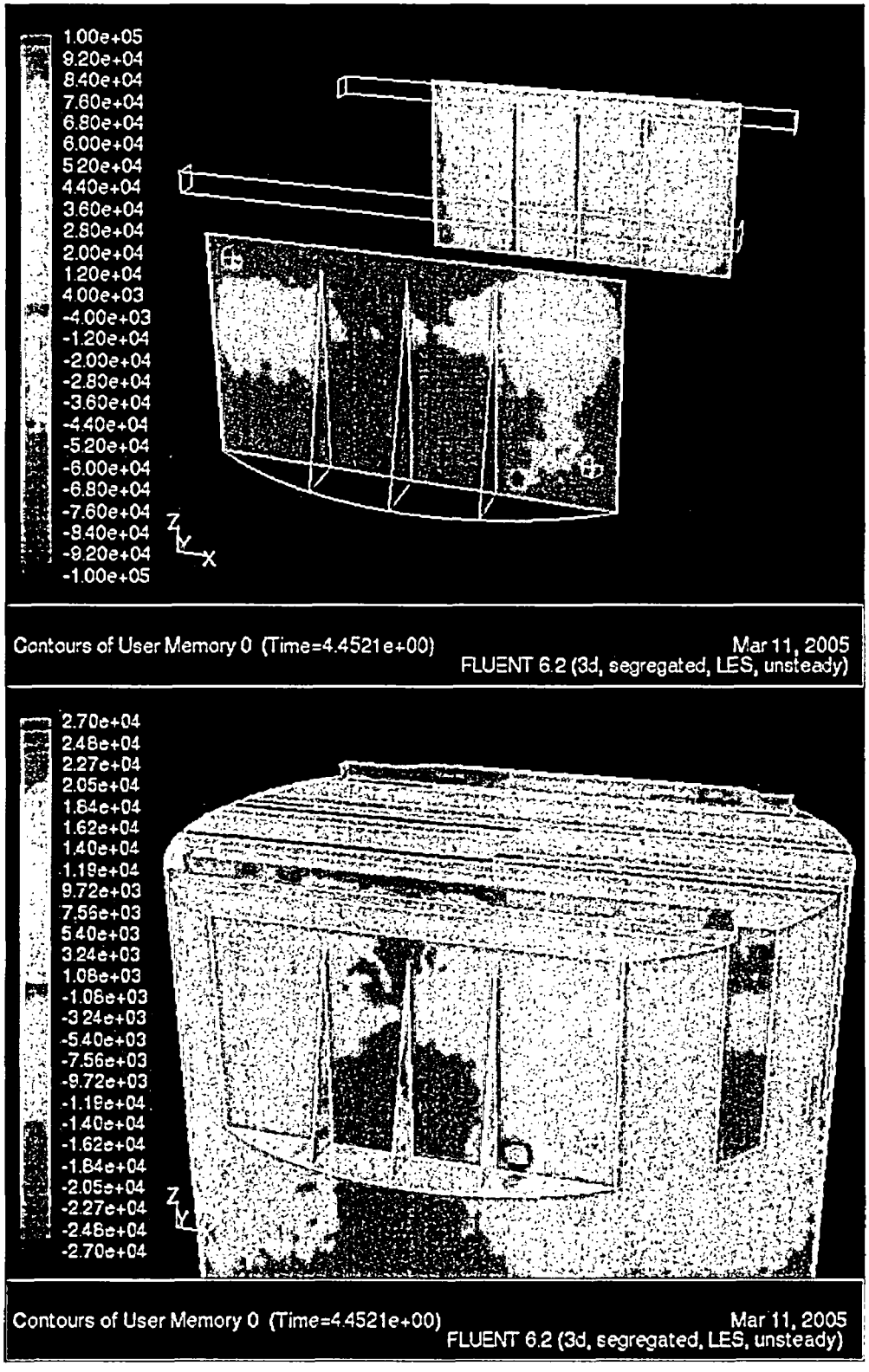

Time 4.45 Seconds

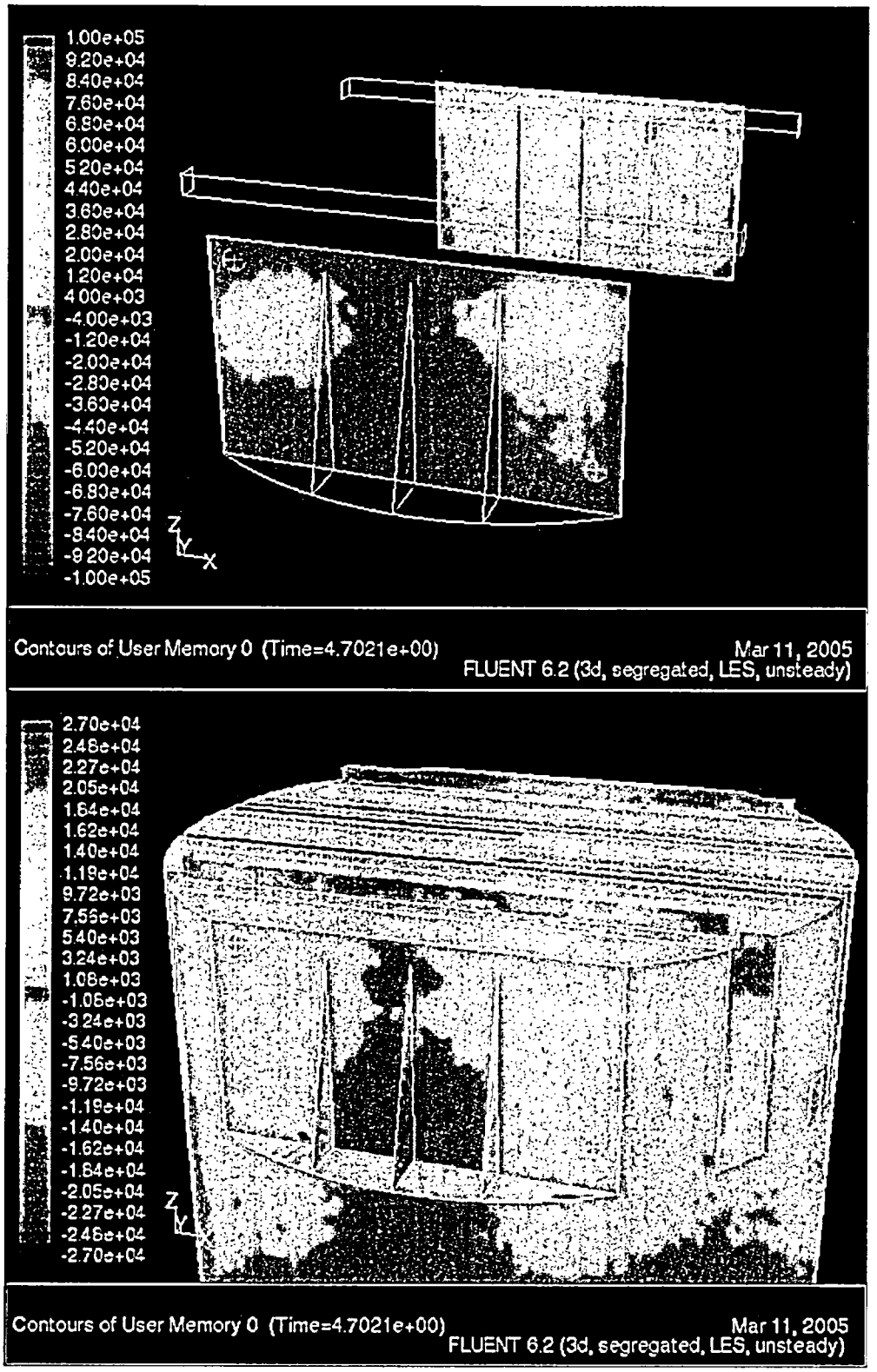

Time 4.70 Seconds

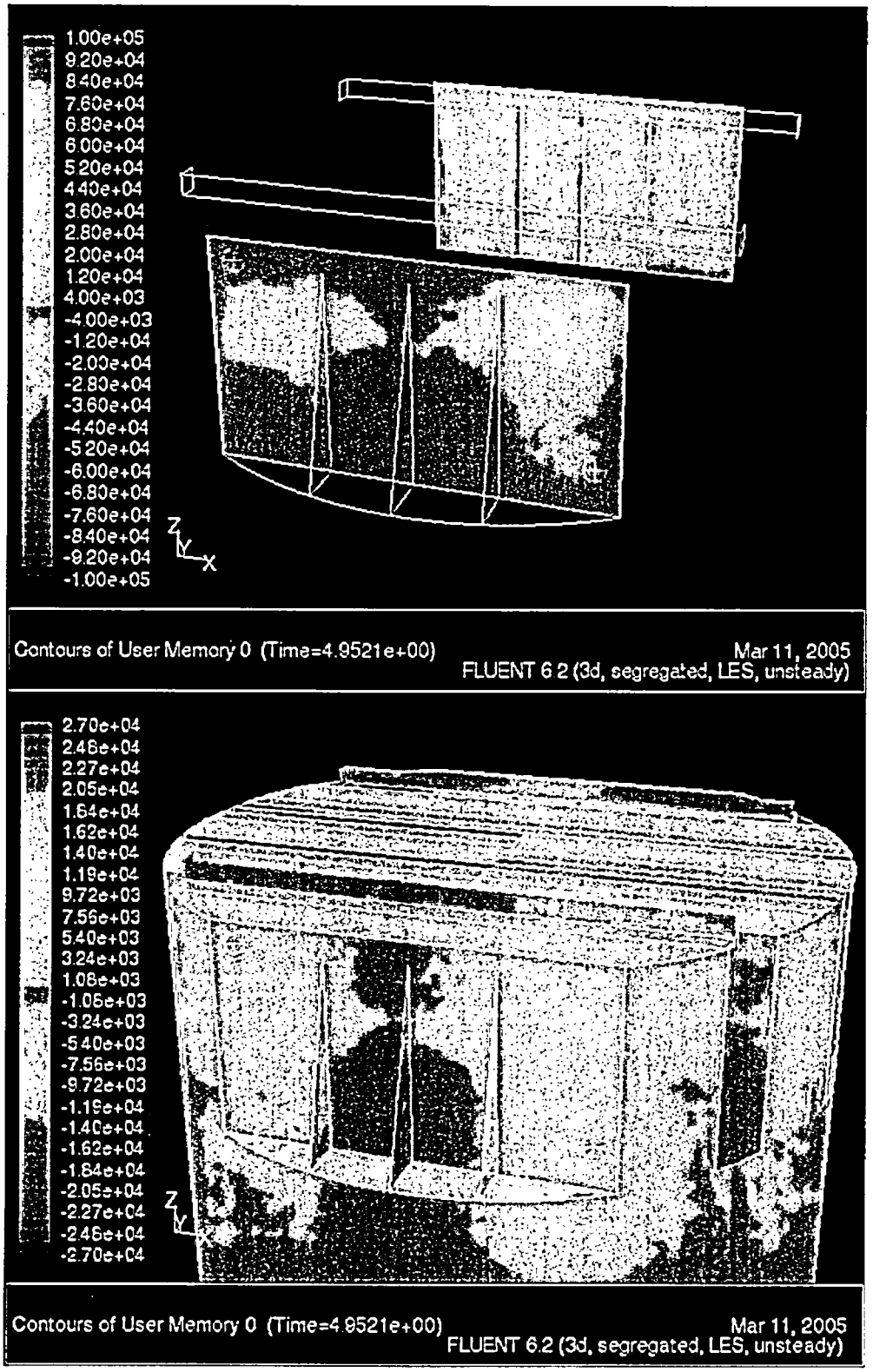

Time 4.95 Seconds

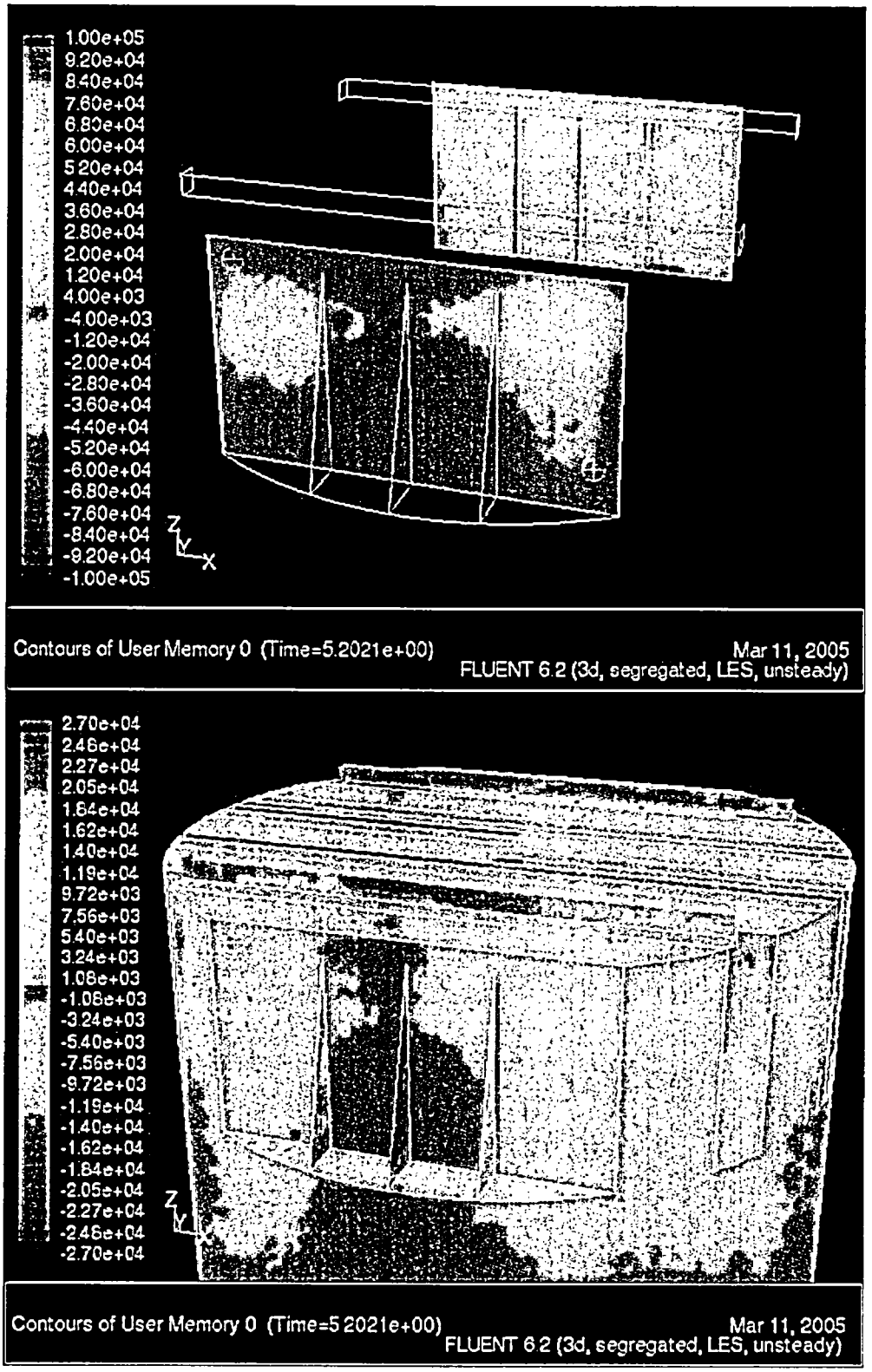

Time 5.20 Seconds

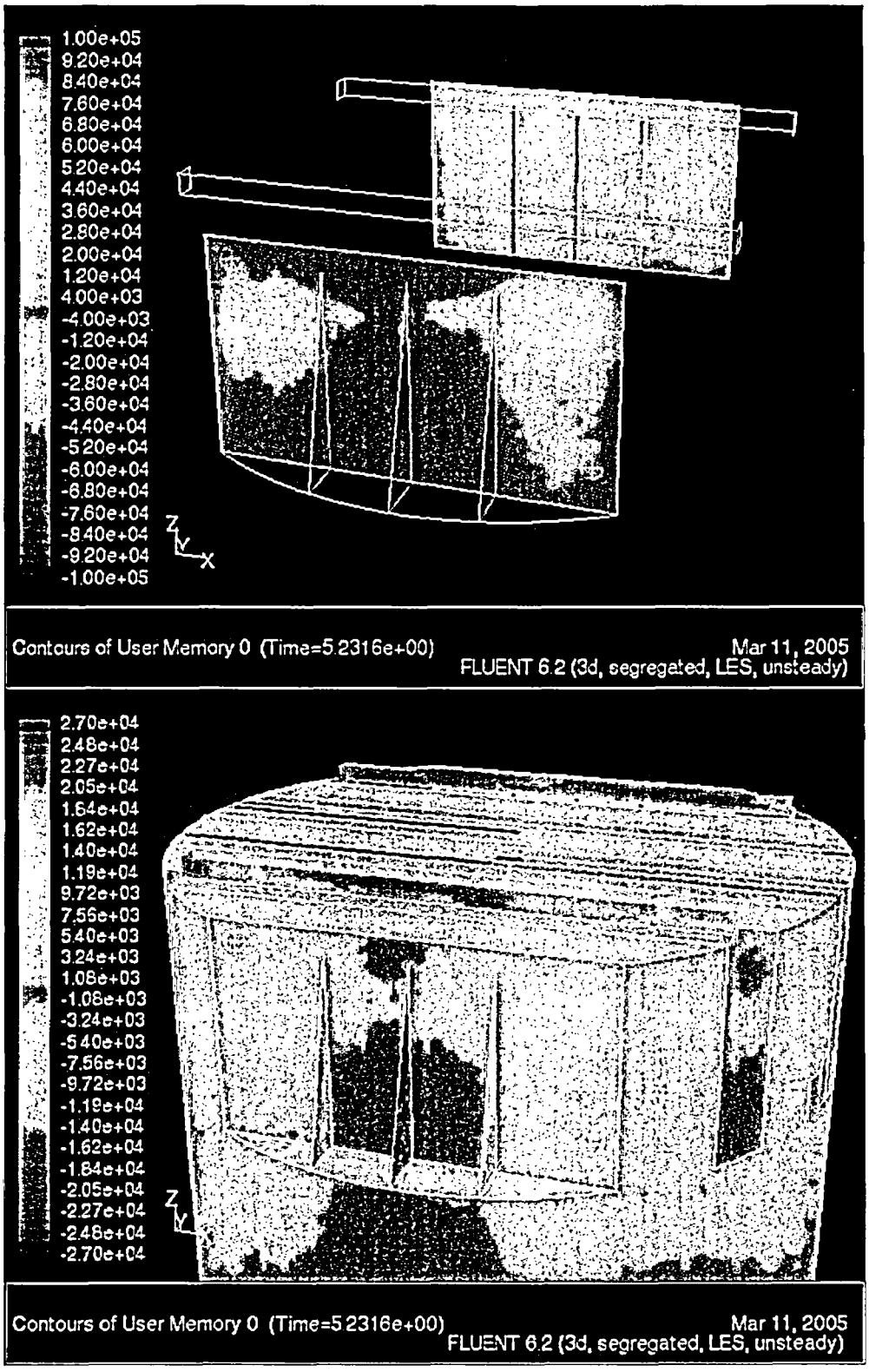

Time 5.23 Seconds

Appendix A.2. Pressure contour plots from the 18 full data sets for 120% Load.

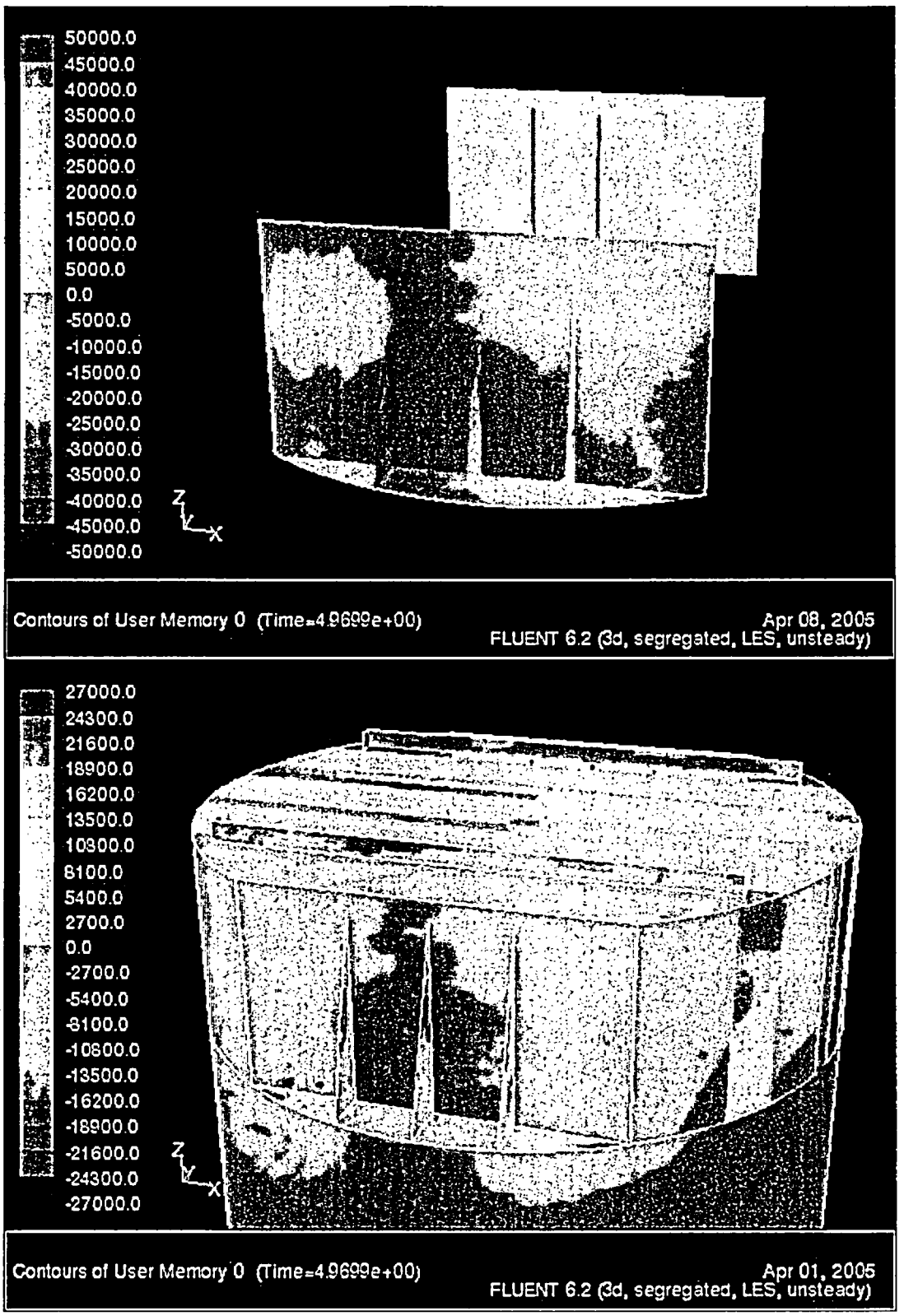

Time 4.97 Seconds

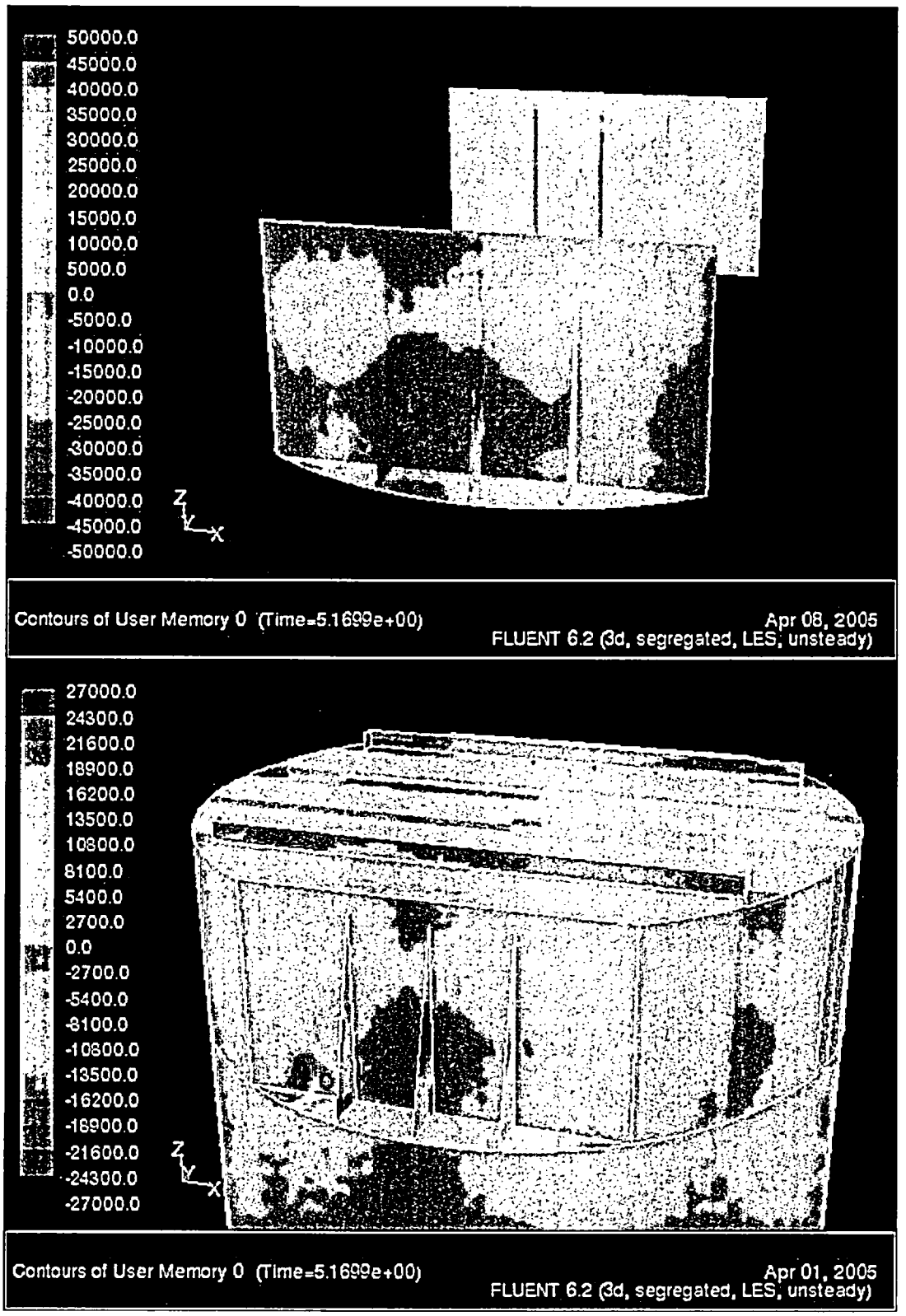

Time 5.17 Seconds

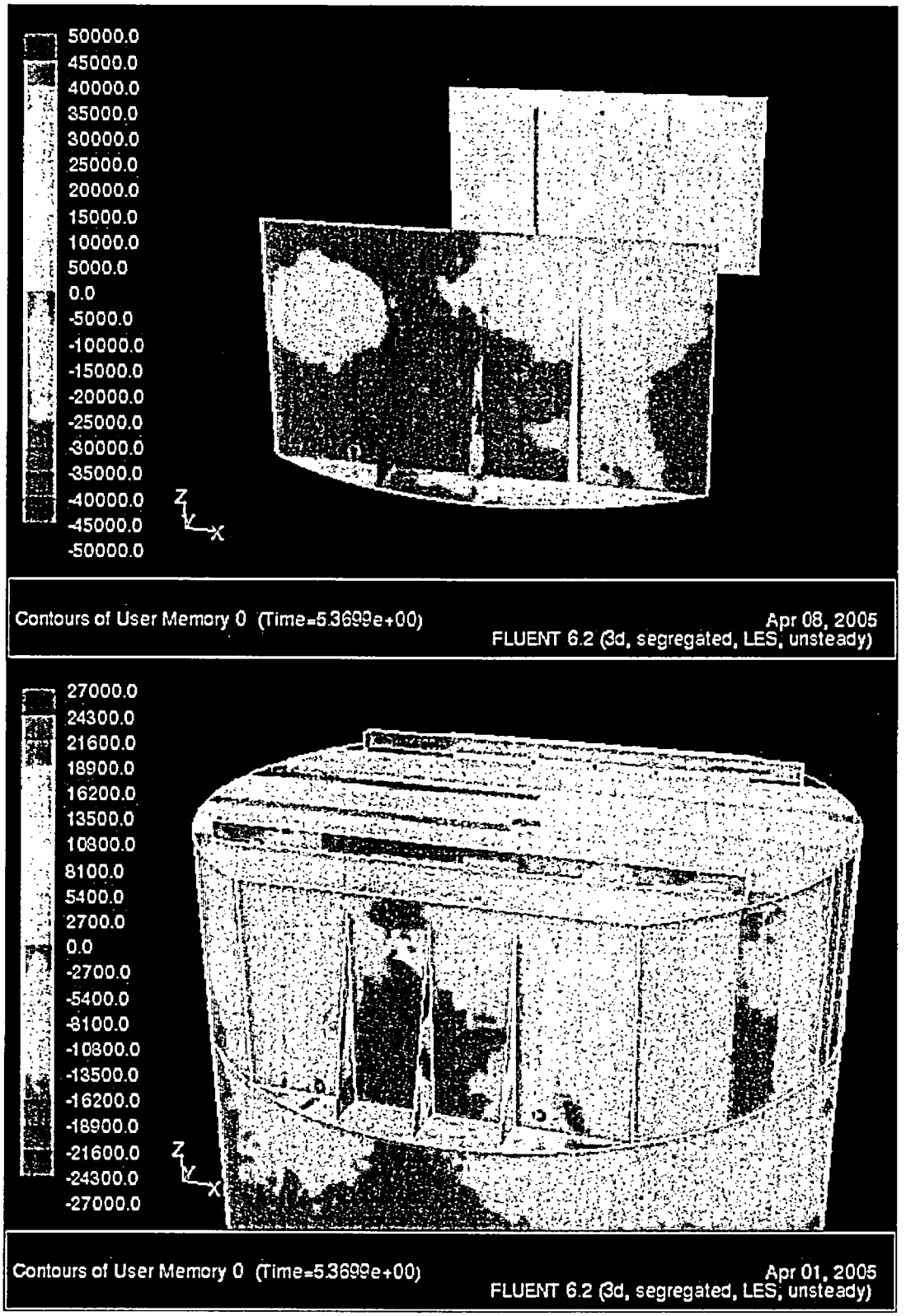

Time 5.37 Seconds

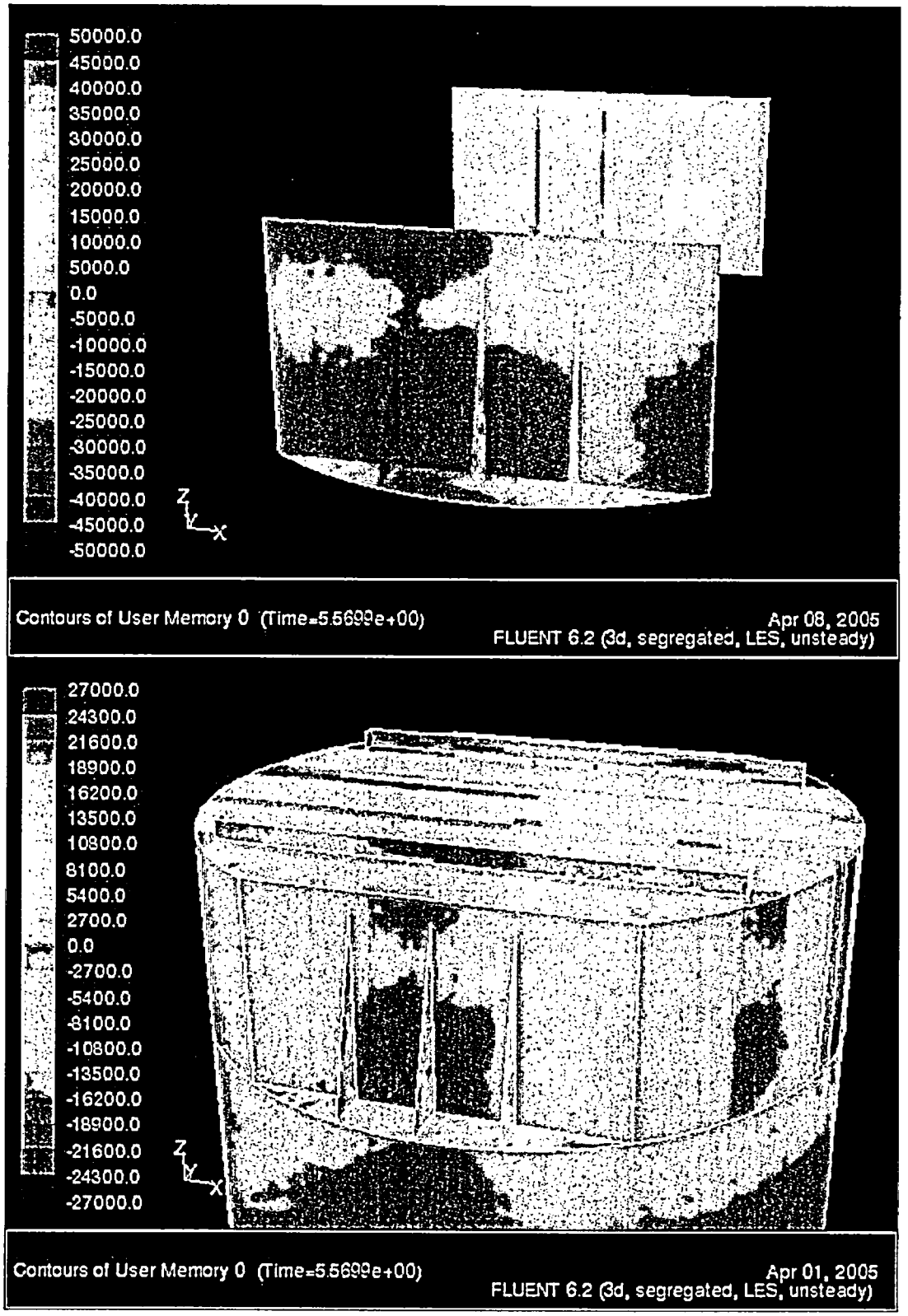

Time 5.57 Seconds

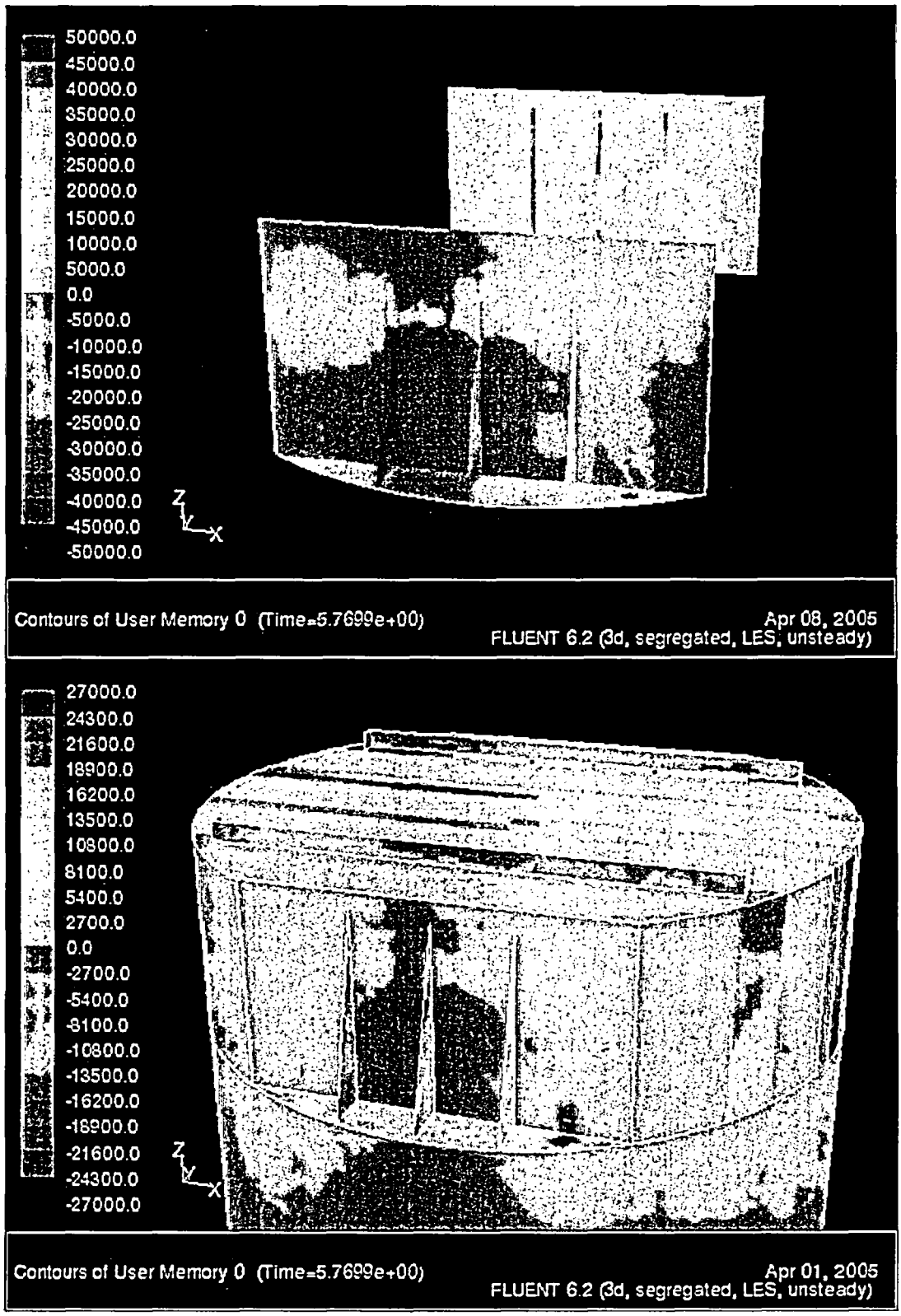

Time 5.77 Seconds

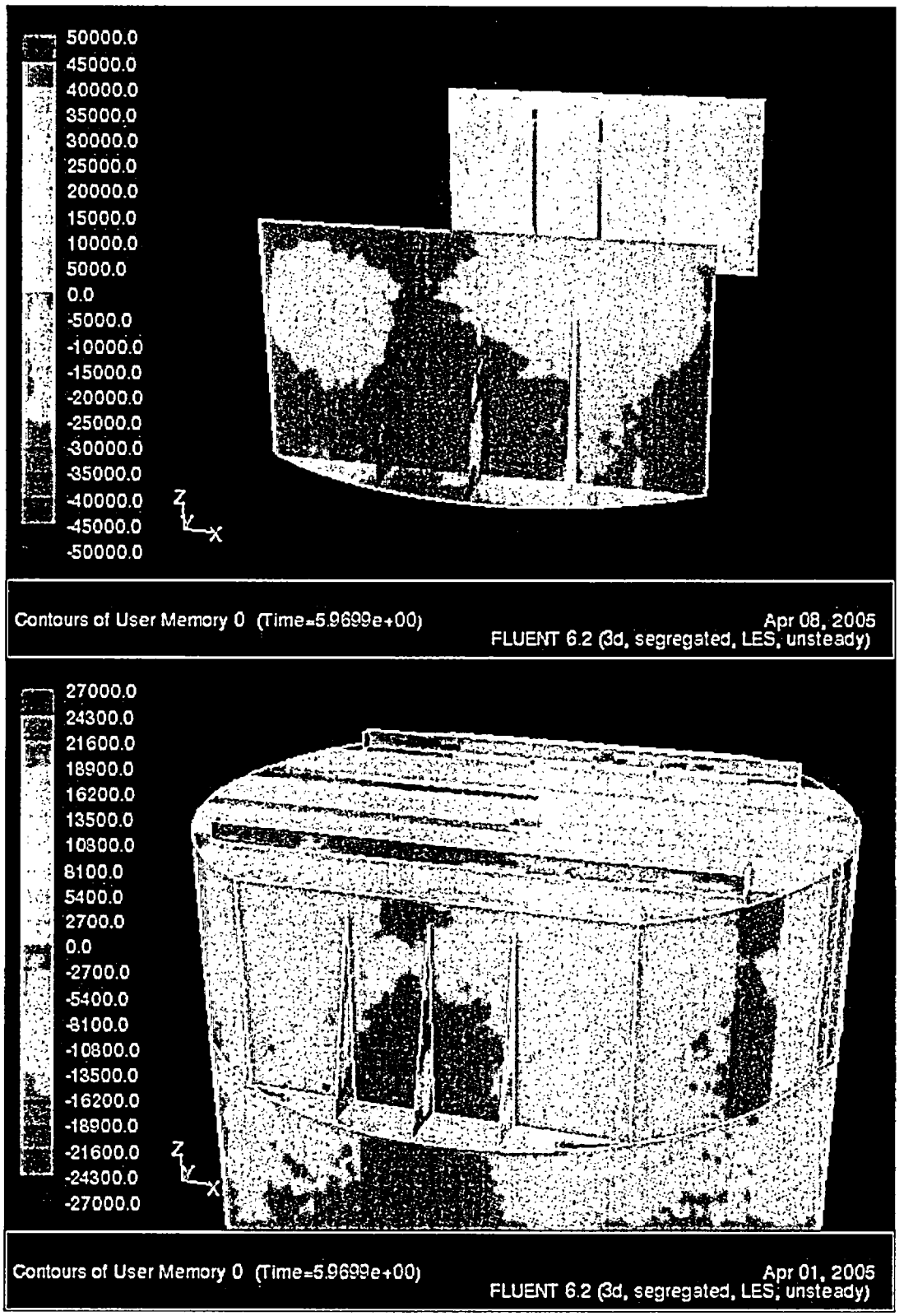

Time 5.97 Seconds

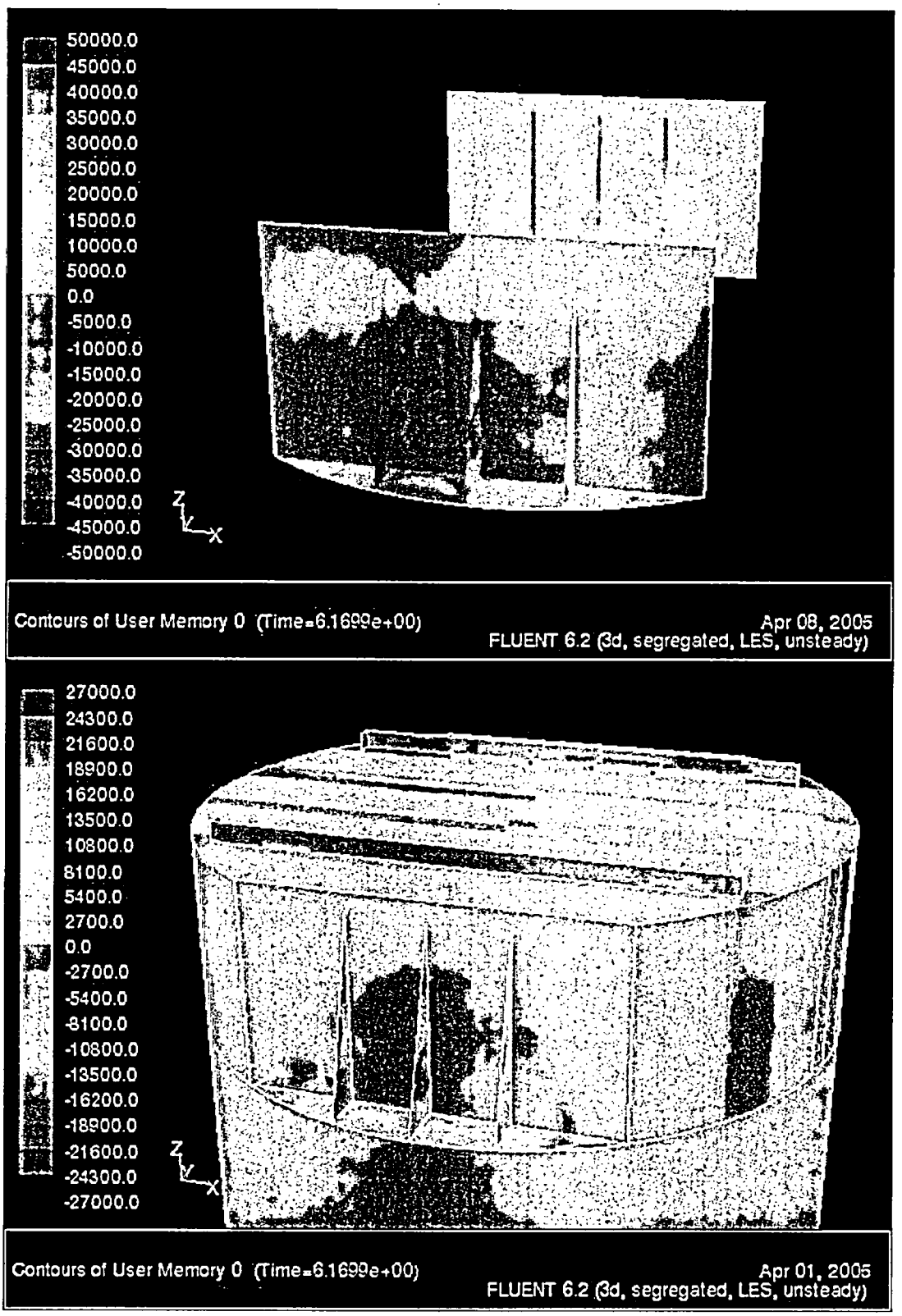

Time 6.17 Seconds

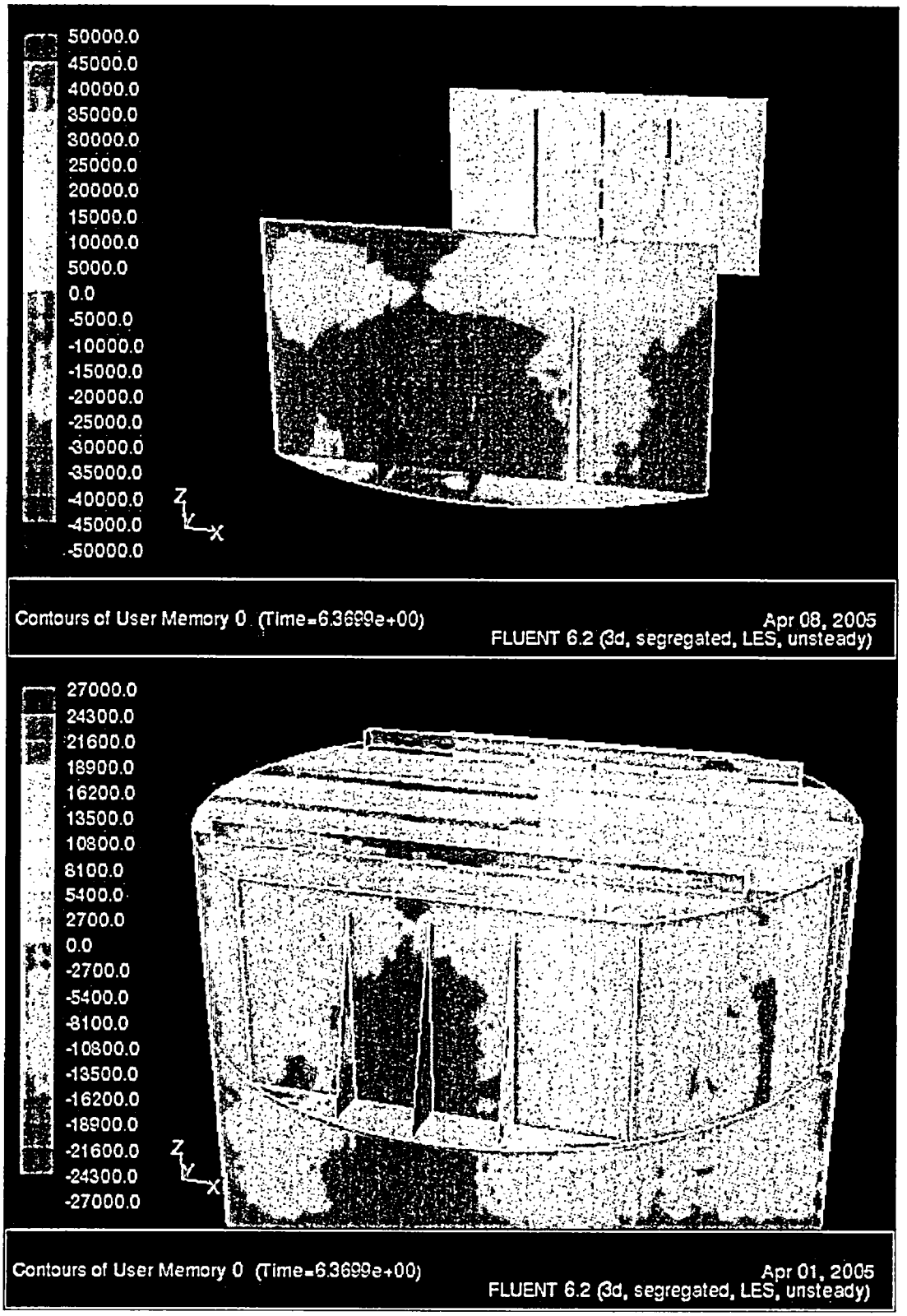

Time 6.37 Seconds

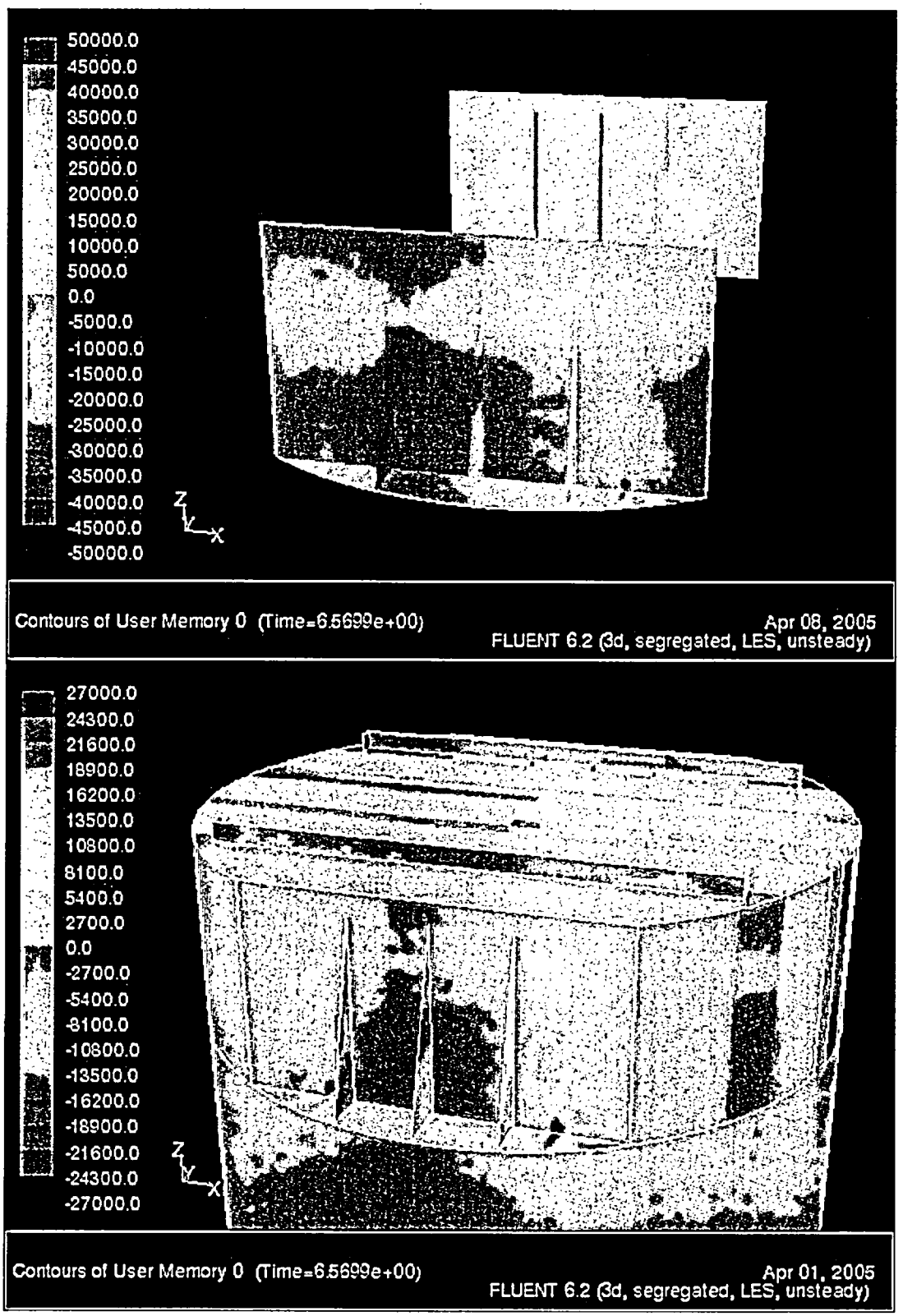

Time 6.57 Seconds

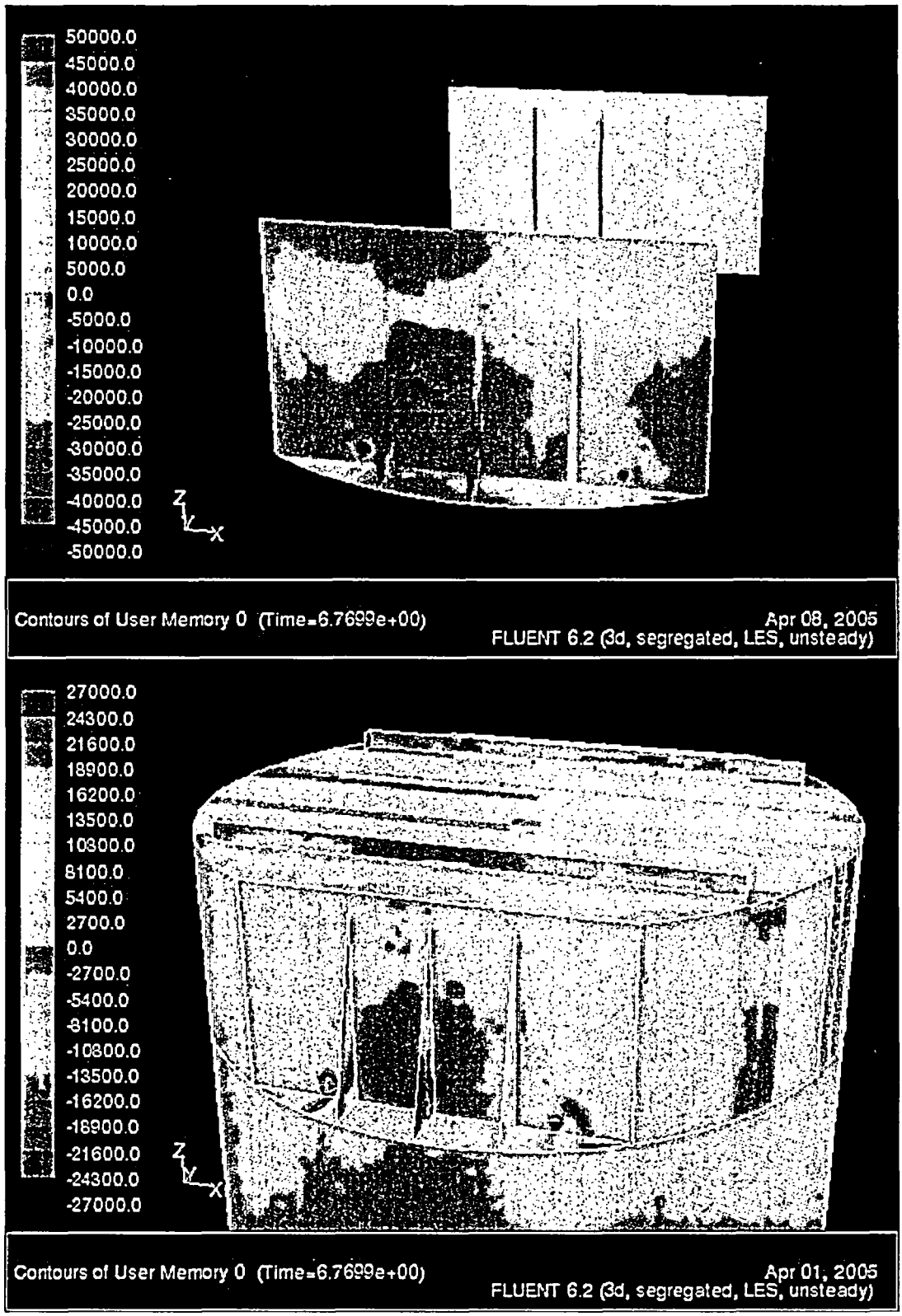

Time 6.77 Seconds

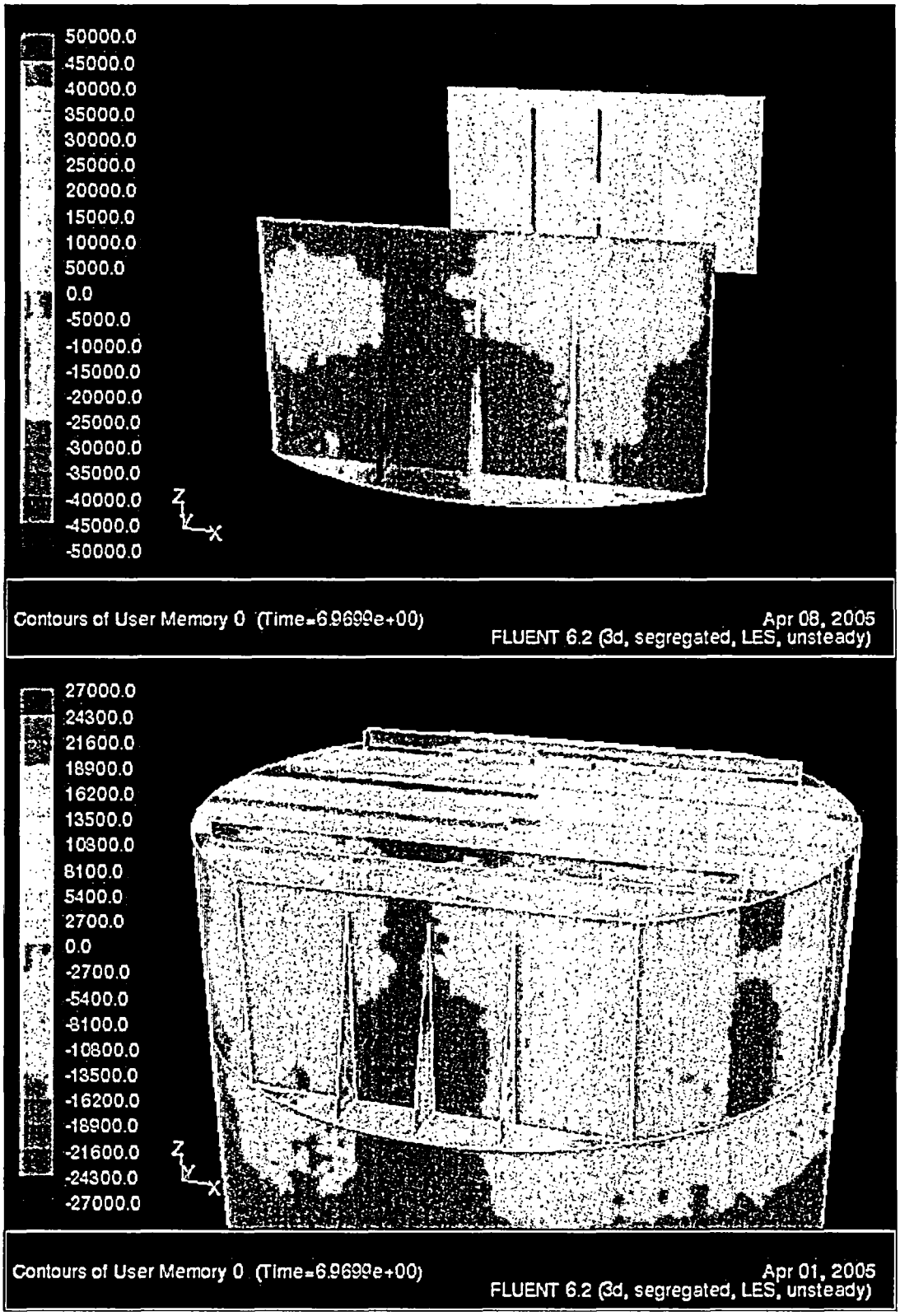

Time 6.97 Seconds

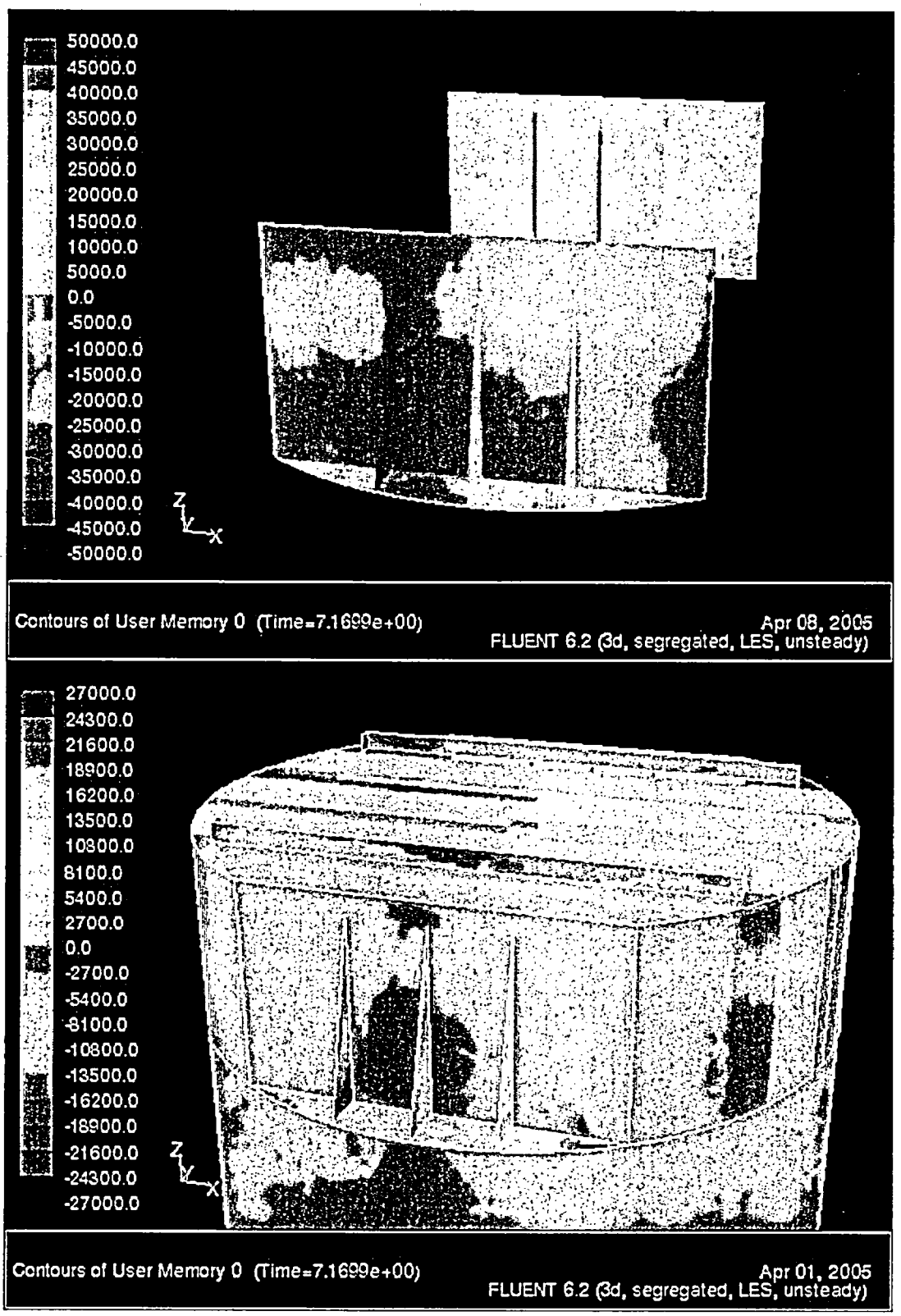

Time 7.17 Seconds

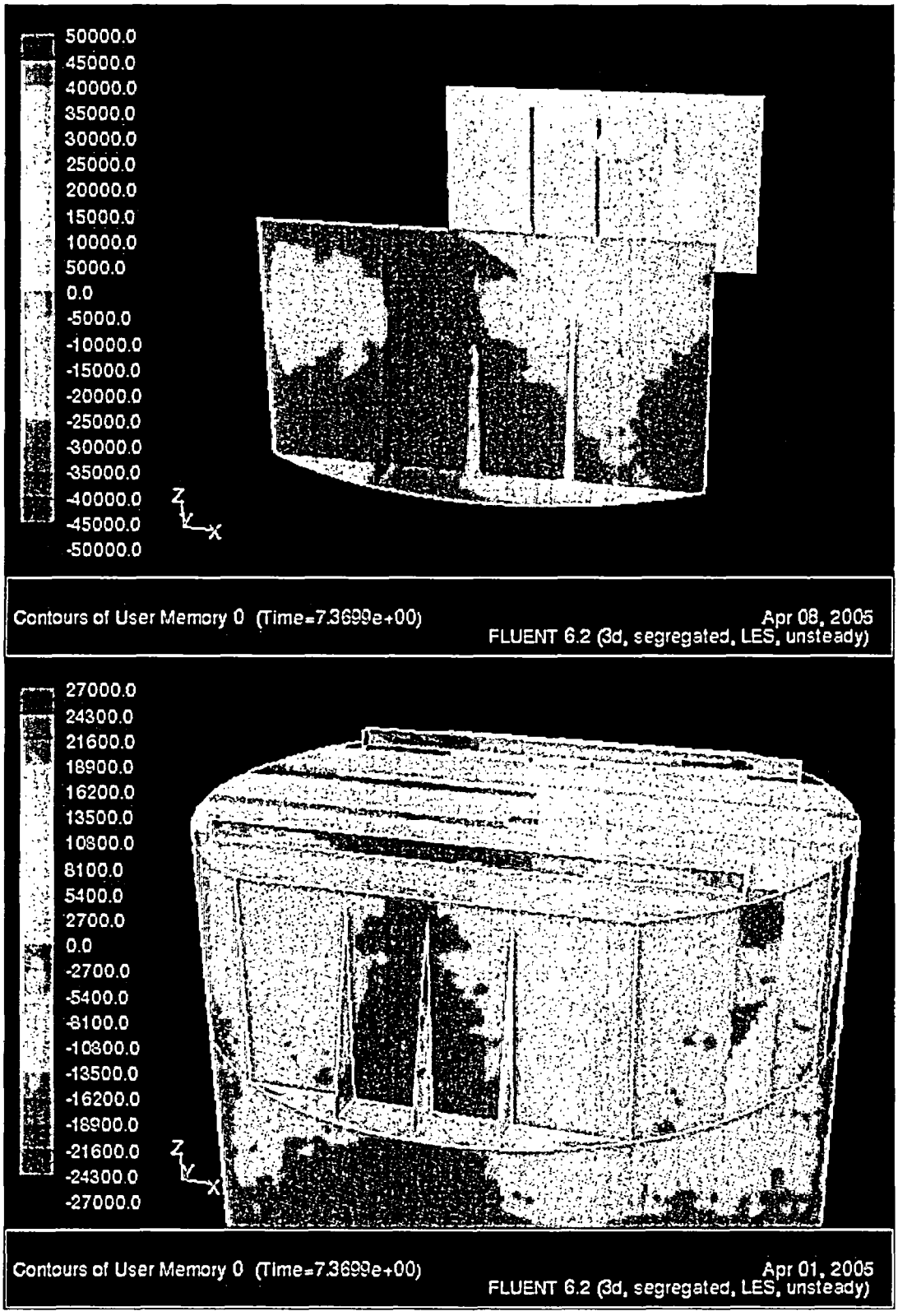

Time 7.37 Seconds

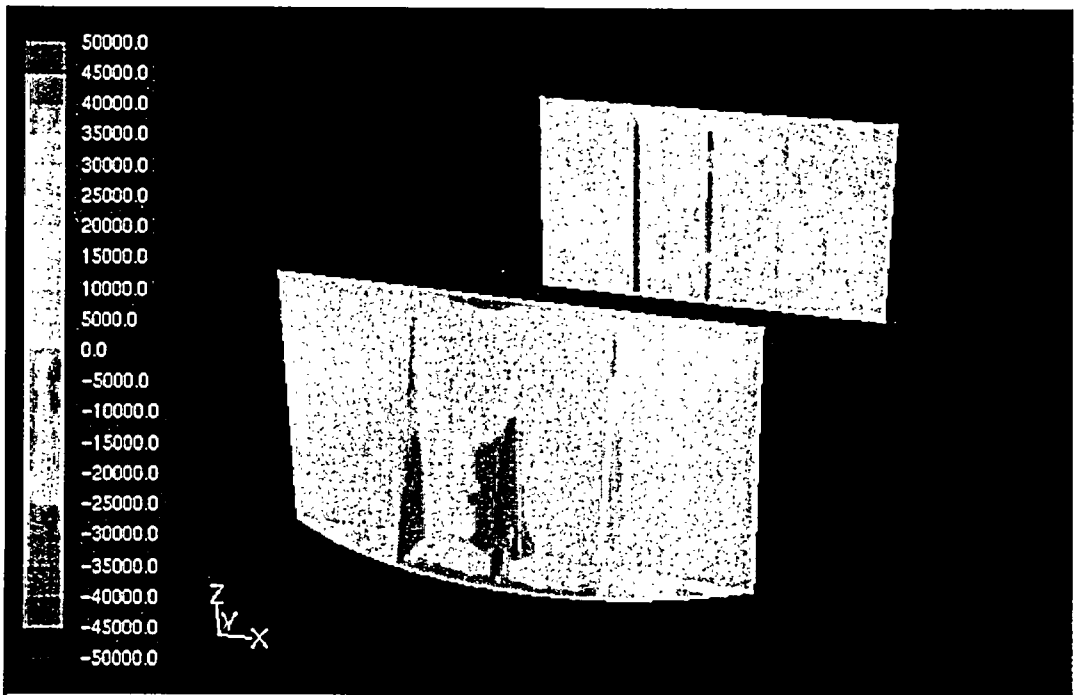

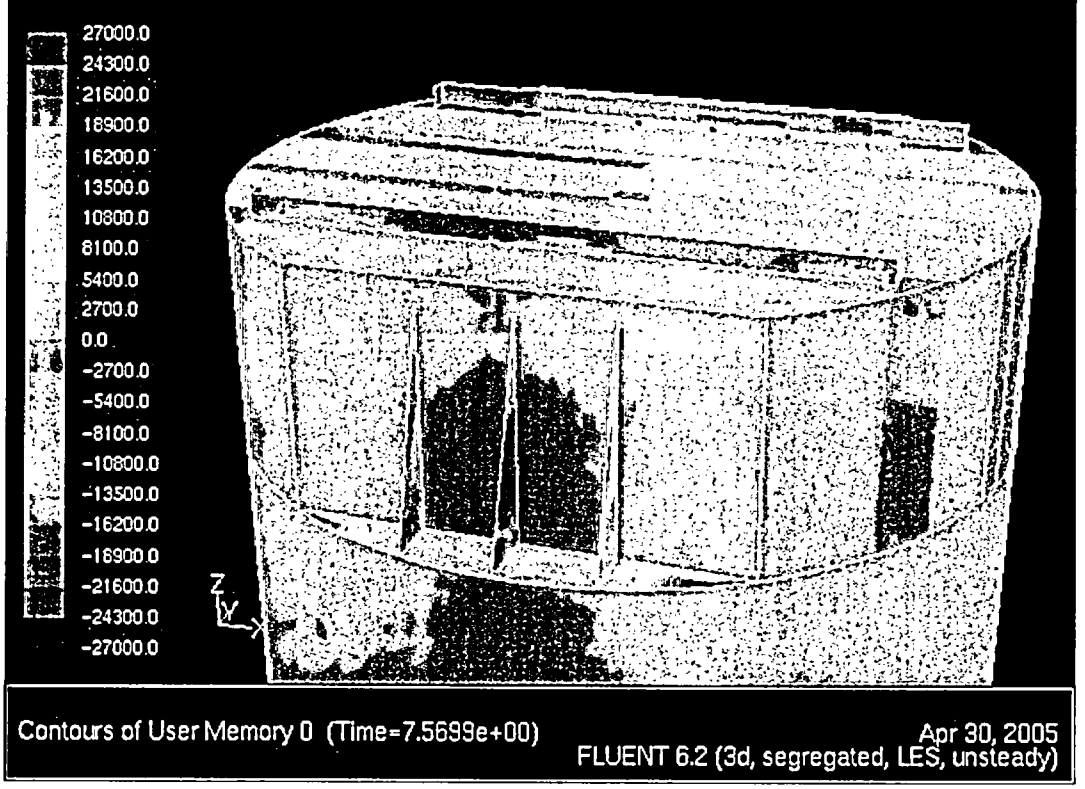

Time 7.57 Seconds

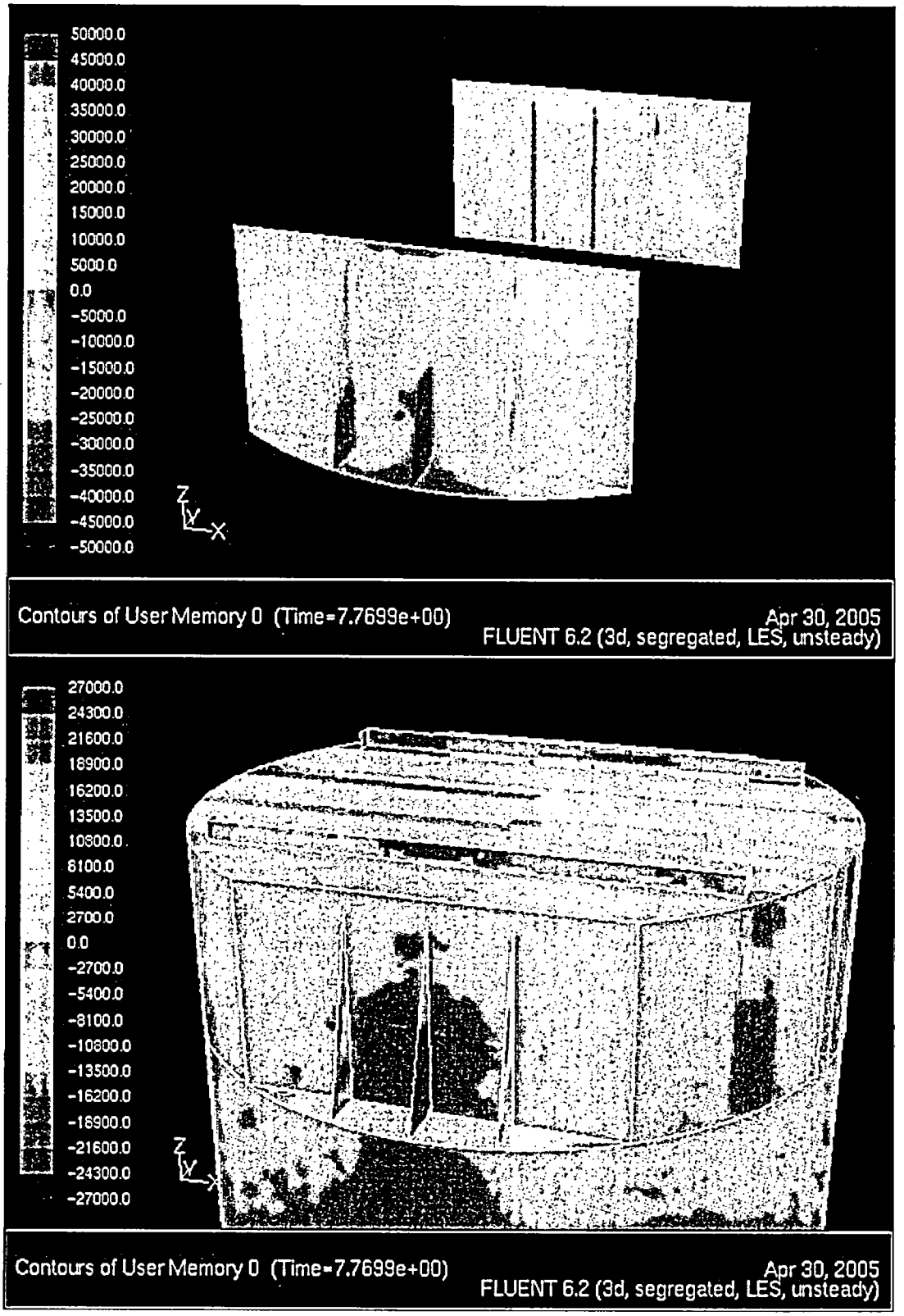

Time 7.77 Seconds

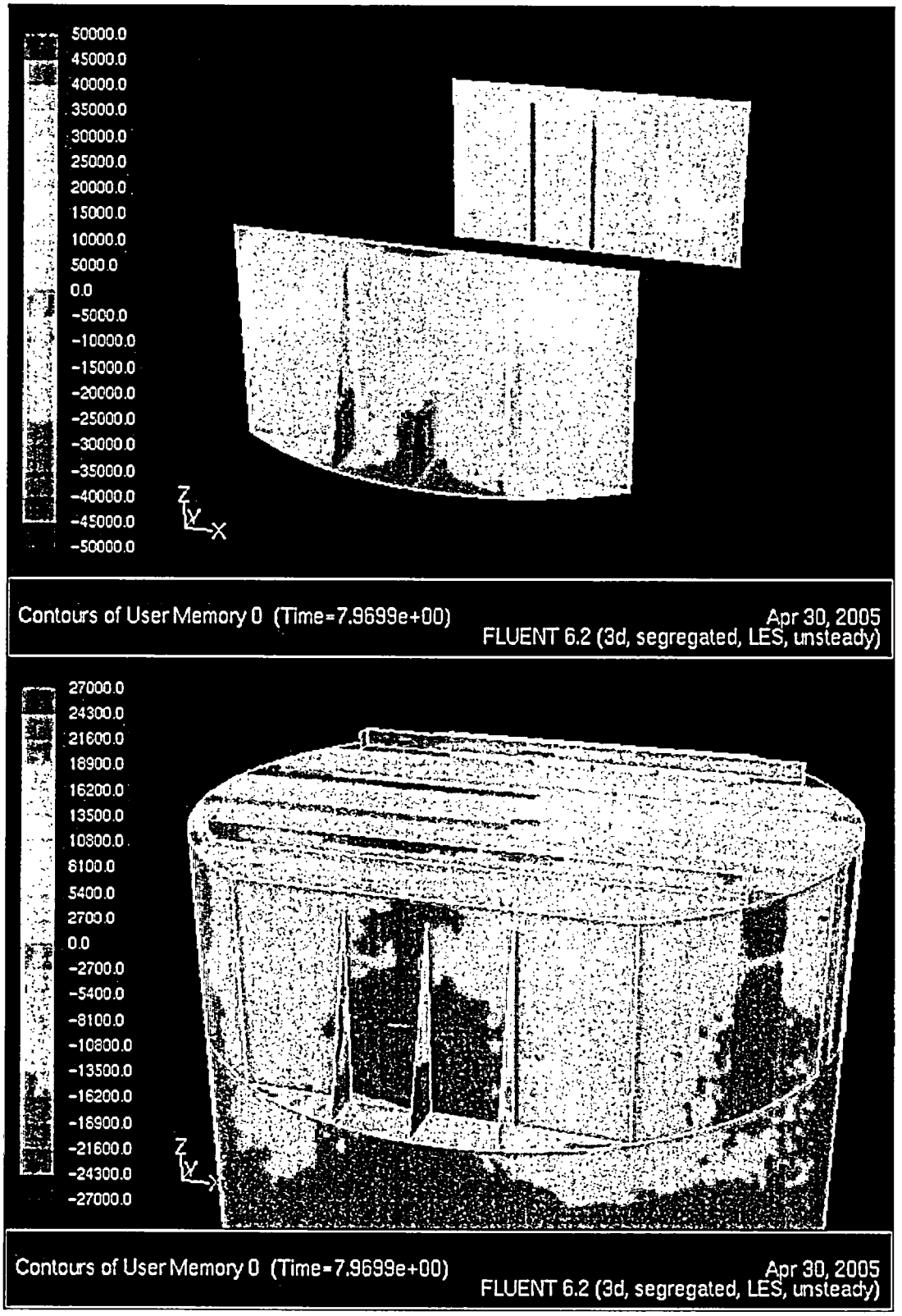

Time 7.97 Seconds

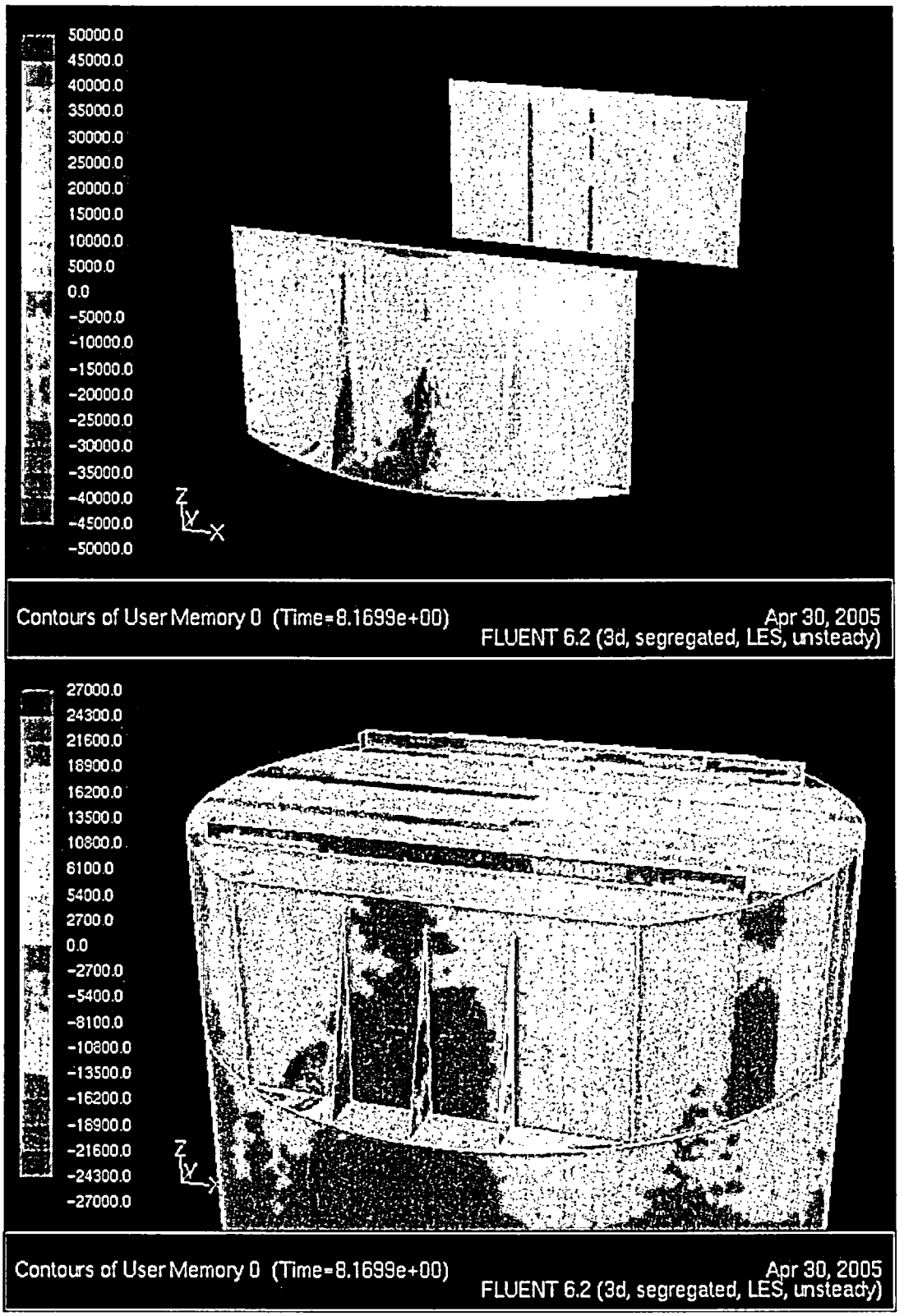

Time 8.17 Seconds

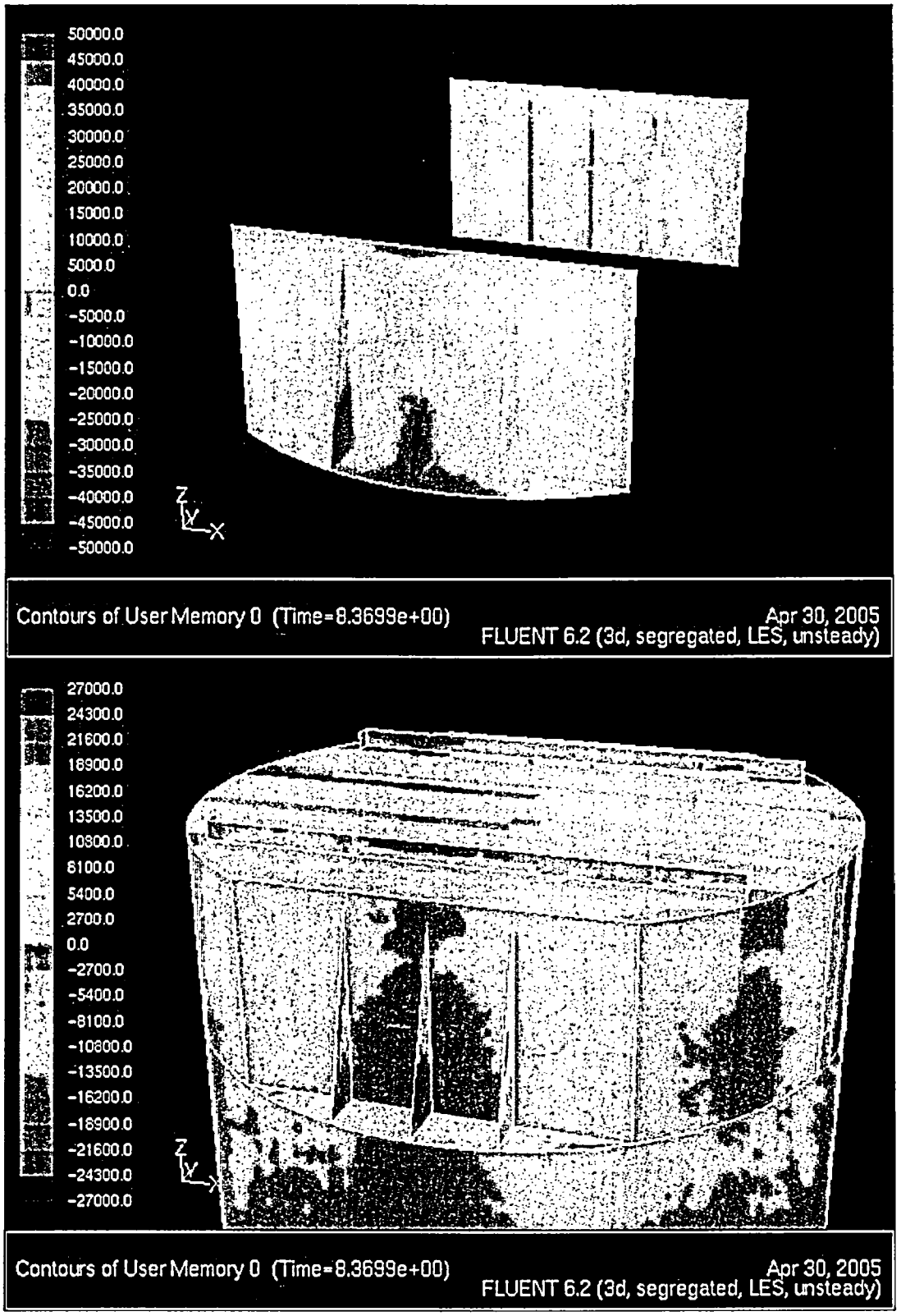

Time 8.37 Seconds